Beam theory and finite element approaches to modelling the stresses in the second metatarsal during running

Submitted by Matthew Arrun Ellison, to the University of Exeter as a thesis for the degree of Doctor of Philosophy in Sport and Health Sciences, March 2020.

I certify that all material in this document which is not my own work has been identified and that no material has previously been submitted and approved for the award of a degree by this or any other University.

(Signature) ……

Abstract

Stress fracture of the second metatarsal is a problematic injury amongst runners, requiring long recovery times. The physiological mechanisms by which a stress fracture may develop are reasonably well understood, however there is poorer understanding of the training variables which may lead to increased risk of injury. This is compounded by the difficulty of directly measuring metatarsal stress. The aims of this thesis were to develop both 2D beam theory and 3D finite element models with participant-specific parameters to investigate the stresses experienced by the second metatarsal during running. The models would be used to answer an applied question regarding the differences in second metatarsal stress between rearfoot (RF) runners and non-rearfoot (NRF) runners.

A single data set was collected consisting of 20 runners, including 12 habitual rearfoot and 8 habitual non-rearfoot strikers. Synchronised force, pressure and kinematic data were collected during barefoot running (3.6 ms^{-1}) in addition to three plane magnetic resonance data of the right second metatarsal of each participant.

The first modelling study developed and evaluated a 2D beam theory model incorporating vertical and horizontal ground reaction forces under the metatarsal head and toe and utilising participant-specific geometrical information from magnetic resonance images. Peak stress and input variables were compared between RF and NRF groups and statistical parametric mapping analysis allowed comparison of the stress time histories between groups. Results demonstrated that ground reaction forces under the metatarsal head were greater in the NRF group at the time of peak stress, but that peak stress did not differ between groups. The SPM analysis found greater stress in the NRF group during early stance.

The second modelling study developed and evaluated a 3D finite element model, incorporating distributed loading and soft tissue effects between the metatarsal head and the ground. A two-part metatarsal bone consisting of trabecular and cortical layers was reconstructed from magnetic resonance images, in addition to the soft tissues surrounding the metatarsal bone. Three time points during stance were analysed; maximum braking (minimum horizontal ground reaction forces), maximum vertical ground reaction force, and maximum propulsion (maximum horizontal ground reaction forces). Maximum von Mises stress and input variables were compared between groups at all three time points. Results showed that vertical ground reaction forces under the metatarsal head were greater in NRF runners at all time points, but stress did not differ between groups at any time.

When using the two models the same overall findings were observed, suggesting that external forces do not represent internal loading well. The magnitudes of stress were not different between groups at the time of peak stress (2D model) or the times of maximum braking, maximum vertical ground reaction force or maximum propulsion (3D model), suggesting that habitual foot strike modality does not affect the risk of stress fracture via this mechanism.

Acknowledgements

This thesis would not exist without the following people:

Firstly, the people who generously gave their time to participate in my study.

Secondly, my supervisory team. Dr. Hannah Rice has been a constant voice of support for my work and her invaluable advice, whether related to this thesis or otherwise, has pushed me to find solutions to the many problems and pitfalls associated with scientific study. Prof. Akbar Javadi has always found time to listen and advise on the computing aspects of this study. I have enjoyed working with you both for the last three years.

Thirdly, Dr. Mohammad Akrami, whose guidance with the process of using the Abaqus software package saved me from premature baldness on more than one occasion.

Fourthly, the support of my family and friends. My parents, without whom I could not have given up work to become a full-time student. The friends I made during the creation of this work, Jonathon, Pat, Pete, Paola and Matt all need special mentions for the pick-me-up chats we had in the office, and my best friends Dan and Sue who still believe I am making robot feet. Lastly my wife Lucy, for whom I could write another thesis detailing the many ways that she has supported me, but won't, because one is enough. Safe to say, the inventive methods she has developed to turn a frown upside down have astounded me.

Special mention to the EPSRC who paid for all this.

Table of Contents

List of Equations

List of Tables

Table 17: Range of motion in degrees between foot segments during running stance in the sagittal and frontal planes

List of Figures

Figure 15: Forces and dimensions considered in the mathematical model. Note: lm represents metatarsal length, l_t represents toe length, r_1 and r_2 represent the lower and upper radii of the metatarsal head, α represents the angle between the metatarsal and the horizontal, P represents the long and short plantar tendon forces, F_{ax} represents the axial compression force, F_{sh} represents the shear force, M_{be} represents the midshaft bending moments, σ_d and σ_s represent the dorsal and plantar midshaft stresses, ε represents the distance from the lower surface of the metatarsal head to the plantar tendon and θ is the angle of plantar tendon action.

Figure 16: Free body diagram for the toe – F_{tz} and F_{ty} represent the vertical and horizontal ground reaction forces acting under the toe, F_{jz} and F_{jy} represent the vertical and horizontal joint contact forces at the MTP joint.

Figure 17: Free body diagram for the metatarsal – F_{mz} and F_{my} represent the vertical and horizontal ground reaction forces acting under the toe.

Figure 18: The heat map of pressure distributions overlaid with the mask outline and section lines (right), the final pixel mask for comparison.

Figure 19: A: Original image of cross section, B: Image with altered contrast, C: Initial edge detection, D: Final edges with centroid plotted in blue.

Figure 20: Outline of cross section divided into triangles, with the centroid of each triangle plotted as circles.

Figure 21: scatter plot displaying individual peak stress values plotted against body weight for rearfoot (RF) and non-rearfoot (NRF) strikers.

Figure 22: Comparison of dorsal stress between foot strike types. Negative values represent compression. Vertical shaded area shows areas of significant differences.

Figure 23: t values for a comparison of dorsal stress between foot strike types across the whole of stance. Area below the alpha line is significant.

Figure 24: Comparison of plantar stress between foot strike types. Negative values represent compression. Vertical shaded area shows areas of significant differences.

Definitions

RFS – Rearfoot Strike

NRF – Non-Rearfoot Strike

FE – Finite Element

GRF – Ground Reaction Force

vGRF – Vertical Ground Reaction Force

hGRF – Horizontal Ground Reaction Force

CSA – Cross-Sectional Area

MTP – Metatarsophalangeal

Declaration, Publication and Communications

Declaration

The material contained within this thesis is original work conducted by the author. The following communications and publications are a direct consequence of this work.

Communications

BASES Biomechanical Interest Group, April 2018, Salford

Inter-segment foot kinematics during running with different habitual foot strike patterns. Oral Presentation

World Congress of Biomechanics, July 2018, Dublin.

The influence of habitual foot strike modality on metatarsal stress during running. Poster presentation.

UK Association of Computational Mechanics, April 2019, London.

Developing a Finite Element Model to Investigate Second Metatarsal Stress during Running. Oral Presentation.

International Society of Biomechanics, July/August 2019, Calgary.

Using a finite element model to investigate second metatarsal stress during running. Oral Presentation

1. Introduction

Running is a fundamental and ubiquitous human movement pattern. The popularity of running as a sport has been increasing since the 1970's (van der Worp et al., 2015) and many people take up running as a hobby either for competitive reasons or for the numerous health benefits it provides. In England a recent survey (Sport England, 2018) suggested that 15.4% of the population had run at least twice for exercise in the preceding 28 days. This gives an estimate of 6.9 million people running on a regular basis in this country alone. Comparison with the previous year's survey suggests that this number is stable in England.

Recreational running takes place over a range of distances; long distance running begins at a distance of 5 km and proceeds up to marathon distances and beyond. Part of the appeal of running is the lack of required equipment or specialist skills needed to take it up and as a result of this running takes place in many environments with many variations in training parameters. As a result, it is unclear as to which particular environments and training factors are best for performance and injury prevention.

Running is an effective way to build cardiovascular fitness and has numerous well-documented health benefits. Importantly, physical fitness is strongly linked with longevity (van der Worp et al., 2015, Fields et al., 2010) with regular physical activity reducing the risks of coronary heart disease, cerebrovascular disease, hypertension, type II diabetes, various cancers, and osteoporosis (Lee et al., 1997). A recent study has suggested that physical inactivity is responsible for 6% of coronary heart disease burden worldwide, 7% of diabetes, and 10% each of colon and breast cancers (Lee et al., 2012) and the same study also suggesting that inactivity is responsible for 9% of premature mortality, while another

systematic study (Samitz et al., 2011) suggests that vigorous exercise and sports shows the largest reduction in all-cause mortality with moderate activities of daily living being beneficial, but to a lesser extent. Other studies have specifically associated running or jogging with reduced mortality and disability (Chakravarty et al., 2008, Lee et al., 2014, Schnohr et al., 2013, Wang et al., 2013). Given its associations with health benefits and longevity it appears that promoting running as a sport or recreational activity is a simple and effective way to increase public health and reduce burden on health systems, particularly for non-communicable diseases that appear later in life.

Any exercise regimen or sports training brings with it the risk of injury, with certain injuries associated with certain kinds of training. For long distance runners, there is a particularly high incidence of lower limb injuries, with one systematic review finding the incidence to range from 19.4% to 79.3% across the 17 studies it included (van Gent et al., 2007). The most injured site was the knee (7.2% to 50%) followed by the lower leg (excluding the foot) (9% to 32.2%) and then the foot, which contributes between 5.7% and 39.3% of injuries. If these figures are representative of the population as a whole then this represents around 407,000 injuries to the foot per year due to running in England alone, based on the estimate of running participation stated above (6.9 million) (Sport England, 2018).

Injury is detrimental as it diminishes the pleasure derived from exercise and limits participation, sometimes for an extended period of time, or may cause a permanent withdrawal from the activity. Injury can be divided into two categories depending on how they occur; acute injuries happen suddenly and can be traced back to a single incident, whereas overuse injuries occur gradually. Most injuries in running are overuse injuries with one study suggesting that they represent 80% of all running injuries (van der Worp et al., 2015).

One type of overuse injury common to running is stress fracture of the lower limb. These injuries typically manifest as small cracks on the bone, often with bony edema. Stress fractures represent a particular burden, in that the time taken to heal and therefore return to training is long - of the order of 12 weeks for metatarsal stress fractures (Wood et al., 2014). Matheson et al. (1987) suggests that stress fracture accounts for 20% of sports medicine clinic visits from athletes and it is not clear if this figure has changed in more recent years. The second metatarsal (MT2) is a problematic site of stress fracture (Bennell et al., 1998, Bennell et al., 1996, Milgrom et al., 1985, Gross and Bunch, 1989, Iwamoto and Takeda, 2003, Orava, 1980, Firminger et al., 2017) with between 8% and 23% of all stress fractures in the athletic populations studied occurring in the metatarsals, and 80% of these located at the second or third metatarsal (Firminger et al., 2017). Based on previously outlined estimates, this suggests that approximately 110000 – 300000 runners will experience a metatarsal stress fracture in England each year. Of those, 88000 – 240000 will be located in the second or third metatarsals. It would therefore be beneficial to understand the particular factors and possible training errors that lead to this injury, such that preventative measures or interventions can be taken to reduce the risk of injury.

Metatarsal stress fractures have been observed all along the shaft (Orava, 1980), with non-proximal fractures more likely than proximal fractures (Chuckpaiwong et al., 2007). Murphy et al. (2003) found that intrinsic factors such as foot morphology and decreased bone mineral content were risk factors for lower limb stress fracture. However, they found that other intrinsic factors such as gender, height, weight and body fat percentage did not differ between athletes developing stress fractures and those that did not. This suggests that stress fracture is likely to be caused by a complex interaction of extrinsic factors, such as training

choices, and intrinsic factors, such as foot morphology, leading to increased loading in certain areas of the bony tissue. It is generally agreed that stress fractures are caused by repeated loading cycles at sub-failure load magnitudes (Milgrom et al., 2002) and due to this, understanding the repeated loading which the tissue undergoes is likely to provide invaluable information regarding causes and mechanisms for the development of this type of injury. As such, quantifying the loading experienced by the bones during running is warranted.

Foot strike modality defines the manner in which the foot meets the ground during the running stride. Changing the kinematics of the foot at the point of impact with the ground has implications for the loading of foot tissues. For example, Nunns et al. (2013) found that those who landed on the more anterior parts of the foot had greater plantar pressures under the metatarsal heads. It is likely, therefore, that foot strike modality could affect the loading experienced by the metatarsal bones, and through this influence the risk of stress fracture.

Direct measurement of forces acting on internal tissues of the body is difficult and invasive to carry out, therefore a mathematical modelling approach is often used to estimate these factors (Nunns et al., 2017, Gross and Bunch, 1989). For 3D models with continuous geometry such as models of bones, the finite element method is appropriate for investigating loading and stress (Halloran et al., 2009).

Models of varying complexity have been used in the past to investigate loading in the foot. However, in general, these models have been either over-simplified, non-participant-specific or used to investigate loads not relevant to running, such as quiet standing or walking (Stokes et al., 1979, Jacob, 2001, Gross and Bunch, 1989, Nunns et al., 2017, Gefen, 2002, Lemmon and Cavanagh, 1997). Development of a model specifically investigating the loads in the second

metatarsal during distance running would allow the identification of training variables that contribute to stress fracture injury and therefore allow interventions to reduce this injury type to be assessed.

This thesis focusses on the challenge of measuring bone loading in the second metatarsal during running, developing both 2D beam theory and 3D finite element approaches to estimating bone stresses. These modelling approaches are evaluated and compared. They are also used to answer an applied question: how do stresses in the second metatarsal compare between two groups habitually using differing foot strike modalities?

2. Literature Review

A review of existing literature is important in order to understand previous research and the current level of knowledge regarding the aetiology of this injury, and therefore to plan where future studies may contribute to the body of knowledge. In this review the current theory of stress fracture and risk factors is investigated, including the methods of measurement of these risk factors.

2.1 Stress Fracture of Bone

In order to understand and interpret how any measured or modelled loads might affect bony tissue and possibly cause injury, an understanding of the human skeletal system is needed. This review section covers the structure and function of bones and includes relevant physiological processes that influence how a bone may react to a particular loading scenario.

2.1.1 Bones and their Function

Bones are the individual components of the framework of the skeleton, which makes up the underlying structure of the human body. The function of the skeleton and therefore bone is both mechanical and physiological.

From a mechanical perspective the geometry and material composition of bones enable the skeleton to have structure and shape, articulate joints and facilitate movement by acting as levers and allowing muscles to transfer forces from one part of the body to another. The bones of the skeleton are often classified by their shape, which also defines their function. For example, the flat bones of the skull are primarily suited for protection, whilst long bones such as the femur are suited for force transmission and leverage. The metatarsals follow the classic shape of a long bone, having a narrow cylindrical shaft (diaphysis) and wider flared ends (epiphysis) which articulate with other bones (Figure 1).

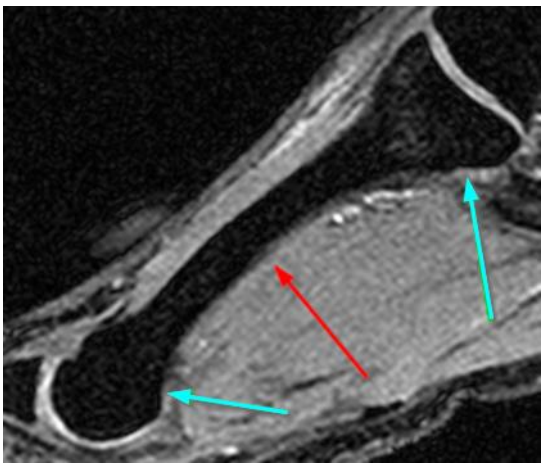

Figure 1: An MR image of the second metatarsal, showing long narrow shaft (red arrow) and wider ends for articulation (blue arrows).

A fact of the design of the human body is that most of the muscles and joints work at a mechanical disadvantage. This creates certain benefits, for example when flexing the leg, the foot will move much faster than the flexor muscles contract in the thigh, and there will be no “web” of muscle between the thigh and shank to hinder the movement or range of motion (Martin et al., 2015). However, a simple mathematical calculation will reveal that the forces produced in the muscles and therefore transmitted by the bones are an order of magnitude higher than the weight of the foot. An example of such a calculation relevant to the metatarsals can be seen in a study by Stokes et al. (1979) where it was shown that the second metatarsal had a maximum axial force equivalent to 84% BW acting on it during normal walking and was subject to a bending moment of 1.4 BW·m. For consideration it should be noted that each foot distributes the force over a number of metatarsals and soft tissues and that the second metatarsal is a small bone, with a typical cross sectional area of less than $2x10^{-4}$ m^2 at the midshaft (Gross and Bunch, 1989). In addition each foot contains approximately 1.4% of total body mass (Dempster, 1955), meaning the metatarsal experiences axial forces equivalent to 60 times the weight of the foot. Therefore, the bone must be capable of withstanding almost the full bodyweight of a person during a dynamic

movement despite its very small size. For more vigorous activities such as running or jumping, forces can be much higher, of the order of several times bodyweight depending on the activity.

An evolutionary adaption to favour speed and easy movement has resulted in the need for bones to be resilient to large forces and to do this over the course of many loading cycles throughout a lifetime. Bony tissue is therefore extremely strong and has several adaptations that facilitate effective force transmission. It is described in the literature as “A hierarchically-organised material that is constructed as a fibre-reinforced composite material.” (Martin et al., 2015). Meaning that the structure at the nano or micro-scale directly affects the performance of the material on a macro-level and that it is not comprised of a single material.

Bone has a multi-material composition that allows it to be both strong and flexible (Martin et al., 2015). However, it also allows it to be anisotropic and its strength in a particular direction is dependent on the arrangement of the fibres. In normal, healthy bones the fibres align to provide greatest strength in the direction of greatest loading. For example it has been shown that the trabeculae structures lie in lines that correspond to the principle stress lines seen under loading (Martin et al., 2015, Yettram and Camilleri, 1993). In long bones this generally occurs in the direction parallel to the longitudinal axis of the bone, however metatarsal bones present one of the few examples where this is not the case. As a result of their location and orientation they are loaded at the distal end almost perpendicular to the longitudinal axis of the shaft (Figure 2). Simple geometry suggests that this will result in a larger than usual amount of bending in the shaft when compared with other long bones.

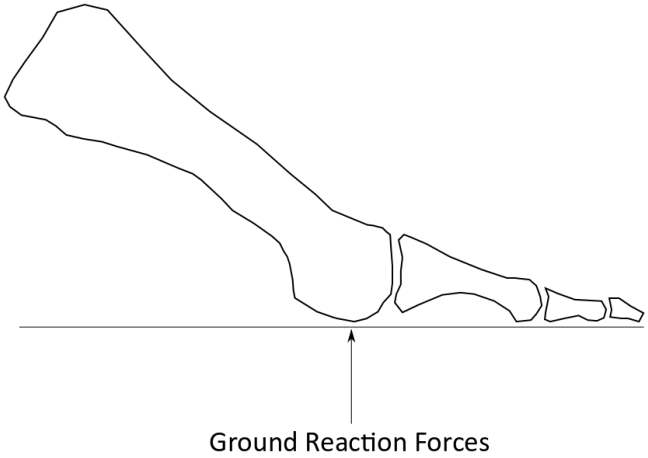

Figure 2: Schematic of the second metatarsal and toe, showing typical angle made with the ground and loading forces

Two types of bony material, known as trabecular or cancellous bone and cortical or compact bone, make up a whole bone. In addition to these two distinct types of material, the bone can also be highly organised, described as lamellar, or disorganised. Cortical bone can be found on the outside of bones, it is dense and well organised into sheets of lamellar bone layered on top of one another. In a long bone, the diaphysis is mostly cortical bone. Trabecular bone is found inside the cortical layers and has a sponge-like and less organised appearance. In a long bone, the epiphysis contains the majority of the trabecular bone (Figure 3).

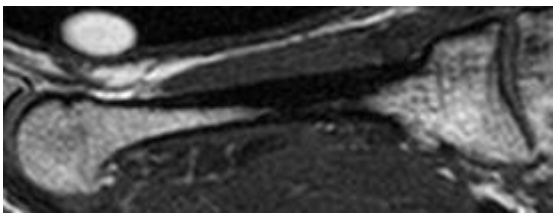

Figure 3: A weighted contrast MR image of the second metatarsal, a lighter colour on the image represents less dense bone material. The trabecular bone represents a large portion of the bony material especially at the epiphysis, whilst cortical bone is much more prevalent in the diaphysis.

Mechanically the two forms of bone are different in their resistance to compressive and tensile forces. For cortical bone the ultimate stress is 195 MPa under longitudinal compression compared to 133 MPa under longitudinal tension, making the bone approximately 1.4-1.5 times stronger under compression than

tension. This is important as the bones in the body are most commonly loaded under compression. Trabecular bone has a much lower threshold, between 1.4 – 5.6 MPa under both compression and tension. Additionally cortical bone is much weaker in the transverse direction than longitudinally (133 MPa for compression, 51 MPa for tension) (Martin et al., 2015).

2.1.2 The Bone Remodelling Process

Due to the large and repetitive forces that bones are subjected to, the ability to repair themselves and adjust their shape and mechanical properties according to the loading they are subjected to is a very important function. In fact, the ability to repair damage allows the bones to balance tissue mass against strength in a way that is not seen in materials outside of nature. A lighter bone is theoretically less strong than a heavier bone, yet a bone's ability to repair damage means it can afford to be lighter to optimise performance. Lighter bones will allow better performance of the organism, for example moving the same limb with a lighter bone will require less force and therefore will cost less energy, or the same force will allow the lighter limb to move faster.

There are three main processes for mechanical adaptation of bones to occur: growth, modelling and remodelling. Growth is the process by which a bone gains mass by calcifying cartilage. It occurs during the formative years of life and ends after puberty, therefore from an injury perspective it is not relevant to this thesis. Modelling can change the shape of a growing bone by adding or removing bone material in the required areas. This is useful as whilst a growing bone will gain mass, it will not necessarily be mechanically sufficient to manage the loads of a growing human body without a change in shape. Remodelling is a process that occurs throughout a person's lifetime and it is the process by which existing bone is replaced by new bone. Existing bone is replaced when it is damaged or

mechanically fatigued. The bone that it is replaced with is usually more resilient to the loading that caused the damage. In this way, whilst the size and shape of a bone may not change, remodelling allows the mechanical properties to vary and be sufficient for the loading experienced. The remodelling process is thought to be heavily involved in the development of stress fracture (Lassus et al., 2002).

Remodelling occurs at sites all over the skeleton simultaneously, but the process at each site will follow the same pattern, called ARF: Activation, Resorption and Formation. In the activation stage, loading of the bone causes both chemical and mechanical triggers to activate a basic multicellular unit (BMU) at the site of damage. The BMU consists of osteoclasts and osteoblasts which act to resorb and form bone respectively. Initially the osteoclasts will act to resorb bone in a tunnel (in bone) or trench (on the surface of bone) shape, roughly 200 μm in diameter (Martin et al., 2015, Schaffler and Jepsen, 2000). The resorption progresses at around 40 μm/day along the tunnel and 5 μm/day in a radial direction. Once a cross section of the tunnel has reached maximum diameter, osteoblasts act to replace the bone. The progress of formation is much slower than resorption. A complete cross section of tunnel can be excavated by osteoclasts in around three weeks, however, it will take osteoblasts around three months to refill it. The complete remodeling of the whole tunnel will take approximately four – six months.

The processes by which a BMU is activated are currently unclear, however mechanical loading is generally held to be a primary driver. Activation is thought to be controlled in part by a mechanostat principle (Frost, 1987). This states that there is a minimum effective strain required to activate a remodelling response, this is postulated to be a range rather than a point, and the theory states that only strains outside this range evoke a response. Consistent strains below the range

cause a negative response, causing an overall loss of bone, strains above this range cause a positive adaptive response thereby increasing bone mass. The loading factors to which bone is sensitive appear to be a combination of magnitude, frequency and rate and are governed by the principles of mechanotransduction (Duncan and Turner, 1995) stating that physical loading is converted to biological signals which are in turn acted upon by cells. Loading magnitude is generally given in units of microstrain (με). In experimental testing, it appears that the response mechanism activates to keep strain between 2000 με and 3000 με in vigorous activities. For example, if a particular activity causes strains above this range then the remodelling process will cause the bone to be mechanically stronger such that the activity causes lower strain levels. Conversely, consistently low levels of strains will cause the bone to lose strength overall.

In addition to the magnitude of strain, the frequency of loading and the rate of loading contribute to the activation of a remodelling response. For example very low magnitude strains repeated with relatively high frequency will contribute significantly to bone's adaptation response. The manipulation of frequency, magnitude and rate can be shown to maintain the same bone mass (Qin et al., 1998). For example 10 minutes of daily loading at 1 Hz requires 700 με to maintain mass, but 10 minutes of daily loading at 30 Hz requires only 400 με to maintain mass. By increasing the daily loading and frequency still further, strains of magnitude of only 100 με can be seen to maintain bone mass. Similarly studies manipulating the rate of loading whilst keeping the magnitude as a constant show that increased rate induces a larger bone response than a lower rate (Mosley and Lanyon, 1998). This is important as running will subject the tissues of the foot to increases in all three factors in comparison to other daily activities, such as

walking. These factors can be manipulated by the runner. For example, increasing the step rate will increase the frequency of loading whereas footwear may influence both the rate and the magnitude of loading.

Activities that the body is unaccustomed to are likely to cause an adaptive response, and this adaptive response will result in bone loss as osteoclasts tunnel out sections of bony tissue before any gain in strength is created. For the running population the nature of training is such that there will be periods where purposeful overloading is required to increase performance. This usually takes the form of increasing distance or velocity, which will result in a change in loading magnitudes, rates, and frequencies as well as the overall number of loading cycles. In this case unaccustomed loading does not require a novel movement pattern, merely a manipulation of training factors. In conclusion, for the running population, a change in training variables could initiate a healthy remodelling response. If the new loading is not excessive, this may weaken the bone in the short term, but given a sufficient recovery period, will result in a stronger bone in the long term. If the remodelling process is interrupted or loading is ongoing during this phase then the chance of fracture may be increased, as outlined below.

2.1.3 Fracture via Fatigue

In general a material can be made to fail in two ways: in the first a load is applied that is greater than the ultimate stress of the material and this causes immediate failure; in the second a load less than the ultimate stress is applied repeatedly or constantly (called fatigue and creep respectively). In the case of stress fracture development, immediate failure is irrelevant, and will therefore not be considered here. In most materials both constant and repeated loading types can occur simultaneously. For example in bones, creep occurs from the constant support of

bodyweight, whilst fatigue occurs from daily activities such as walking or running. Although creep and fatigue are closely related, stress fracture in running is assumed to be caused by fatigue and this will be the focus here. When repeatedly loaded sub maximally, bone will develop microcracks (cracking on the microscale), which impair the normal mechanical properties of the bone as a whole. Increased cracking decreases the elastic modulus of bone, exacerbating the effect of further loading by allowing increased deformation, ultimately leading to further cracking. In a simple model the bone will fail if the accumulation rate of damage from fatigue outpaces the remodelling repair rate. However because the remodelling process removes bone tissue before it is replaced, if too much remodelling is activated in a particular section of bone then the removal of tissue may result in failure. From the perspective of stress fracture development, the fatigue life of bone is inversely related to the magnitude of any repeated loads (Edwards et al., 2009) meaning that as the magnitude of loading increases the number cycles needed to cause failure will decrease.

In general the laminate and fibrous nature of bone is advantageous in terms of microcracking. As a crack propagates it moves through many different materials and the differing properties allow it to be deflected along a direction that is less problematic, for example along the lines of lamellar tissue, which prevents transverse cracking. This increases the amount of cracks and therefore how much fatigue damage a bone can endure before failure when compared to a non-laminate material (Martin, 1992, Najafi et al., 2007). When considering the metatarsals specifically, work has been done to compare the strains at sites commonly associated with stress fracture such as the second metatarsal and sites not associated with this injury, such as the fifth metatarsal (Donahue et al., 2000). Findings from this study indicate that whilst sites commonly injured

experience greater strains, the density of cracking between the two sites was not different. This indicates that increased strain alone will not necessarily lead to increased cracking in the bone, and suggests an additional process, such as remodelling must also occur in order to lead to injury.

2.1.4 The Role of Remodelling in Stress Fracture

Studies have shown that *ex-vivo*, bone can withstand between 1000 and 1000000 cycles of loading at a strain level of between 5000 με and 10000 με (Burr, 1997, Carter et al., 1981). However physiological loading levels are far lower than this typically around 2500 με in compression (Schaffler and Jepsen, 2000, Schaffler et al., 1989). It has also been shown that testing cortical bone within these physiological ranges did not result in bone failure even after 10 million cycles (Schaffler and Jepsen, 2000) although a loss of up to 10% of stiffness was observed. This reduced stiffness is indicative of mechanical fatigue, with the majority of this occurring in the first 2 million cycles after which a period of stability was observed. This supports the theory of failure prevention by material design discussed above. The initial loss of stiffness corresponds to the creation of new cracks, which are then propagated extremely slowly due to the design and structure of the material. This further suggests an interim process may be responsible for the formation of stress fractures.

From an applied perspective, there is additional evidence that a remodelling process produces a long term protective effect from data in military recruits engaged in differing activities prior to commencement of training. Those who engaged in ball sports had a lower incidence of stress fracture than those who participated solely in long distance running, whilst those who only swam had the highest incidence (Milgrom et al., 2000). It was suggested this is due to the higher strains experienced in ball sports eliciting a large remodelling response and

strengthening the bones over time, which has a protective effect when undertaken at an appropriate time before military training.

A sudden increase in repetitive activity can cause damage exceeding the tissue's ability to repair itself and may lead to fatigue failure (Schaffler and Jepsen, 2000). Starting an intense programme of physical training such as military training will induce a large remodelling response (Popovich et al., 2000) potentially weakening the bone and subjecting it to increased risk of fracture. However, studies have shown that a remodelling response is not always needed to produce fatigue failure of bone, particularly in the metatarsals where metatarsal strain was found to be 5315 με when barefoot jogging when tested with a bone staple strain gauge (Milgrom et al., 2002). *Ex-vivo* studies suggest this would be enough to cause failure within a physiologically reasonable number of cycles (1000 – 100000 cycles) (Milgrom et al., 2002). Further to this, an intervention programme designed specifically to reduce stress fracture in military recruits by incorporating a rest week in the physical training regimen found no difference in incidence between intervention and control groups (Popovich et al., 2000). However, the remodelling process generally takes far longer than one week so it may be that a single week of rest was insufficient. A 12-month study in track and field athletes found no difference in bone turnover between those that developed stress fractures and those that did not (Bennell et al., 1998) suggesting that the activation of remodelling alone may not lead to stress fracture. Supporting theory suggesting a combination of factors, including both high strains and remodelling activation leads to stress fracture development.

In conclusion, current literature suggests stress fracture is likely caused by a sudden increase in loading factors whether by increasing the training load of an already established movement or by loading in an unusual or physiologically

poorly adapted manner. Remodelling can play a part in this as it will be highly activated under these conditions due to a sudden accumulation of microdamage, and thus will cause the bone to further become weakened for a period of time during which loading is still ongoing. In this case failure to complete remodelling prior to repeating the loading conditions that led to its activation can lead to an injury such as stress fracture. In addition it is possible that in some areas of bone, such as the metatarsals, the loads experienced during running and jumping are great enough to cause fatigue failure without a remodelling response. However, due to the mechanostat response, running is likely to be beneficial to bone health in the long term as long as remodelling recovery time is sufficient and loads are not too excessive.

2.2 The Human Foot – Anatomy and Function

The human foot is the region of the body distal to the tibia and fibula, it is the interface between the body and the ground and as such it performs many functions linked to locomotion and balance. Due to the number of mechanical functions it performs it is complex with many different bones and active and passive soft tissues. This section will briefly lay out the function and anatomy of the foot, with a focus on the metatarsal and how it behaves during various activities.

2.2.1 The Purpose of the Foot

The main function of the entire lower limb is to support the weight of the body through the various activities humans engage in, ranging from quiet standing through propulsive locomotion and the impact of landing from running or jumping. A second major function of the lower limb is to move the body through these activities, providing the propulsive power for the wide range of activities suggested above (Drake et al., 2015). As the interface with the ground, the foot

is both the last link in the kinematic chain for providing forces against the ground for locomotion and the first link in the chain for the management of impact and landing and as such transmits very large forces. During running the impact peak in the vertical ground reaction force is typically around 2.2 BW (Cavanagh and Lafortune, 1980) and the active peak of forces provided by the body for push off is around 2.8 BW (Cavanagh and Lafortune, 1980). During more vigorous activities such as jumping this can be much higher, of the order of 14 BW (Allen et al., 2012). In order to provide efficient locomotion, the foot provides energy storage and release, with the structure of the foot compressing under the load of landing and then releasing during propulsion (Ker et al., 1987). This is provided by the arch-like structures of the foot where the bones are not laid out flat to the ground and support is provided by the soft tissues (Drake et al., 2015). These functions require a complex anatomy such that the foot can withstand the very large loads it is subjected to, but still effectively store, release and transfer energy.

2.2.2 Bones of the Foot

The foot consists of 29 bones, laid out broadly in four sections, the most distal aspect of the foot is made up the phalanges. Connecting the phalanges to the midfoot there are five metatarsal bones, proximal to these there are the tarsal bones, comprising of the cuneiforms, navicular and cuboid bones, and lastly the large talus and calcaneus bones which support the heel and articulate the ankle joint (Figure 4). The metatarsal bones join with the tarsal bones at the tarsometatarsal joints, which allow only limited sliding to occur (Drake et al., 2015), the second metatarsal articulates with all three cuneiform bones which makes its tarsometatarsal joint particularly restrictive. In addition the five metatarsal bones are joined at their distal ends by the deep transverse metatarsal ligaments which limits their ability to move independently (Drake et al., 2015).

There are two arches in the foot, the primary arch is the longitudinal arch, which is formed between the calcaneus and the heads of the metatarsals (Figure 5), there is also a transverse arch under the metatarsals, which is supported by the transverse metatarsal ligaments. The arches, combined with the action of the passive and active soft tissues of the foot allow the foot to both store energy elastically in the plantar soft tissues but also to mitigate large impacts by allowing the foot to deform upon landing (Kelly et al., 2018a, Kelly et al., 2018b).

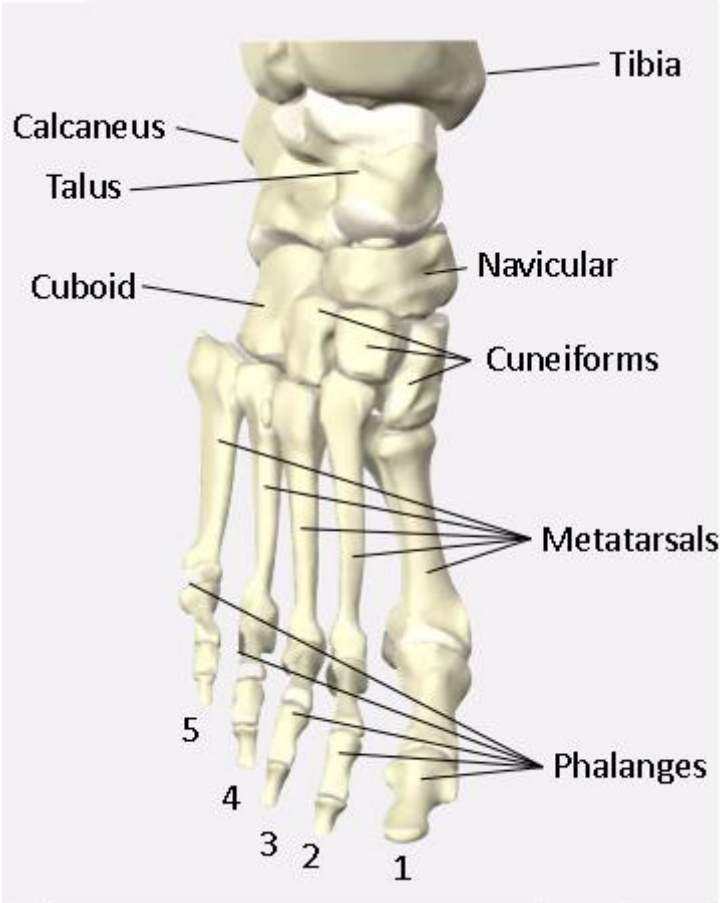

Figure 4: The bones of the human foot

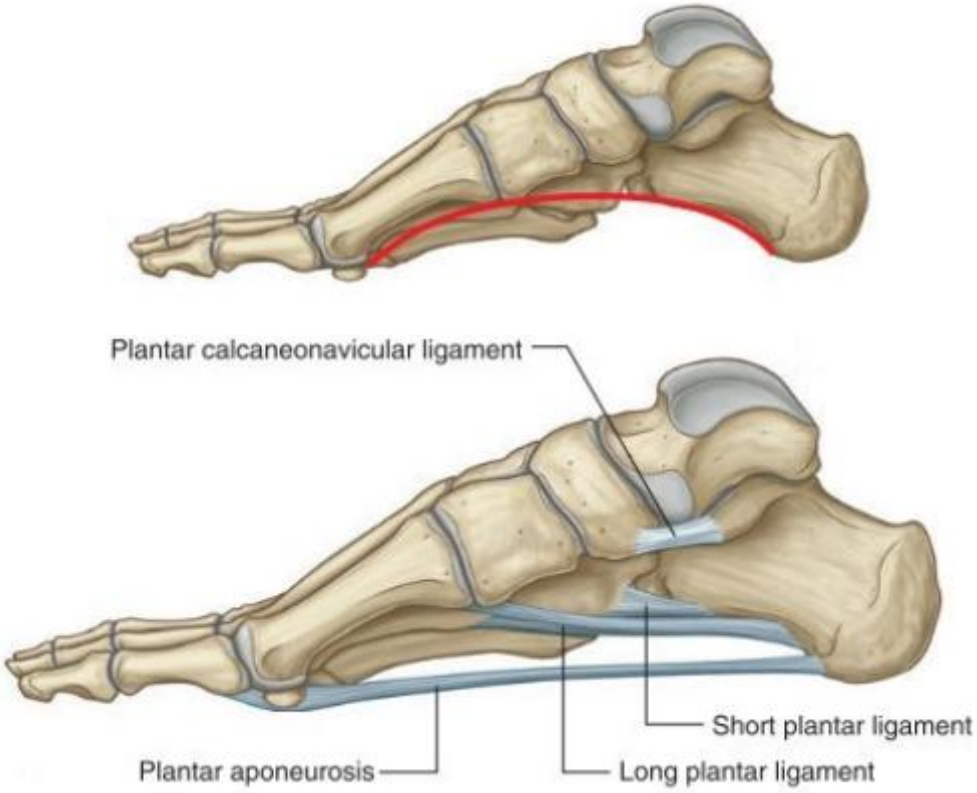

Figure 5: Sagittal aspect of the foot from the medial direction. Top: the arch of the foot. Bottom: the supporting soft tissues for the arch (Drake et al., 2015)

2.2.3 Soft Tissues of the Foot

The foot contains a number of different types of soft tissue relevant to locomotion and impact management, including ligaments holding the bones in position, intrinsic muscles and a specialized fascia known as the plantar aponeurosis. Of interest to the second metatarsal are the two plantar ligaments (short and long) shown in Figure 5 which act between the calcaneus and the metatarsal and contribute towards holding the arch in position. The plantar aponeurosis, also shown in Figure 5, is a thickened fascia that is connected to the base of the calcaneus and runs down the sole of the foot, where it diverges into individual elements and passes under the metatarsophalangeal joints to merge with the ligaments, bones and skin of the phalanges (Drake et al., 2015). Its purpose is not only to support the functioning of the arch of the foot, but also to act as a protective layer on the sole of the foot (Drake et al., 2015). Muscle tendons also

act to support the arch of the foot, in particular the tendons of the flexor digitorum brevis and flexor digitorum longus muscles attach to the plantar aspect of the phalanges and act to cause flexion in the metatarsophalangeal joints. The flexor digitorum brevis muscle is intrinsic to the foot, attaching to the base of the calcaneus and lying directly superior to the plantar aponeurosis whilst the flexor digitorum longus has its origin on the tibia and is responsible for plantarflexion of the foot as well as flexion of the phalanges (Drake et al., 2015).

2.2.4 Injury to the Foot Bones

During normal locomotion such as walking and running, forces are transferred between the floor and the body via the foot, and the arch of the foot depresses both to mitigate the force and to store energy (Kelly et al., 2018a). Due to the nature of the soft tissues of the foot, much of the arch deformation can be accounted for by the stretching of the plantar soft tissues discussed above (Li et al., 2017). However, due to the limited movement available at the tarsometatarsal joints, the long thin bones of the metatarsals will deform by bending when the force is sufficient. As discussed in section 2.2.3 repeated loading of this nature can lead to failure by material fatigue, especially if the loading is repeated during the remodelling process of the bone. Another route to injury is if the protective soft tissues are impaired from taking the strain of loading from locomotion, for example due to a deformity of the foot, injury to the soft tissues, or through training choices, such as footwear or technique.

2.3 Risk Factors and Aetiology for Metatarsal Stress Fracture

Having discussed the biological processes by which a stress fracture may occur, this section will discuss variables related to running that have been shown to be linked to stress fracture of the second metatarsal through prospective or retrospective studies. Also included are variables that may affect internal loading

of the metatarsal bones and therefore increase risk for injury either directly or through initiating a remodelling response. In general, the factors directly relating to second metatarsal stress fracture in distance runners are not well understood, although more detailed understanding would be beneficial for the reasons outlined in chapter 1. This review will cover factors that have been investigated in relation to stress fractures in varied body locations, factors that have been linked to more general lower limb injuries in runners, and factors linked to stress fracture of the metatarsals and other bones in different populations, such as military recruits. Whether these factors may have a bearing on the risk of second metatarsal stress fracture in distance runners specifically will be considered.

2.3.1 Factors Linked to General Lower Limb Overuse Injury in Runners

Several recent systematic reviews have investigated the association between overuse injuries and various training, environmental and individual variables. A review of running injury studies noted that whilst many factors contribute towards injury development, there was strong evidence only that reduction of weekly mileage was helpful in prevention of injury (Fields et al., 2010). This study included all injuries requiring at least one day of missed training and identified those running more than 40 miles.week^{-1} at particular risk of an injury. From the perspective of stress fracture formation, a larger number of loading cycles will occur as running distance increases, leading to increased opportunity for cracking to occur on the bone. In addition, greater mileage is likely to lead to greater fatigue, particularly in those who are purposefully increasing their mileage to induce training adaptations. Fatigue can influence the activity of muscles, which have been shown to provide resistance to bone bending and shear forces (Scott and Winter, 1990). Fields et al. (2010) also noted that a sudden change in training variables or an erratic schedule is linked to injury, finding that one third

of runners studied had changed their schedule or shoes immediately prior to injury. As noted in section 2.1.4 unaccustomed loading is a primary driver in activating a remodelling response, which is one of the mechanisms that may lead to stress fracture. Previous injury has also been shown to increase the risk of subsequent injury (van Gent et al., 2007, Fields et al., 2010). Although the studies reviewed do not suggest a mechanism for this, previous injury was defined in most cases as having occurred in the preceding 12 months, suggesting that returning to training or increasing training intensity could be responsible.

2.3.2 Factors Related to Training

We have seen from the review of the mechanisms by which stress fractures occur in section 2.1.4 that either a remodelling response must be initiated whilst loading continues or stress in the metatarsal must be high enough in magnitude over a large number of cycles for a stress fracture to form. Therefore it is assumed that in the case of sufficient rest between activities of high loading magnitudes, or in cases where the stresses on the bone are low enough that microcracks do not form, a stress fracture will not occur. Factors considered in this section are those that allow the loading magnitude or frequency to be modified in various ways.

It has already been discussed that unaccustomed loading of bone is highly likely to result in microcracking and therefore lead to the formation of stress fracture (section 2.1.4). Loading on the bone itself can be greatly affected by the surrounding muscles, be it the timing of their activation or the amount of force they produce. Muscle activation can influence the bending experienced by the bone, whilst well timed activation can reduce it. In the tibia, the plantarflexor muscles have been shown to contribute to reduced bone bending and bone shear (Scott and Winter, 1990), and simple models of the forefoot which include the forces from the flexor digitorum brevis and flexor digitorum longus show that

these muscle forces act to reduce the bending in the metatarsal from the ground reaction forces under the forefoot (Stokes et al., 1979). Factors that could affect the timing or magnitudes of these muscle forces include the intrinsic muscle strength and the ability of the muscle to withstand fatigue. If the muscular forces are reduced due to fatigue or low muscle strength then this model suggests that the bending and shear forces experienced by the metatarsal will increase. This is supported by the work of Arndt et al. (2002), (2003) who used bone staples to directly measure bone strain in the second metatarsal. Fatigue was induced via 3 hours of treadmill walking whilst wearing a backpack containing 45% bodyweight (Arndt et al., 2003) or through walking up to one hour (Arndt et al., 2002). Findings from both studies indicated that fatigue increases compressive and tensile forces measured on the shaft of the metatarsal, regardless of load or footwear. Plantar pressure distribution was also shown to change with fatigue with participants experiencing greater pressure mostly under the 1st metatarsal and hallux pre-fatigue but loading metatarsals 2 – 5 more post-fatigue. The 1st metatarsal is well adapted to greater loads, being shorter and thicker than other metatarsals. As load is distributed away from it towards metatarsals 2 – 5 post fatigue the risk of injury in the thinner metatarsals will increase. In addition, later peak plantar pressures under the metatarsals were associated with 3rd metatarsal stress fracture in a prospective study (Rice, 2015). It was theorised that this later peak pressure was the result of reduced plantarflexor muscle forces contributing to forward locomotion. However it should be noted that the third, not second, metatarsal was investigated here and that the population were military recruits, and that whilst measurements were carried out during running, the recruits were required to complete other tasks which could contribute to bone loading in the forefoot as part of their training, such as loaded carriage, and therefore the data

from this study are not definitive. In addition this prospective study did not find any differences between calf girth and bimalleolar breadth in recruits who sustained a stress fracture of the third metatarsal and those that did not, suggesting similar muscle sizes, and therefore forces, between groups.

The stiffness and hardness of footwear and running surfaces have also been implicated in injury risk. Minimalist shoe types are popular amongst recreational runners (Firminger and Edwards, 2016) and are designed to more closely mimic the experience of running barefoot than traditional shoes, whilst providing some protection from sharp objects. They are characterised by minimal cushioning, high flexibility of the sole and a flat profile. In particular they have been linked to increased metatarsal stress fracture (Cauthon et al., 2013, Salzler et al., 2012), however, it is not clear from the literature whether the increase in injury is from the altered biomechanics, which tend to move the centre of pressure at landing in a more anterior direction (Firminger and Edwards, 2016), the lack of cushioning, which may change impact forces and loading rates during stance, or from some contribution of the two. It is strongly indicated from the literature in section 2.1 that altered biomechanics will adjust bone loading and that an acclimatisation period is recommended when making major changes to training parameters. In the two papers cited above, the longest transition period in the runners who sustained a second metatarsal stress fracture was only two months, and four of the nine stress fracture patients across the studies reported having no transition period at all. Therefore it is unclear whether the shoes would cause the same injury levels in runners who transitioned over a period of time closer to the time taken to complete remodelling (around four to six months (section 2.1)). Minimalist footwear has been seen to increase the loading at the metatarsophalangeal joints (Firminger and Edwards, 2016), which is likely to

increase the load on the metatarsal bones. However, it is not clear whether this increase is due to the change in cushioning of the shoe, or the change in kinematics. There is evidence of an interaction between the choice of footwear and kinematics, as shown by Rice et al. (2016), who compared habitual forefoot runners to rearfoot runners in both cushioned and minimalist footwear finding that both the magnitude and loading rates of the ground reaction force were lowest in minimalist shoes when running with a forefoot strike, and that magnitudes and loading rates were highest in forefoot runners in a cushioned shoe. This suggests that footwear can influence loading on the structures of the foot. However, recent literature has suggested that external measures of force do not correlate well to internal loading in the tibia (Matijevich et al., 2019), and this may also be the case in the metatarsals.

An additional consideration which may affect the risk of stress fracture is sudden changes in training variables, such as increased running mileage or training frequency. Studies suggest that frequently changing shoes may be a risk factor for lower limb injury in general, and that for men, restarting running after a break may increase injury risk (van der Worp et al., 2015). Several studies have investigated the physical preparedness of military recruits with regard to their training activities prior to basic training, finding that a history of physical activity was protective against stress fracture in general, with a longer history offering more protection (Lappe et al., 2001). Another study found that engaging in strength training for the lower limbs for longer than seven months prior to engaging with basic training lowered the risk of stress fracture (Rauh et al., 2006). Although these two studies were both conducted on female military recruits rather than a mixed cohort of runners, it does support the theory that by engaging in activities that load bone, the bone can adapt to higher loads and therefore the

risk of stress fracture in other activities can be reduced. It can be inferred from this that habituation to higher loads or training intensities is an effective way to reduce the risk of stress fracture.

2.3.3 Individual Factors

In this section factors that cannot be easily adjusted by the athlete will be discussed. Studies have been conducted to assess whether aspects of foot geometry can be responsible for increased metatarsal stress fracture risk in runners. Drez et al. (1980) conducted a study of relative bone lengths and suggested that changing the ratio of lengths of the first and second metatarsal does not increase risk of stress fracture in the metatarsals. However a recent modelling study found that bony geometry was the largest determinant factor on the stress seen in the third metatarsal (Nunns et al., 2017). However other factors may mitigate the large loads estimated in areas of high risk geometry. For example the model did not account for surrounding soft tissues, or muscle activation, which can act to reduce bending on the metatarsal during stance.

Foot arch height has been identified as an indicator of injury risk in the lower limb, with a high arch associated with fifth metatarsal stress fracture, however the same study also detected more stress fractures of the second and third metatarsals in low arched participants (Williams Iii et al., 2001). An earlier study associated low arch height with an increased risk of metatarsal stress fracture (Simkin et al., 1989) in military recruits. This suggests that an arch height that is too high or too low could be a cause of increased stress fracture risk through differing mechanisms. For example, a high arch is associated with high plantar pressures under the metatarsal heads, which has in turn been suggested as a mechanism of stress fracture formation (Nagel et al., 2008), which is supported by the findings of Dixon et al. (2019) who identified a link between high arch and

second metatarsal stress fractures in a prospective study. Finite element models of the foot also confirm that those with high arches experience greater strain in the metatarsals (Sun et al., 2012). Conversely in a low arched foot, the metatarsals are more parallel with the ground and therefore may be in a position to experience greater bending from ground reaction forces.

The quality of bony material as measured by bone mineral density has been shown to be a determinant of bone strength (Martin et al., 2015), and has also been shown to be lower in those that develop stress fractures (Välimäki et al., 2005). Therefore lower bone mineral density can be considered a risk factor for stress fractures. There are many factors that can affect the mineral density of bones including age, gender, smoking and alcohol consumption among others, specifically: older age, female gender, and smoking is associated with lower bone mineral density (Krall and Dawson-Hughes, 1993), however, these variables are beyond the scope of this thesis.

2.3.4 Kinetic and Kinematic Variables

Research into the association between biomechanical variables and the risk of stress fracture is limited. A prospective study indicates that higher foot abduction during running is a predictor of second metatarsal stress fracture (Dixon et al., 2019), and a retrospective study (Dixon et al., 2006) found that those previously injured displayed an earlier peak eversion during stance, suggesting more time spent in the propulsive phase of stance when the metatarsal heads are loaded. This longer loading period for the metatarsals may represent an increased injury risk for these individuals, but any internal loading mechanisms suggested by studies of this nature are speculative and quantification of the internal mechanics of the metatarsal is needed for fuller understanding.

Foot strike modality is a method of describing the manner in which a runner interacts with the ground at the foot-ground interface. In general runners can be categorised based on whether they contact first with their heel (rearfoot strike, RFS) or not (non-rearfoot strike, NRF) (Nunns et al., 2013), with each type displaying distinct kinematic and ground reaction force time histories. Rearfoot striking is associated with an early impact peak in the vertical ground reaction force time history (Figure 6) and high vertical force loading rates (Lieberman et al., 2010). In non-rearfoot groups the impact peak is less distinct in the time domain and the loading rates are in general lower than for a rearfoot runner (Ahn et al., 2014). There is debate in the literature regarding the benefits of a particular modality over others, with some literature suggesting benefits in performance (Ahn et al., 2014) and a reduction in injury (Lieberman et al., 2010, Cheung and Davis, 2011, Diebal et al., 2012) for non-rearfoot modalities, and others disputing these (Hamill and Gruber, 2017). Generally the injuries claimed to be reduced by a non-rearfoot strike occur more proximally than the metatarsals, for example at the tibia (Lieberman et al., 2010). A study of 1065 military recruits running barefoot with their habitual running technique (Nunns et al., 2013) found both peak pressure and impulse to be significantly higher under the second metatarsal in those who ran whilst landing on their forefoot compared with those who landed on their heel or midfoot. This suggests that a non-rear foot strike may cause greater loading in the metatarsals, due to the higher anterior pressures underneath the metatarsal heads. This theory is further supported by recent finite element models comparing forefoot and rearfoot loading types in single participants (Li et al., 2017, Morales-Orcajo et al., 2018) where it was found that

an overall higher stress level was found in the metatarsals in the forefoot loading condition.

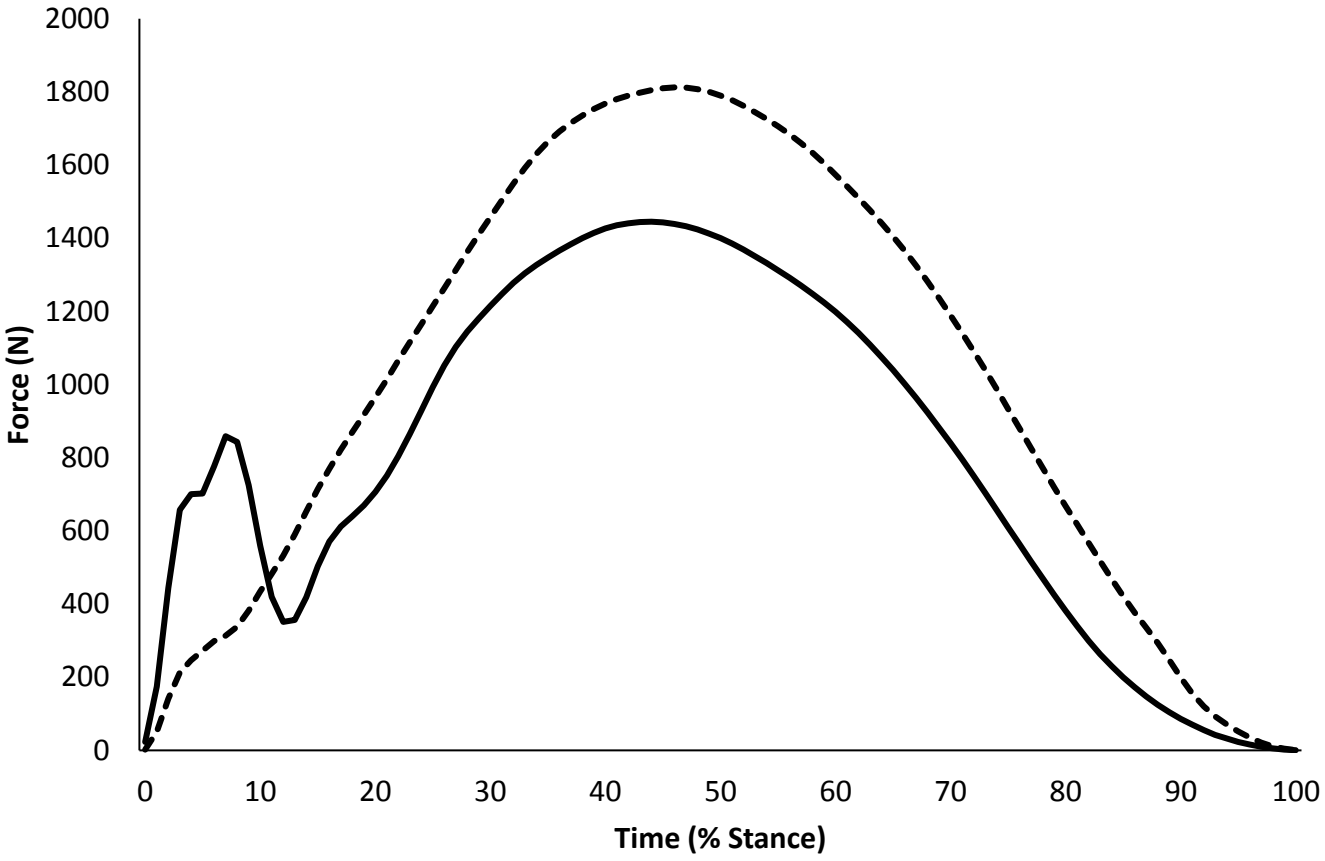

Figure 6: Typical vertical ground reaction force traces for a forefoot runner (dashed line) and rearfoot runner (dotted line).

2.4 Approaches to Estimating Loading in Biomechanics

Based on the previous section, it is clear that in order to understand stress fracture risk, measurement of the loading experienced by the bone is important. Comparing the internal loading experienced during different conditions allows us to infer which of the conditions is likely to produce a remodelling response in the bone for example. Considered here are the current methods and past methods used in the field of biomechanics to measure or estimate internal forces with both the various advantages and limitations of each method discussed and possible sources of error.

2.4.1 Direct Measurement using Invasive Methods or Cadavers

The gold-standard method of investigating the forces in a system is usually to attempt direct measurement. In the case of bone strain this is done through the use of a staple strain gauge or similar. This method requires surgical attachment at two sites along a bone and the participant must complete weight-bearing movement trials directly after this surgery if the influence of human locomotion on bone strain is to be investigated. Previously this method has been used to investigate stress fracture risk in the metatarsals (Arndt et al., 2002, Arndt et al., 2003, Milgrom et al., 2002) and the measurements showed a reasonable match with previous 2D beam theory models used to estimate internal forces in these bones such as the models of Stokes or Gross and Bunch (Stokes et al., 1979, Gross and Bunch, 1989). The surgical procedures used in these studies allows for a high validity of assessment, however the limitations of this method are significant. Namely the nature of having a surgical device attached whilst performing tasks such as running may change biomechanical variables and confound results, it is difficult and in some cases unethical to recruit participants from target populations for an invasive procedure, contact time with these participants will be limited due to the nature of the devices and repeating measures is unlikely to be practical as it would require a second surgery. Given the level of agreement with various simple models it is often not justifiable to perform this kind of invasive procedure. In the previous studies, due to low participant numbers no statistics were able to be performed, thus weakening the value of the results.

Another direct measurement method is to use cadaveric specimens in all or part of investigation. Manter (1946) performed a study on the loading in the metatarsals using cadaveric feet whereby the feet were placed in a jig and quiet

standing was simulated through loading the talus. The ratio of pressures was calculated using the size of impression each bone made in clay. This method has obvious limitations in that the loading may not be true to life and that measurement of the impressions in clay are prone to error. Another more complex study used a rig to animate a cadaveric shank and foot (Sharkey and Hamel, 1998), applying realistic muscle forces via actuators and verifying results via ground reaction forces. The forces transmitted via the tibia were measured directly. However the validity of using cadaveric specimens is questionable as the feet may have come from the elderly or from those suffering various pathologies, rather than the healthy populations this thesis is investigating. Designing and building such apparatus is also costly and time consuming. Technological advancements have allowed us to assess pressure and forces between the participant and environment *in-vivo* quickly and easily, rendering some forms of cadaveric study obsolete.

2.4.2 Estimation Based on Directly Measured External Variables

Measurement of kinetic variables at the foot ground interface has become exceedingly common in biomechanical studies, generally via the use of force plates and plantar pressure sensing systems.

Previous work has used external force data to understand injuries. For example in a retrospective study Dixon et al. (2006) found that peak horizontal forces were applied more laterally during the braking phase of stance and were lower during the propulsive phase of stance in those who had suffered a stress fracture. Studies of this nature are very useful and informative, but require access to sufficient injured and non-injured participants and it is not possible to infer whether the injury was the cause or was caused by the differences seen. Another option is to use a more powerful prospective study, where cause and effect for

injury can be suggested. However large numbers of participants are required before enough injuries occur to reach statistical power. Dixon et al. (2019) performed such a study, where later peak pressures were found to increase the risk of third metatarsal stress fracture. In this case 1065 Royal Marine recruits were followed and only seven second metatarsal stress fractures were observed. It would be very useful therefore to directly estimate internal load from external forces. Many studies infer that a direct increase in externally measured forces, such as higher peak plantar pressures under the metatarsal heads in toe runners, would lead to higher forces experienced by the whole metatarsal (Nunns et al., 2013). However, more recent research has suggested that external force does not necessarily correlate to internal loads (Matijevich et al., 2019) where 76 out of 80 computed correlation coefficients between ground reaction force metrics and tibial loading metrics indicated that higher ground reaction force metrics did not correlate strongly with higher tibial forces. It has not been determined whether this is also the case in other parts of the body, such as the metatarsals. When considering just externally measured forces as a measure of bone loading, any inference to internal loading must be evaluated carefully, using appropriate musculoskeletal modelling to calculate joint contact forces, rather than the net forces acting at a joint, as net forces calculated using inverse dynamics methods may underestimate the actual forces experienced by bones (Vigotsky et al., 2019).

2.4.3 Estimation using Mathematical Models and Simulation

Due to the limitations and difficulties of using direct measurement or inferring internal loads from external measures listed above, often a mathematical model is used to represent the human body or part of it. These models use inputs that are measured from experimental procedure, such as ground reaction forces

measured via force plates and will output an estimation of variables that are difficult to measure, such as the loading experienced internally by a bone. This thesis develops and uses both a 2D and a 3D model, ranging from simple geometry to fully 3D continuum mechanics, to investigate metatarsal stresses during running. Thus an in depth review of approaches to modelling along with their benefits and limitations is warranted.

Computer simulation is a powerful tool for investigation as it allows estimations of variables that would otherwise need to be measured using invasive methods or that are difficult to measure experimentally (Halloran et al., 2012). In addition a simulation can be run many times without fatigue and will perform identically every time. This allows investigation where only one variable is allowed to change, thereby quantifying the effect of that change alone. Conversely, with *in-vivo* studies a participant can perform only so many trials before fatigue influences their gait and they may not perform in the same manner each time, in particular when asked to change one variable. For example, when changing running velocity or footwear type, a human participant will unconsciously adapt other parts of their technique and therefore the effect of a single change cannot be quantified (Yeadon et al., 1990).

In order to assess its usefulness, any model must be evaluated. Without adequate evaluation the results and predictions given by the model may not be relevant to the system modelled (Yeadon and King, 2002). In order to be considered valid, a model must be tested for internal consistency and to ensure the laws of physics are upheld, for example conservation of momentum or energy are not violated. It should also be compared to some real life measurable performances and a good match must be established. Upon evaluation, it may be found that the model is limited in some way that allows it to answer only certain

research questions. It is also useful to evaluate the sensitivity of models to perturbations in input values or the determined model parameters.

As this thesis relies heavily on various modelling techniques, it is useful to review both previously used modelling techniques and historical findings of relevance to internal foot loading. The following subchapter explores these in detail.

2.5 Models of the Foot in the Literature

In the past, models have been used to investigate sporting performance (Alexander, 1990, Allen et al., 2010, Hiley and Yeadon, 2005), injury causes (Mills et al., 2008) and to inform clinical procedures and interventions (Chen et al., 2015a, Erdemir et al., 2005, Hsu et al., 2008, Lemmon et al., 1997b, Isvilanonda et al., 2012, Wu, 2007). For each problem investigated a specific model must be designed, with thought given to the complexity of the model. A model that is too simple will give outputs that diverge from real life (Mills et al., 2008); conversely an overly complex model will be computationally expensive and may obscure intended results. Computational expense is usually measured in the time taken for a model to run on a given computer system and generally increases with the complexity of the model. Some more complex models can take of the order of weeks to run on a high performance computing platform. A model should be made complex enough to give accurate outputs as verified by the evaluation methods chosen, but care should be taken to reduce any complexity or calculations that provide only limited contributions to the accuracy of the results. Often a model could be made more accurate by adding complexity, however a balance is needed to ensure a small gain in accuracy does not cause a large increase in computing time.

2.5.1 Beam Theory Models

For many studies of bones and their loading, the bones are considered to be beams, that is, their diameter is small compared to their length. From an engineering perspective, bending occurs in a beam if a transverse load is applied to it, or an axial load that is offset from the longitudinal axis is applied. Bending refers to the deflection of a beam due to this force, and results in stresses distributed along the beam. For simple estimations of these stresses, the whole system can be considered to be in quasi static equilibrium, where the deflections of the beam and therefore the stresses do not vary with time. A cantilever model is often used for the bones of the foot. In this case, the beam is assumed to be fixed at one end, and the forces are applied at some distance from the fixed point. A simple diagram of this is shown in Figure 7. This leads to deflections where-by the side opposite that which the force is applied to is shortened, experiencing compressive stresses and the side the force is applied is lengthened, experiencing tensile stresses. In addition to these stresses, some shear stresses will be created. The tensile and compressive stresses from a purely perpendicular force will be equal and opposite in direction, but if forces acting along the length of the beam are introduced, then this is added linearly to the bending stresses.

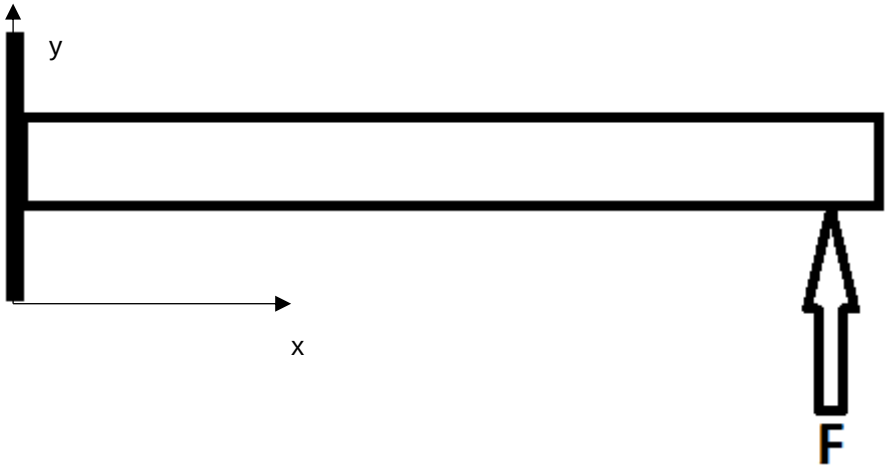

Figure 7: A cantilever beam, fixed at the proximal side and with force F acting vertically upwards

The nature of the geometry of the system means that greatest deformation occurs at the edges of the beam, and therefore the stresses are maximal here. There is also an internal line that can be drawn down the centre of the beam where no length change occurs with bending, and therefore there is no stress. This line is called the neutral axis.

In order to calculate the bending stress in a beam, the following general equation is used (Equation 1).

$$\sigma_x = \frac{M_z y}{I_z}$$

Equation 1: Equation for calculating stress in a simple beam, σ_x is the bending stress, M_z is the bending moment about the neutral axis z, y is the perpendicular distance to the neutral axis and I_z is the second moment of area about the neutral axis

In the case of bones, often the cross section is not symmetrical, in which case a more complicated equation is necessary (Equation 2)

$$\sigma_x(\mathrm{y},\mathrm{z}) = \frac{M_z I_y - M_y I_{yz}}{I_y I_z - I_{yz}^2} y + \frac{M_z I_z - M_z I_{yz}}{I_y I_z - I_{yz}^2} z$$

Equation 2: Equation for calculating stresses in an asymmetric beam, y and z are coordinates of the location of the stress on the cross section, M_z and M_y are the bending moments about the centroid, I_y and I_z are the second moments of inertia about the y and z axes, I_{yz} is the product moment of area

From an applied perspective, the greatest stress is usually of most interest. This lies at the periphery and can be assumed to lie at zero on the neutral z axis, leading to the reduction of the second term of the equation to zero. In addition, that shafts of long bones are often close to symmetrical, making the simpler equation suitable. Beam theory models using modern computation techniques are generally computationally inexpensive, although, they can be calculated by hand or with limited calculation aids, as was done in older models such as Stokes et al. (1979) which is very time consuming. These models tend to consider forces and kinematics in two dimensions and whilst they may incorporate some participant-specific aspects such as bone cross-sections, many parts are highly simplified. For example, bones are normally considered to be fully rigid rods. Any

joints between body segments tend to be considered as frictionless and forces are generally described as acting at points rather than being distributed over a surface. These simplifications have the advantage of allowing quasi-static equilibrium to be used to calculate any unknown forces in the system. A disadvantage of this level of simplification is the difficulty in mathematically describing the effects of easily deformed soft tissues such as the plantar fat pad, leading to an assumption that externally measured forces are applied directly to rigid internal components such as bones, which may lead to overestimation of internal forces.

An early beam theory model estimating the forces acting under the metatarsal heads and at their bases is that of Stokes et al. (1979). By modelling each ray of the foot in 2D and simplifying the geometry of individual metatarsals by considering the heads as the radii of two circles, forces were estimated during normal walking for each metatarsal. Subsequent research has built upon this simple model, adapting it to use more complex geometry involving all of the joints of the toes and estimating joint contact forces and tendon loading in the first and second rays (Jacob, 2001).

The model was adapted to consider the metatarsal as a hollow elliptical cylinder and investigate stress during running (Gross and Bunch, 1989). All values pertaining to the geometry of the metatarsal were gathered from previous literature thus were not specific to each participant. Results showed that the second metatarsal bore the greatest bending strain (6662 με) and shear forces (203 N), correlating with evidence that it is one of the more common sites for stress fracture. However when compared with experimental data from bone strain gauge studies, the values reported were high. Milgrom et al. (2002) reported strains of 5315 με and 1891 με during barefoot jogging, assessed using strain

gauges in two participants. This is lower than the value of Gross and Bunch, especially when considering that the modelled strain included only the value due to bending, and did not consider the additional strain that would be experienced due to longitudinal compression of the metatarsal bone. It is not clear from this study whether the apparent overestimation of strain values is due to the aforementioned limitations of considering bones as rigid rods with external forces applied directly, or whether other simplifications of the study such as the non-participant-specific geometry may account for it.

As the human body is made of irregularly shaped solids rather than the simplified perfect geometry used in the above models, one way to increase the accuracy of a model is to increase the geometrical complexity and make it more similar to the real structure of the tissues studied. This has become more feasible with the increased access to non-invasive scanning methods such as magnetic resonance imaging and computed tomography. Work by Nunns et al. (2017) is a recent example of a study of stresses in the third metatarsal bone that has been carried out using a geometrically accurate model of the bone. They found that individual geometry has a large effect on the internal stresses of the bone. The model relied on a long digitization process whereby each coronal MRI slice was digitised with 96 individual markers, used to create 96 irregular triangles making up the plane of a single slice of the bone (Figure 8). From this, inertial information was reconstructed.

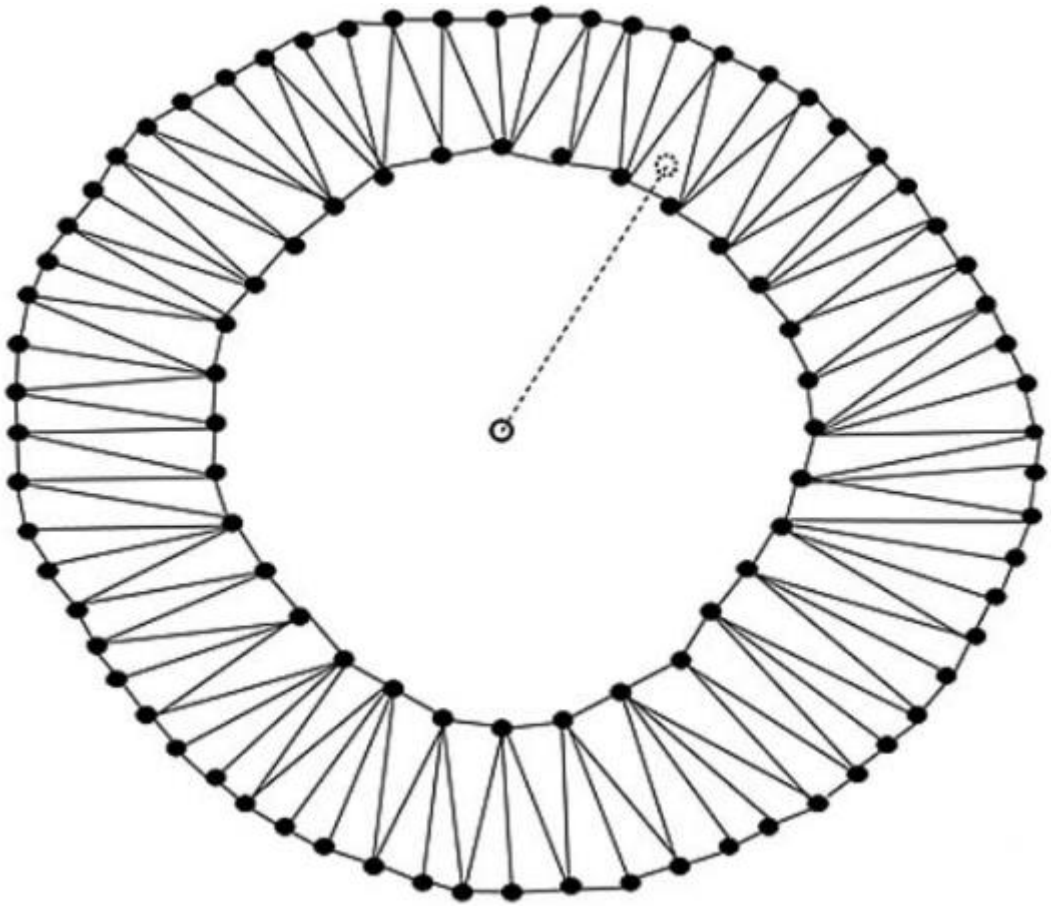

Figure 8: A 2D slice through the metatarsal bone, showing the triangles used to find inertial information of the slice (Nunns et al., 2017).

The bone was modelled as a fixed cantilever similar to that of Stokes et al. (1979) and Gross and Bunch (1989) but without the consideration of the toe and plantar tendons. Tensile and compressive normal stresses were calculated on the uppermost and lowermost surfaces of the bone. Average compressive stress was 114.43 MPa, equivalent to 6731 με (using a Young's modulus of 17 GPa). These values were again far higher than strains recorded in strain gauge studies (Milgrom et al., 2002), although it should be noted that the strain gauge study measured only the second metatarsal, compared to the third here. The results of this study also showed that variation in geometry can lead to mechanically deficient areas of the bone where stress fracture may be likely and that the lowest cross sectional area of bone is not necessarily the point of greatest stress, although mathematically it is always the point of greatest axial stress. This

supports findings by Orava (1980) showing stress fractures occur anywhere along the shaft. Whilst this study provides powerful insight into the effects of geometry on bone stress it is limited by several factors. Firstly, it does not account for any soft tissue interactions such as plantar tendons, the aponeurosis, or the plantar cushioning soft tissue which have been shown to significantly change the distribution of stresses in the foot (Lemmon and Cavanagh, 1997, Gefen, 2002). Additionally, the effect of forces under the toe and its influence on the metatarso-phalangeal joint were not modelled. The geometry, whilst generally accurate, is simplified into slices 5 mm apart. Based on this, in future research a model made up of a continuous mesh to represent the bone geometry may show additional insights into stress distributions. Additionally the effects of plantar tissue forces should be modelled.

2.5.2 The Use of the Finite Element Method for Modelling the Foot

One way to increase the ability of a model to answer a specific question is to make the model more complex. For answers to questions regarding optimal limb movement and sequencing a model consisting of rigid rods and ideal hinges will often suffice (Halloran et al., 2009). However, when impacts or internal loading are investigated, we can see from the studies in section 2.5.1 above that rigid rods may overestimate loading and it would be of benefit to include a method of including soft tissues which deform (Halloran et al., 2009). Soft tissues and their deformation has been included in some rigid rod models, in the form of spring like elements and wobbling masses (Pain and Challis, 2006) and have been shown to be important in reducing system loading. However despite the addition of these elements to beam theory models, they are still limited to rigid rods and point loads. To accurately examine the effect of some technical or environmental change on internal loading of components of the foot, forces acting on a single

bone must be modelled in the most realistic manner possible. This requires an accurate rendering of muscle actions, soft tissue effects and importantly the mechanical properties of the bone itself. One technique by which realistic deformation of bones under the influence of forces applied and distributed via soft tissues can be modelled is the finite element (FE) method.

Finite element analysis is a method for estimating both the deformation of and the resulting stresses in a system. Its benefits are that it can be used to calculate stresses and strains in almost any geometric shape and the level of detail and accuracy calculated can be scaled. It allows for interactions between different parts and accounts for the material properties of differing parts of a model. FE analysis is a widely used method for investigating the loading of the human body and there are many well evaluated models in the literature with varying levels of complexity and with varying approaches to model design that have been specifically designed to look at the lower limb and foot. This section will cover in more detail technical aspects of some relevant examples.

Finite element models of the foot in the literature are designed for a variety of purposes, for example, the investigation of stresses or effects of changes in properties in plantar soft tissues (Natali et al., 2010, Telfer et al., 2016, Thomas et al., 2004, Gefen, 2003b, Chen et al., 2010, Actis et al., 2006, Lemmon and Cavanagh, 1997, Yarnitzky et al., 2006), or plantar aponeurosis (Gu and Li, 2012, Cheung et al., 2004, Cheung et al., 2006, Chen et al., 2015b, Cheng et al., 2008, Gefen, 2003a) to investigate specific foot pathologies (Morales-Orcajo et al., 2015a, Guiotto et al., 2014, Garcia-Gonzalez et al., 2009, Brilakis et al., 2012, Isvilanonda et al., 2012, Wu, 2007, Gefen, 2002), to design footwear or insoles for specific purposes (Spirka et al., 2014, Yu et al., 2008, Chen et al., 2015a, Actis et al., 2008, Hsu et al., 2008), or to investigate whole foot loading under

various circumstances (Qian et al., 2010b, Qian et al., 2010a, Qian et al., 2013, Spyrou and Aravas, 2012, Sun et al., 2012, Cheung et al., 2005, Camacho et al., 2002, Antunes et al., 2008, Akrami et al., 2017, Chen et al., 2001a, Gefen et al., 2000, Hannah et al., 2012, Jacob et al., 1996). However there are relatively few studies designed specifically to investigate metatarsal stresses (Budhabhatti et al., 2007, Garcia-Aznar et al., 2009, Gu et al., 2011) and only a small subset of these look specifically at aspects of running and their effect on metatarsal stresses (Firminger et al., 2017, Li et al., 2017, Morales-Orcajo et al., 2018). In the following section, relevant aspects of the existing model designs above are discussed. Each of these uses differing approaches to both modelling the structure of the foot and to driving the model, based both on the research question and available computational power. These approaches give each model its own merits and disadvantages.

2.5.3 Previous Finite Element Models of the Foot and Their Design Considerations

2.5.3a Defining Model Geometry

Having formulated research questions and hypotheses often the first step in the construction of a finite element model is to consider the geometry to be included in the model. There are several considerations at this stage, such as how many parts the model should have and how complex the geometries of parts can be. Often the complexity of these parts is driven by the available computing power, with the advent of more powerful computing facilities allowing more complex models to be developed. One of the first FE models of the foot in the literature is that of Nakamura et al. (1981). In this model the geometry of the bones of the foot, the soft tissue and the sole of a shoe were considered. However the model was highly simplified in 2 dimensions, with all the bones of the foot considered as

a single homogenous planar layer. Similarly the soft tissue was considered a single 2D layer bonded to the bony tissue at the sole of the foot and the sole of a shoe was then bonded to this. This simplification allowed the whole foot to be represented by just 342 elements, allowing computation with the facilities of the time. Simplifying the bones of the foot by merging them together in order to reduce computational expense is seen in other studies. For example Jacob et al. (1996) investigated the stresses in the arches of the foot. However the individual bones constituting the arches were merged to give a medial and lateral arch in three dimensions. This allowed articulation and whilst reducing the problem to just 1475 elements to represent the bones.

It should be noted that recent FE models of the foot can have upwards of several hundred thousand elements allowing much more complex regions of the foot to be differentiated and modelled with high fidelity. It is useful to bond the layers of bone and soft tissues together as modelled by (Nakamura et al., 1981) as this means the model allows no movement between these tissues, which is assumed to occur in vivo. Although in reality the bond between tissue layers is unlikely to be perfect, the properties of any interface between two tissue types would be very difficult to quantify.

Later studies have built upon this simplified geometry to provide more realistic foot models and answer more specific research questions. For example a study by Yettram and Camilleri (1993) used more complex bone geometry to investigate whether cancellous bone orientation aligns with the predicted lines of high stress in a loaded calcaneus bone. The complex internal geometry of the bone was segmented using a cadaveric calcaneus bone sliced in the sagittal plane. Each slice was x-rayed and a 3D shape was built up from these slices. This method of building fully 3D representations of body parts using image slices

is a common method today, particularly as magnetic resonance imaging and computed tomography have become more widely available.

As seen in the previous paper by Nakamura et al. (1981) it can sometimes be useful to combine several body parts into one geometry for the purposes of the model, as this allows for simplification of segmentation and usually results in reduced computational expense. Whilst considering bones to be fused is one way to reduce the complexity of a model's geometry, another method is to narrow the scope of the model to a smaller area, containing fewer bones. For example, Lemmon and Cavanagh (1997) investigated the effect of toe tendon forces on plantar pressure loading under the foot. They reduced the problem to just two bones in two dimensions, a metatarsal and a toe, with a single tendon under the toe and the metatarsal base fixed in position. Soft tissue was represented by a simple continuum surrounding the bones. Similarly in 3D, Budhabhatti et al. (2007) considered the first ray of the foot during walking, including the first metatarsal, and hallux bones, with a homogeneous soft tissue surrounding this. This method of representing the metatarsal bones as a fixed cantilever has been used previously in the beam theory models described in the previous section (2.5.1) (Stokes et al., 1979, Gross and Bunch, 1989) and has been developed since into recent models with highly detailed single bones such as the work of Fung et al. (2017) and used to investigate the effect of stride length and minimalist footwear on bone strain (Firminger et al., 2017). These studies developed a model containing just the second metatarsal, fixed at the proximal end. Geometry was taken from computed tomography scans. Forces such as ground reactions and joint reactions were applied to regions of the bone based on the 2D beam theory model of Stokes et al. (1979). This model used just 28,660 elements compared with similarly detailed whole foot models where 221,722 elements are

needed (Akrami et al., 2017, Akrami, 2016), nearly a ten-fold increase. The model developed by Firminger et al. was able to discern the effects of both stride length and minimal shoes on metatarsal strains, however it includes some limitations that should be considered. Computed tomography is a highly valid method for acquiring bone geometry allowing for easy segmentation based on the Hounsfield unit, which also allows density to be estimated. However it used x-ray radiation, which has risks for participants and so is less ethical to use than magnetic resonance scans. The model itself performed well when compared to a controlled experiment on cadaveric metatarsals, but its validity when used for studies of living runners is less clear. The forces applied accounted for the effects of the plantar tendons via the joint reaction forces applied, but did not account for any cushioning or redistribution of ground reaction forces applied by the soft tissues in the sole of the foot.

The effect of a model's complexity on its ability to produce high quality prediction of plantar pressure data has been investigated by Actis et al. (2006). A range of 2D models were developed along the second and third rays of the foot and loaded to represent the push off phase of gait. All models had a fused rear foot section, separate metatarsal and phalange with corresponding cartilage, encapsulating soft tissue, and a shoe represented by a total contact insole bonded to a sole. In the most complex model, a plantar fascia element was included as was a plantar tendon for loading the phalange which was fully articulating with cartilage between segments. Simpler models had either fused the phalange segments, excluded the tendon or the fascia or used a combination of these approaches. The models were evaluated against experimental plantar pressure distributions. The full model had very close agreement to experimental pressure data. Models that reduced the number of phalange bones, removed only the fascia, or

combined both these simplifications showed limited deviation from experimental results. However those models that removed the tendon or both tendon and fascia had a greater deviation from experimental results. It should be noted that as this model applied both linear and rotational loads to the ankle, the tendon and fascia would be needed to transfer these forces towards the forefoot. When considering the specific deigns required by other models for investigation of metatarsal stresses these tissues may not need to be present, and the research questions any model is developed to answer will inform which simplifications should be made. Overall, this study shows that simplification of geometry is an effective way to reduce modelling time and that whilst simplifications inevitably change results, usually away from those measured experimentally, if simplifications are chosen with care the deviation from experimental values can be limited.

The selection of model geometry is important both to give results that are a close fit with experimental validation and to manage computational expense. When considering the stresses in the second metatarsal, the anatomy of the foot is such that the bone is surrounded on three sides at its base by the bones of the midfoot and the first and third metatarsals, suggesting that there is limited movement at this joint and that modelling using a fixed cantilever approach as seen in the literature is appropriate (Fung et al., 2017, Lemmon et al., 1997a, Gross and Bunch, 1989, Stokes et al., 1979, Nunns et al., 2017, Firminger et al., 2017). However, the surrounding tissue complexity depends on the research question, for example if the question is concerning the formation of ulcers in the foot as in Gefen (2003b) then the plantar soft tissues and their mechanics are a very important consideration and must be included. However the study of Firminger et

al. (2017) was able to discern differences in metatarsal stresses with no soft tissue modelling.

2.5.3b Material Properties

Each individual part of a model must be assigned a specific set of material properties in order to complete subsequent analysis. These must be carefully considered with appropriate constitutive material models selected that allow the model to closely replicate the *in-vivo* properties of various body tissues. However, it is possible in certain cases to simplify the properties of parts to facilitate improved computational speed. In this section the material property choices of several models in the literature will be considered and the possible effects of this choice on the model outcomes will be discussed.

In the early model of Nakamura et al. (1981) the bone, soft tissue and shoe sole are all considered to be homogeneous and isotropic, with the bone being linearly elastic and the soft tissue being non-linear. It is known via mechanical testing in vitro that these tissues are non-homogeneous, and bone in particular is non-isotropic (Martin et al., 2015) which as mentioned in section 2.1 allows it certain beneficial performance characteristics *in-vivo*. However these simplifications allow a model to be constructed far more quickly and for computation time to be reduced. In addition the use of computed tomography scanning and magnetic resonance imaging has become far more readily available since these studies were completed and allow new methods to model the non-isotropic and non-homogeneous natures of the bony tissues. A recent example of this is the work by Fung et al. (2017) whose model consists of a single metatarsal bone with material properties at any point along the bone defined by an optimised density function, using the apparent density of the bone taken from a computed tomography image. Results showed that the predicted strains in the model

formed a relationship with the experimental strains with R^2 of up to 0.96. Depending on the scanning methods used it is not always possible to measure density of the material, for example, when using magnetic resonance imaging, it is possible to distinguish between cortical and trabecular bone, but not the changes in density in areas of cortical bone. Another study compared two foot models, identical, except that one had homogenous bones and the other distinguished between cortical and trabecular bone (Garcia-Aznar et al., 2009). In this case the homogenous bone was found to underestimate stress distributions when compared to the non-homogenous model. Therefore in order to investigate stress distribution within bony structures, the inhomogeneous nature of bones must be modelled.

Studies investigating the effect of soft tissue properties on the stresses in diabetic feet have found that adjustment of soft tissue properties such as decreased thickness, increased hardness or changing the isotropic nature of the soft tissues increases the stresses both at the foot-ground interface and at the inner interface of the soft tissue where it meets hard tissue (Thomas et al., 2004).Cheung et al. (2005) modelled the soft tissue as a hyperelastic material and investigated the influence of a five-fold increase in stiffness. The results showed that whilst the simulated plantar pressure increased by up to 35%, peak bone stresses increased by 7%. These results suggest that the choice of soft tissue properties does affect bone stress, and that investigating a model's sensitivity to these changes should be part of any evaluation procedure for a model.

2.5.3c Loading and Boundary Conditions

Once suitable geometry and material properties have been decided, the modelled parts must be assembled and loading and boundary conditions applied. In the case of the foot the model must be constrained such that it best represents the

movement that would occur *in-vivo*, but allow loads to be applied that replicate the loading seen in experimental studies. In the foot there are two main sources of loading, the loading from the weight of the body at the foot ground interface and the loading from the musculature of the lower limb activating to produce the movement seen. In the foot this internal loading is caused by the actions of the calf plantar flexor muscles such as the soleus and gastrocnemius acting on the Achilles tendon, the dorsiflexor muscles such as the tibialis anterior and the internal foot muscles such as the flexor digitorum brevis.

Earlier finite element models often considered only passive forces, for example by estimating the total weight bearing at the ankle in quiet standing and applying this at the ankle joint. This is the case in the early models such as those of Nakamura et al. (1981) and Yettram and Camilleri (1993). Despite the non-participant-specific loading of Yettram and Camilleri (1993) findings indicated good agreement between lines of principle stress and the lines of cancelli found using neutron diffraction, suggesting that internal bone loading can be accurately modelled using these methods. However loading in this manner is limited, and for investigation of more dynamic movements such as running, methods of loading must be more detailed, for example by including muscle actions.

There are several methods to model muscle actions in a participant-specific manner. A participant can be asked to perform a series of contractions in a rig designed to measure forces and then these measured forces can be applied to the model, this is a common method of driving joint motion in musculoskeletal models. For models examining internal forces, where the effect of individual muscles on bone stress is examined, this method is of limited use, as the muscle forces are combined into one force vector. Muscle forces can be inferred from a combination of electromyography-used to measure individual muscle activation

levels - and estimates of each muscle's maximum force production capability. An inverse dynamics approach can be used to calculate forces at a joint level, based on measured ground reaction forces and kinematics and this can be used to drive a foot model from a single joint. For example Qian et al. (2013) used a single rotational force and two linear forces calculated at the ankle to drive a dynamic 2D finite element model of the whole foot. Further calculations can be performed to resolve this force into individual muscle forces using a static optimisation algorithm. This approach can be used to drive 3D foot models that include forces and motions at the ankle such as Akrami et al. (2017) where six muscle forces were applied to the foot via tendon lines of action, allowing for the effects of an individual muscle's action on stresses in other tissues to be examined.

Whilst the geometry and loading methods employed by studies such as Akrami et al. (2017), Wu (2007) or (Chen et al., 2012) may be highly realistic and include the stresses on the metatarsal bones among other outputs, they are also extremely complex, requiring the segmentation of many tissues, the implementation of interactions between these tissues as well as the generation and application of any forces considered. This leads to long development times and high levels of computational expense, resulting in studies of single participants, reducing their ability to be used in applied studies. Studies focussing on only one aspect of the foot such as a single metatarsal bone (Firminger et al., 2017) or foot ray (Budhabhatti et al., 2007, Lemmon and Cavanagh, 1997) can greatly reduce the time needed to segment tissues and for the model to run, allowing more data to be analysed. The model developed by Firminger et al. (2017) has been used to answer applied questions regarding stresses on the second metatarsal during running. This model is essentially a 3D representation of the beam theory model of Stokes et al. (1979) whereby a combined force made

up of the joint contact forces and vertical ground reaction force acting under the metatarsal head was calculated applied directly to the metatarsal head. The model is notable for its simplicity, and its excellent comparisons with *ex-vivo* experimental strain gauge data (Fung et al., 2017). The model reported a 95th percentile strain of 3110 με in control shoes and 4341 με in minimalist shoes.. However, it did not account for the effects of horizontal ground reaction forces, either applied directly to the metatarsal head or applied under the toes via the joint contact force. It also did not account for the effects of soft tissues and applied forces directly to the head of the metatarsal.

The literature models considered so far have only simulated loading at single points in time, whether during a dynamic movement such as walking and running or simply standing. Due to the large amount of computational power required, a fully dynamic finite element simulation is rarely undertaken. A recent exception to this is research by Qian et al. (2013). This 2D model consisted of a fused sagittal bone slice with only one articulating part at the toe. A single encapsulating soft tissue was included, but no plantar tendon forces or fascia contributions were considered. A comparison was made using the model in a fully dynamic simulation against discrete points of gait calculated in a quasi-static manner around heel strike, mid stance and toe off. Results from the dynamic simulation showed that whilst it can match the general trend of ground reaction forces, it introduces oscillations which are not seen experimentally. This may in part be due to the simplification of bony structure and lack of soft tissue complexity, not allowing the model to absorb the initial force of impact as in vivo. When compared to the quasi-static loading method, it was seen that the dynamic simulation improved the results in some locations and at some time points. There were improvements in the heel region at foot contact (0.01 MPa or 10% improvement)

and in the metatarsal head region during mid stance (0.04 MPa or 33% improvement). However other regions and time points were not different (metatarsal head at toe off) or had poorer performance, such as in the heel region at mid stance (0.02 MPa or 33% poorer) or the toe region at toe off (0.06 MPa or 200% poorer), implying that the increased computing time required for a fully dynamic simulation may not yield better results.

Table 1 shows a summary of relevant literature studies of varying methodologies and their findings related to estimated or measured second metatarsal loading.

Table 1: A summary of literature values for measured and estimated second metatarsal loading during walking and running. Strains are presented in με; stressed are presented in MPa.

Study	Measurement method	Findings (Stress or Strain reported)
Milgrom et al. 2002	staple strain gauge - barefoot	2685 με walking range (2663 - 2707 με)
Milgrom et al. 2002	staple strain gauge - barefoot	3603 με jogging (range 1891 - 5315 με)
Arndt et al. 2002	staple strain gauge - barefoot	1534 (±636) με walking
Gross and Bunch 1989	Beam theory (non-participant specific)	6662 με running
Chen et al. 2001b	Finite element n=1	4 Mpa walking
Gu et al. 2010	Finite element n=1	6.65 Mpa walking
Akrami 2016	Finite element n=1	6.80 Mpa walking
Firminger et al. 2017	Finite element n=14 minimalist shoe	1937 (±452) με median, 4341 (±917) με 95th% strain

2.6 Summarising the Literature, Aims of the Thesis, Research Questions and Hypotheses

2.6.1 Literature Summary

Second metatarsal stress fracture has been identified as an injury that is common in recreational and competitive distance runners, and amongst athletes that include running in their training regimen. The process by which a stress fracture forms is well understood. These occur when strains on a bony site are great enough in magnitude, rate, frequency or duration to trigger a remodelling response, which initially weakens the bone, before strengthening it against the loading that initiated the response. In some activities, the strains placed upon the

bone may cause a stress fracture through fatigue failure in a physiologically reasonable number of cycles without the need for an intermediary remodelling process.

The primary physiological drivers for developing a stress fracture are reasonably well understood: where the bone is poorly adapted to manage the loads it is subjected to, the risk of developing a stress fracture is high. Specific kinematic variables that lead to high bone stresses in the second metatarsal in runners are not well studied, however research on other populations such as military recruits suggests that individual geometry of both the bones themselves and their arrangement as part of the foot are strong determinants of stress magnitude. In addition, it is theorised that loading conditions that increase the magnitude of forces and pressures under the metatarsal heads such as running in minimalist shoes or landing with the more anterior parts of the foot first will increase the loading on the metatarsals. Studies have shown that switching from cushioned to minimalist shoes or barefoot running can cause a stress fracture to occur within a few weeks, but these reports had little or no transition or habituation period and it is not clear whether the cushioning, the change in kinematics, or a combination are responsible.

Mathematical models have been useful in understanding internal loading variables, especially in situations where the direct measurement of loading is difficult or invasive, such as on or within a bone. A number of models of the foot exist, ranging from simple beam theory models to finite element models incorporating all the bones and soft tissues of the foot. However, these models can vary in their ability to answer research questions, each having their own limitations. For example, simple beam theory models do not include the force absorbing effects of the soft tissues, whereas complex finite element models are

time consuming to develop and run and therefore can have limited participant numbers.

Whilst the two modelling methods identified have very different development times and computational expense, a direct comparison of their abilities to estimate internal loading has not been undertaken, and therefore it is not clear whether the potential for increased detail in the results of a finite element model outweigh the potential costs in time and computing power to develop and run them when compared to a similarly designed beam theory model.

Answering applied questions should always be undertaken using the best tool, but accuracy and detail of results are not the only measures of the usefulness of a particular method. The ability to obtain sufficient data from participants, influenced by the time needed to perform the study are also important. For the investigation of internal bone loading in the foot, this review has shown that invasive direct measurement and highly complex models can give highly valid and detailed results respectively, but conducting applied studies with these methods is difficult and limited. Conversely simple models may be able to provide less detailed yet valid results whilst also allowing simulation of the model for larger cohorts of participants for applied studies.

2.6.2 Aims of the Research

There is insufficient understanding of both the risk factors for developing a second metatarsal stress fracture in runners and non-invasive approaches that can perform investigations of this nature. This research aims to develop both a participant-specific two dimensional beam theory model and a participant-specific three dimensional finite element model that can answer research questions centred on the risk of developing a second metatarsal stress fracture. These

models will be used to understand how second metatarsal stresses differ during running in those who habitually run with a rearfoot strike compared to a non-rearfoot strike. Firstly, a two dimensional beam theory model incorporating participant-specific geometry, and experimentally-obtained kinetics and kinematics will be used. Based on the limitations and advantages of this model, a three dimensional finite element model will then be developed and the same data set will be applied. This will allow a comparison of the two models which will improve understanding of the best way to model the stresses in the second metatarsal. This will have applications to the modelling of other body structures as well. Comparing metatarsal stresses between habitual rearfoot and non-rearfoot strikers will provide a novel understanding of how internal bone loading compares between these two groups.

2.6.3 Research Questions and Hypotheses

A flow chart of the research programme can be seen in Figure 9. The initial research questions and the associated hypotheses are discussed below.

1. Does habitual footstrike pattern affect the magnitudes of stresses experienced by the second metatarsal bone during running?

Hypothesis: Based on the literature, it was hypothesised that there would be greater loading under the metatarsal heads in non-rearfoot runners than rearfoot runners. This greater external loading would result in greater stresses acting on the bone.

2. Does habitual footstrike pattern affect the magnitude of stresses experienced by the second metatarsal bone during running when modelled using a 2D beam theory approach?

Hypothesis 1: Externally measured forces under the metatarsal head would not be representative of internal loading when participant-specific geometry and kinematics were included in the model.

Hypothesis 2: There would be greater external and internal second metatarsal loading in non-rearfoot runners than rearfoot runners.

3. Does habitual footstrike pattern affect the stresses experienced by the second metatarsal bone during running when modelled using a 3D finite element approach?

Hypothesis 1: Externally measured forces under the metatarsal head would not be representative of internal loading when participant-specific deformable geometry and distributed loading were included in the model.

Hypothesis 2: There would be greater external and internal second metatarsal loading in non-rearfoot runners than rearfoot runners.

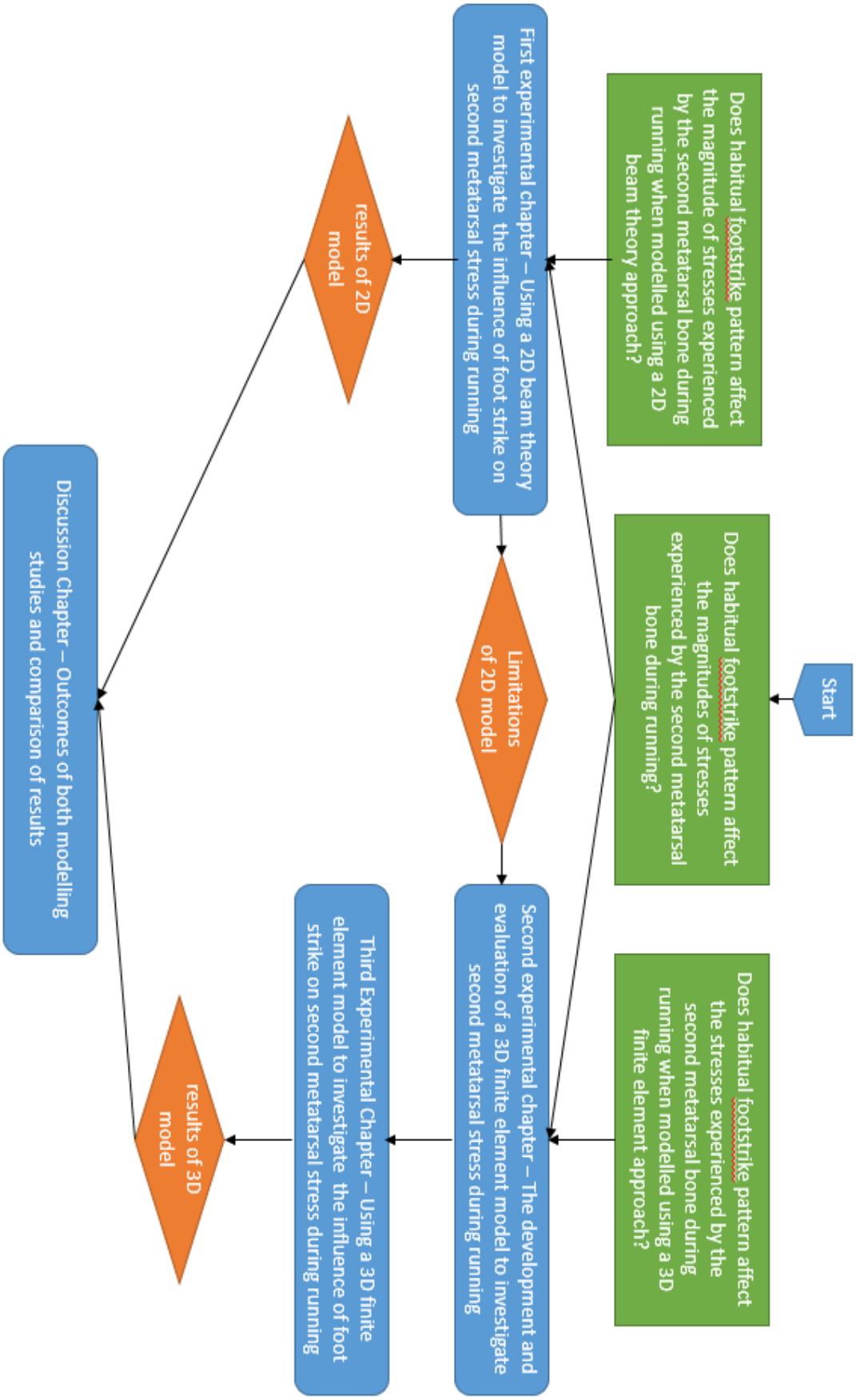

Figure 9: Flow chart of research aims and questions

3. General Methods of Data Collection and Analysis

Detailed methods for each study will be presented in their respective chapter. However to avoid repetition, methods and equipment setup that remain consistent between studies will be described here. Briefly, one set of experimental data were collected, from a group of habitual rearfoot runners and a group of habitual non-rearfoot runners. Two models were developed to quantify metatarsal loading. These models were then evaluated and used to compare these groups of runners, and then the modelling methods themselves were compared.

3.1 Sample Size and Selection

This thesis utilised a single data collection protocol and developed different modelling approaches for their analysis. Based on the literature above, two groups of participants were targeted for recruitment: rearfoot strikers who land on their heel and mid- to forefoot strikers who were grouped together as non-rearfoot strikers. The inclusion criteria for the study were that participants were competitive or recreational athletes aged 18 to 60 years of age who participated in running activity at least three times per week and for a duration of greater than 150 minutes per week. Participants were excluded from the study if they reported any lower limb injury affecting training in the past year. Eligible participants were given information about the study and provided informed written consent. Ethical approval for the study was given by the Sport and Health Sciences Ethics Committee, University of Exeter. Sample size was estimated using G*Power (Faul et al., 2007). Vertical forces under the central forefoot following a change in foot strike were used to determine effect size (Warne et al., 2014) as this is an

important input variable into any model of the foot. 20 participants was sufficient based on an alpha of 0.05 and power of 80%.

Participants were recruited using a combination of non-probability sampling methods - convenience, purposive and snowball sampling. Initial participants were recruited in a typical convenience manner using flyers. Participants were additionally recruited by word of mouth, where non-rearfoot strikers were preferentially selected such that there would be approximately equal groups of rearfoot strikers and non-rearfoot strikers.

In total 20 participants were recruited (10 Female; age 25 ± 9 years; mass 66.5 ± 11.9 kg; height 1.68 ± 0.09 m). No participants reported any current injuries affecting their running regimen and no participants had sustained any lower limb injuries that prevented their normal training within the last year.

In order to assess the participant's foot strike in a habitual running setting, an initial trial was conducted with the participant running at the appropriate speed whilst wearing their preferred running shoes, contacting a pressure plate that was used to determine foot strike pattern. Participants were not informed of the outcome of this trial. Following this, runners completed trials as detailed in section 3.5 barefoot. The barefoot trials were compared to the shod trial to determine whether participants were using their habitual shod running foot strike pattern whilst completing barefoot trials. Foot strike was assigned using the centre of pressure location relative to the foot at the first point of contact according to strike index (Cavanagh and Lafortune, 1980): where this was in the rear 30% of the foot they were classified as rearfoot strikers, all other strike types were classified as non-rearfoot strikers. Examples of these are seen in Figure 10. Two participants displayed a foot strike that was consistently more anterior when running barefoot

than running in shoes, and these participants were included in the non-rearfoot grouping. Two further participants displayed a foot strike that was inconsistent when running barefoot compared to the shod trial, producing some trials displaying rearfoot and some displaying non-rearfoot characteristics. In these cases, extra trials were conducted such that a complete set matching the shod trial were collected. These participants were categorised into the group that matched their shod trial. In all cases, participants were not informed of their foot strike during data collection to avoid influencing their running gait. Of the 20 participants, 12 were classified as rearfoot (N = 12; 7 Female; age 28 ± 11 years; mass 62.6 ± 10.4 kg; height 1.65 ± 0.07 m) and 8 as non-rearfoot (N = 8; 3 Female; age 20 ± 3 years; mass 72.3 ± 12.3 kg; height 1.73 ± 0.09 m). A students T test was used to determine if the groups differed in mass, height or age. No differences in mass or age between groups were found, however the non-rearfoot group was significantly taller than the rearfoot group ($p=0.049$). Within the non-rearfoot group, there were three subgroups of strike types, as defined by Nunns et al. (2013): midfoot runners characterised by landing with the midfoot in the first two frames of contact; forefoot runners characterised by landing on the metatarsal heads in the first two frames of contact, followed by heel touchdown; and toe runners characterised by landing on the metatarsal heads during the first two frames of contact and where the heel never touches the ground. In total there were two midfoot runners, five forefoot runners and two toe runners in the non-rearfoot group.

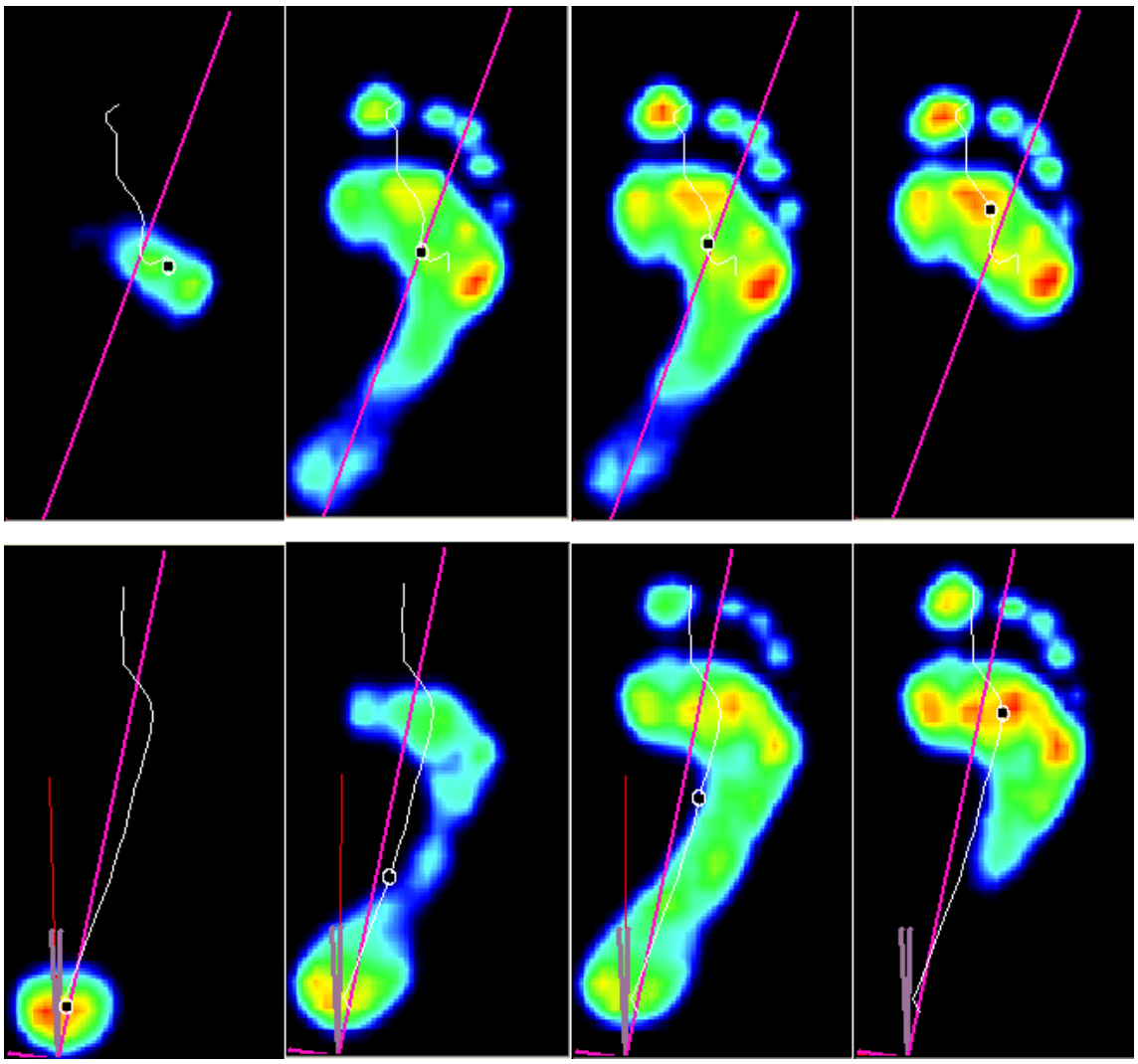

Figure 10: Typical pressure traces for a NRF (top row) and RF (bottom row) strike. From left to right: initial contact, mid-stance, push off.

3.2 Measurement of Kinematics

The motion capture system used for the experimental data collection presented in this thesis is the Codamotion CX 3D motion capture system with four monitors (Coda CX1, Codamotion – Charnwood Dynamics Ltd., U.K.), each containing three motion sensors. Each CX1 unit can measure marker location independently with very low error (±0.05 mm laterally and ±0.3 mm distance from camera). The laboratory setup was such that the origin of the laboratory co-ordinate system was placed at one corner of a force plate (see section 3.3), the x-axis was set in a medial-lateral direction, the y axis in an anterior posterior direction and the z-

axis was set vertically, with positive upwards. All running trials were completed such that the direction of running was in the positive y direction. The cameras were set up and placed to cover a capture area of approximately 5 m by 3 m as shown in Figure 11. As collection was focussed on the right lower limb, the two cameras on the left side of the body were placed to better capture the medial aspects of the right leg and help prevent occlusion of any markers placed there. The right foot and leg were targeted as regions of interest and marker sets were created to capture full movement of the segments of the foot and lower leg up to the knee. Kinematic data were collected in tandem with model development, therefore although data detailing the motions of the individual segments of the foot were captured, after model development only a smaller subset of markers were needed for analysis. The remaining data were analysed and the findings regarding the motions of foot segments during running are detailed in Appendix 2. The CX system allows for a fixed number of markers for a given data collection frequency. Given the detailed nature of the foot and leg complex 19 markers (Coda XM series, Codamotion – Charnwood Dynamics Ltd., U.K.) connected via 6 active drive boxes (Coda QMDB, Codamotion – Charnwood Dynamics Ltd., U.K.) were attached directly to the skin and used to mark strategic bony landmarks of the foot and shank, similar to the Oxford Foot Model (Carson et al., 2001). Photographs identifying marker locations can be found in Appendix 2. To maximise repeatability and reliability between participants the markers were always placed in the same order and the positions of the markers relative to the floor were kept standard using the width of the investigator's thumb.

Marker locations were determined using palpation and were secured directly to the skin or skin tight clothing using both double sided tape and Micropore^{TM} tape (3M, U.S.A.). Loose wires were secured to prevent accidental marker removal

and to prevent wires occluding markers. Data were collected at 200 Hz, kinematic gaps caused by marker occlusion were filled using cubic splines and the complete trajectories were filtered using a butterworth filter with a cutoff frequency of 12 Hz similar to other studies (Rice, 2015).

3.3 Measurement of External Forces and Pressures

External forces acting on the foot were measured using a force plate (AMTI BP400600HF, Advanced Mechanical Technology Inc., U.S.A.), collecting data at 1000 Hz. Co-ordinates for the plate were set to match the kinematic lab co-ordinate system. The force plate analogue signal was converted to a digital input via an amplifier (AMTI OPT-SC, Advanced Mechanical Technology Inc., U.S.A.) and was integrated into the camera system via a control unit (Coda Active CodaHub, Codamotion – Charnwood Dynamics Ltd., U.K.).

Plantar pressures were measured using a plantar pressure plate (RSscan 0.5 m Hi-End Footscan, RSscan – Beringen, Belgium) collecting at the same frequency as kinematic data. The pressure plate was placed on top of the force plate such that the pressure plate was entirely within the boundaries of the force plate, and the force plate zeroed, such that the force collected by the force plate was not affected. The pressure plate was triggered to collect data via the kinematic collection software, and would measure any force greater than 10 N on the plate. Pressure data were collected at 200 Hz using Footscan software (RSscan Footscan Gait v7, RSscan – Beringen, Belgium) connected via an interface box (RSscan Footscan 3D interface box, RSscan – Beringen, Belgium). A runway was constructed from EVA panels such that the pressure plate was flush with the running surface and participants would not have to adjust their stride to account for it. A diagram of the experimental setup can be seen in Figure 11.

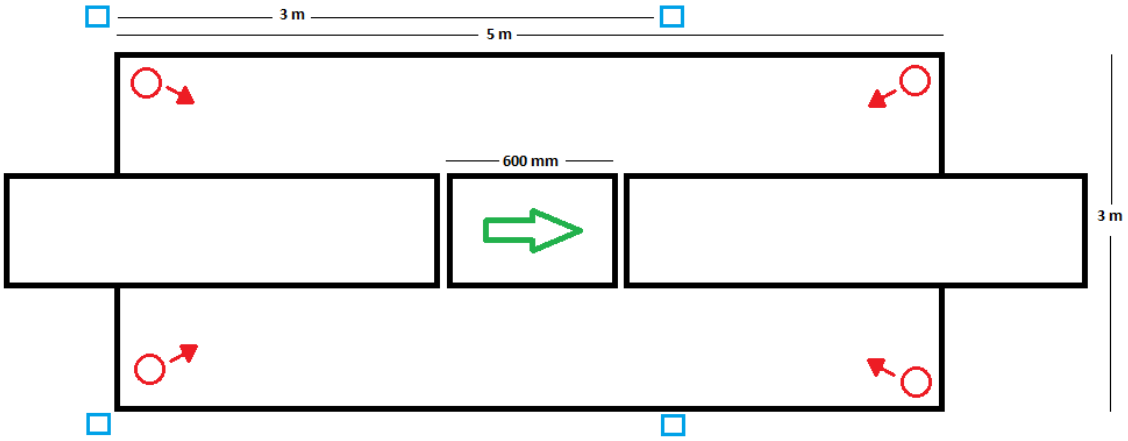

Figure 11: A diagram of the lab layout. Force plate and pressure plate (centre rectangle) with arrow indicating direction of travel, red circles and arrows approximate camera locations and blue boxes show timing gate locations.

3.4 Measurement of Internal Geometry

For accurate estimation of internal forces, the structure of internal tissues must be known. This allows both geometry and mechanical properties to be correctly assigned to parts of a model. In this thesis, Magnetic Resonance Imaging (MRI) was used for all internal geometry. All MRI scans were made in three orthogonal planes in order to facilitate three dimensional reconstruction of tissues at a later date. To determine individual metatarsal geometry, magnetic resonance (MR) images were collected from each participant whilst lying supine within a 1.5 T superconducting whole body scanner (Gyroscan Intera, Philips, The Netherlands). The location of the second metatarsal and phalange was initially identified via palpation and a cod liver oil capsule placed on the foot at that location using micropore tape. Cod liver oil capsules were additionally placed at the head of the first and fifth metatarsals, using the kinematic marker locations. The unloaded foot was then placed against a flat vertical barrier within a quadrature head coil to minimize movement, and to ensure each data set was

acquired with the foot in a similar position. Stacks of MR images covering the whole of the foot and centred around the second metatarsal, as identified in the images from the high intensity cod liver oil capsule, were then acquired in sagittal, coronal and axial planes. In all cases a T1 weighted (repetition time 20 ms, echo time 4.0 ms, flip angle 500) 3D gradient echo sequence was utilised with an in-plane resolution of 0.3 x 0.3 mm and a slice thickness of 0.7 mm. Depending on the imaging orientation, between 60 and 160 slices within a stack were required for full coverage. Typical slices through the metatarsal in all three planes are shown in Figure 12, Figure 13 and Figure 14.

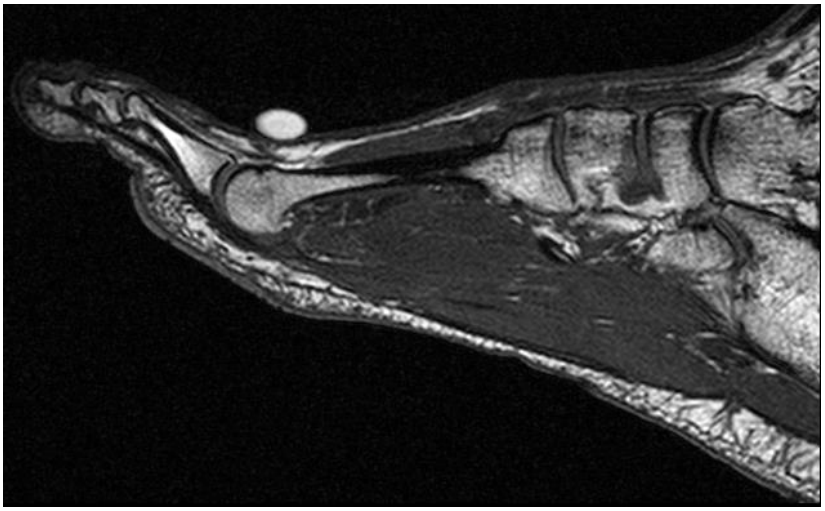

Figure 12: A typical sagittal image slice used to calculate bone geometry

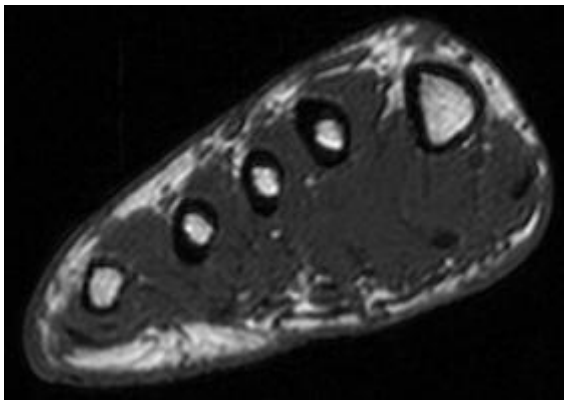

Figure 13: Typical mid-shaft slice used to calculate bone geometry

Figure 14: A typical mid-shaft slice in the transverse plane

3.5 Running Protocol

The participant's height and mass were measured whilst participants wore their own running kit. Synchronised kinematic, kinetic and plantar pressure data were collected during running at a constant velocity of 3.6 ms^{-1}. Trials were completed barefoot. An opportunity to warm up was given and familiarisation trials were completed until the participant was comfortable running at the desired velocity on the surface. Feedback on the running velocity was provided after each attempt. This was obtained using a set of timing gates (Microgate Witty system, Microgate U.S.A., New York, U.S.A.) set up 3 m apart with the force plate in the centre (Figure 11).

The experimental protocol consisted of running at constant velocity ensuring that the right foot contact was within the pressure plate boundaries. A trial was considered successful when the right foot contacted the plantar pressure plate, velocity was registered as 3.6 ms^{-1} (±5%), markers showed good visibility during foot contact with the pressure plate and the investigator observed no unusual movement during footplate contact. In total ten successful trials were recorded

per participant. For the purpose of comparison of the modelling outputs against previous literature measurements of second metatarsal stresses, one participant was asked to conduct 5 trials whilst walking at a self-selected speed in addition to their running trials. The data collection setup was identical for these extra trials.

A detailed description of any analysis of this data for use as modelling inputs can be found in the respective chapters (4 and 5).

4. Incorporating Participant-Specific Geometry in a 2D Beam Theory Model to Compare Metatarsal Stress during Running with Different Foot Strike Patterns

As outlined in the literature review (2.1) measurement of the magnitude of internal stress experienced by the metatarsal is useful when considering the formation of stress fractures. The magnitude of loading on the second metatarsal when using differing foot strike modalities is not well understood. The aim of this study was to develop and evaluate a participant-specific beam theory model to investigate whether the magnitudes of forces and stresses acting on the second metatarsal at the head and mid-shaft during running differ between rearfoot and non-rearfoot runners. Evaluation was conducted using both an input sensitivity analysis and by comparison of the outputs of the model with other models and strain gauge data during both walking and running. It was hypothesised that non-rearfoot strikers would experience both greater external and internal second metatarsal loading than rearfoot strikers during running. Data were collected for this study in line with the procedures outlined in Chapter 3.

4.1 Model Design

The forces acting on the second metatarsal were estimated using a model similar to Stokes et al. (1979) and Gross and Bunch (1989), with stresses calculated at the upper and lower surfaces of the bone at the midpoint of the shaft, using a similar approach to that of Meardon and Derrick (2014).

Figure 15 shows the forces considered in the model. Assumptions in the model are:

1. The MTP joints are frictionless (Stokes et al., 1979)

2. Forces due to accelerations of the components are negligible (Stokes et al., 1979)
3. No extensor muscles act during ground contact (Stokes et al., 1979)
4. The second ray of the foot is independent of other metatarsals and toes (Stokes et al., 1979)
5. The load is shared equally between the long and short plantar tendons
6. The masses of the segments are negligible
7. The forces act at points underneath the metatarsal head and toe
8. Forces and kinematics in the mediolateral direction are negligible

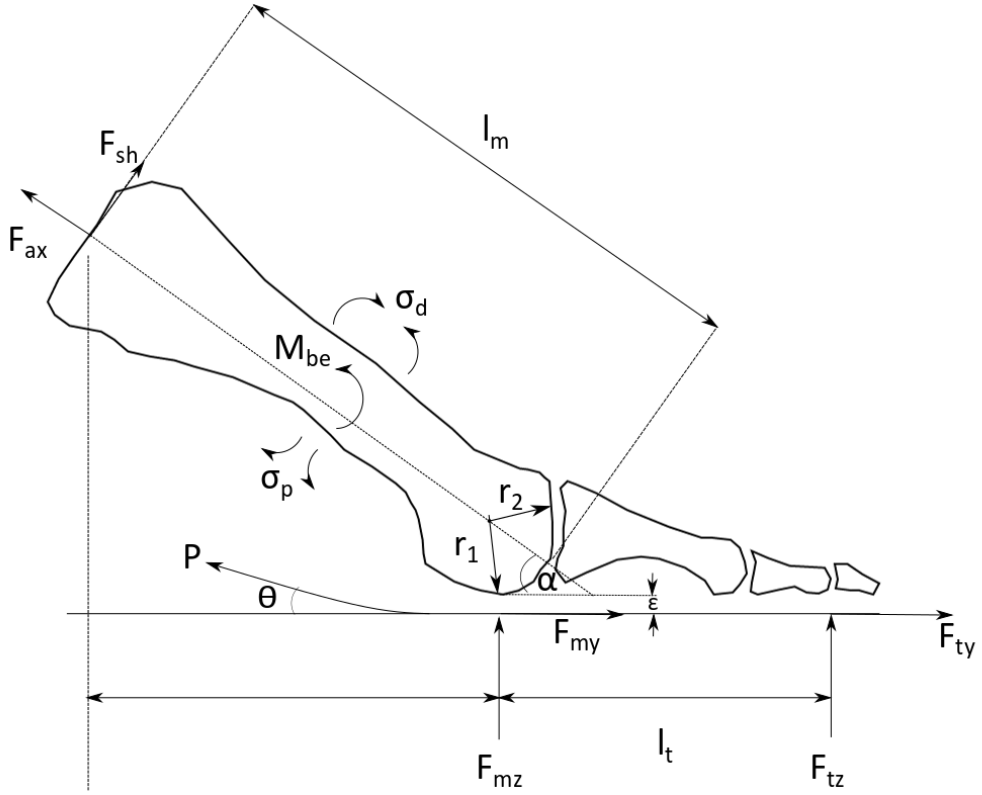

Figure 15: Forces and dimensions considered in the mathematical model. Note: l_m represents metatarsal length, l_t represents toe length, r_1 and r_2 represent the lower and upper radii of the metatarsal head, α represents the angle between the metatarsal and the horizontal, P represents the long and short plantar tendon forces, F_{ax} represents the axial compression force, F_{sh} represents the shear force, M_{be} represents the midshaft bending moments, σ_d and σ_s represent the dorsal and plantar midshaft stresses, ε represents the distance from the lower surface of the metatarsal head to the plantar tendon and θ is the angle of plantar tendon action (adapted from Stokes et al. (1979)).

The forces due to the long and short plantar tendon is therefore simplified to a single force acting to bisect the angle between the two tendons. The angle between tendons (β) was taken to be 10° based on the work of Jacob (2001) using cadaveric measurements, thus θ can be calculated using Equation 3.

$$\theta = \alpha - \frac{\beta}{2}$$

Equation 3: Calculation of the angle of action of the plantar tendons

First the toe is considered in isolation (Figure 16). In equilibrium the sum of linear forces equates to zero, giving equations 04 and 05. Summing the moments acting at the MTP joint gives Equation 6. From these, the joint contact forces and the force in the plantar tendons can be calculated. In this case the joint contact force represents the forces experienced by the metatarsal due to bone on bone contact from the phalange as described by Vigotsky et al. (2019).

$$F_{tz} + F_{jz} + Psin\theta = 0$$

Equation 4: Summing linear forces acting on the toe vertically

$$F_{ty} + F_{jy} - Pcos\theta = 0$$

Equation 5: Summing linear forces acting on the toe horizontally

$$F_{tz} l_t = P(\varepsilon + r_1)$$

Equation 6: Summing moments about the metatarsophalangeal joint

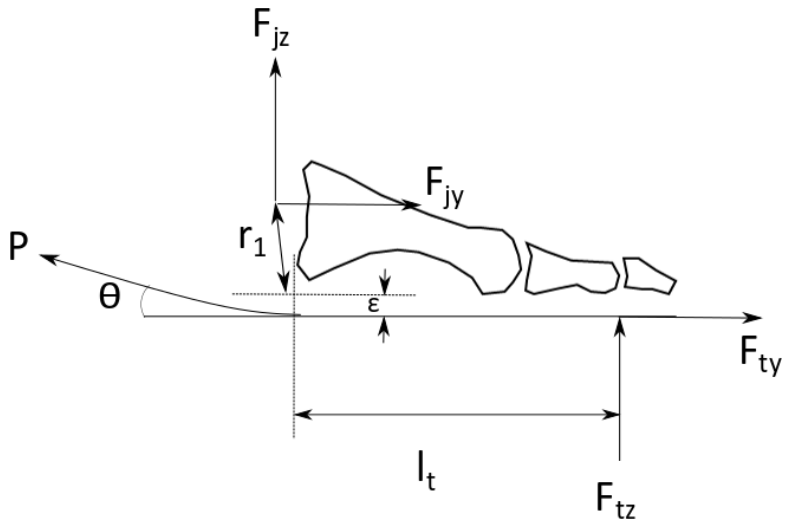

Figure 16: Free body diagram for the toe – F_{tz} and F_{ty} represent the vertical and horizontal ground reaction forces acting under the toe, F_{jz} and F_{jy} represent the vertical and horizontal joint contact forces at the MTP joint.

Now the metatarsal can be considered (Figure 17). Resolving forces axially and perpendicularly gives equations 07 and 08. The bending moment at the mid shaft can be calculated using Equation 9.

$$F_{ax} = F_{mz}sin\alpha + F_{jy}cos\alpha - F_{my}cos\alpha - F_{jz}sin\alpha$$

Equation 7: Calculation of axial forces in the metatarsal

$$F_{sh} = F_{mz}cos\alpha + F_{my}sin\alpha - F_{jz}cos\alpha - F_{jy}sin\alpha$$

Equation 8: Calculation of shear forces in the metatarsal

$$M_{be} = F_{mz}\left(\frac{l_m - r_2}{2}\right)cos\alpha + F_{my}\left(\frac{l_m - r_2}{2}\right)sin\alpha - F_{jz}\left(\frac{l_m - r_2}{2}\right)sin\alpha - F_{jy}\left(\frac{l_m - r_2}{2}\right)cos\alpha$$

Equation 9: Calculation of the moment acting at the midpoint of the metatarsal

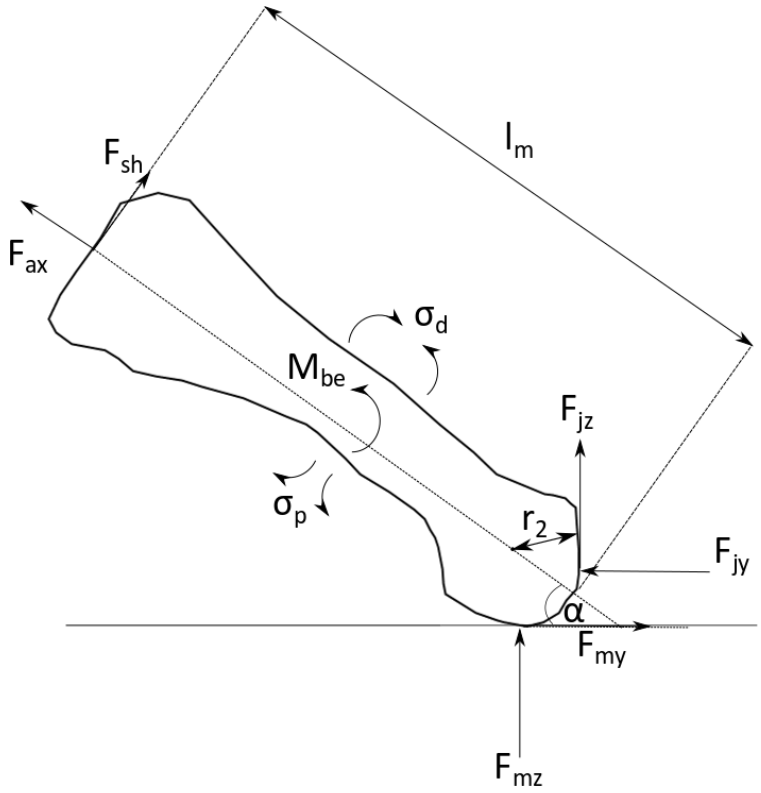

Figure 17: Free body diagram for the metatarsal – F_{mz} and F_{my} represent the vertical and horizontal ground reaction forces acting under the toe.

Lastly, stress can be calculated using these forces and the cross-sectional geometry of the metatarsal at midshaft.

Axially, the stress is given by Equation 10, and bending stress is calculated using Equation 11.

$$\sigma_{ax} = \frac{F_{ax}}{CSA}$$

Equation 10: Axial stress calculation where CSA represents the cross sectional area

$$\sigma_{be} = \frac{M_{be} r}{I}$$

Equation 11: Bending stress calculation where r represents the radial distance from the centre of the bone to the surface, I represents the area moment of inertia of the cross-section

Finally, the mid-shaft stresses at the dorsal and plantar bony surfaces can be calculated using Equation 12.

$$\sigma_d = \sigma_{ax} + \sigma_{be}$$

$$\sigma_p = \sigma_{ax} - \sigma_{be}$$

Equation 12: Normal stress acting on the upper and lower surface of the midshaft, d and p represent dorsal and plantar surfaces, σ_{ax} represents axial stress and σ_{be} represents bending stress

To obtain the estimated ground reaction force under the second metatarsal and toe for input into the model, the pressure in each cell under the metatarsal head and second toe was summed and then calculated as a percentage of the pressure across all cells in that frame of stance. The ground reaction force measured using the force plate was then scaled by this percentage. This was repeated for each frame of stance using a custom Matlab script (Matlab 2016b, MathWorks, MA. U.S.A.). A typical foot outline showing the last, dividing lines and edited pixels can be seen in Figure 18.

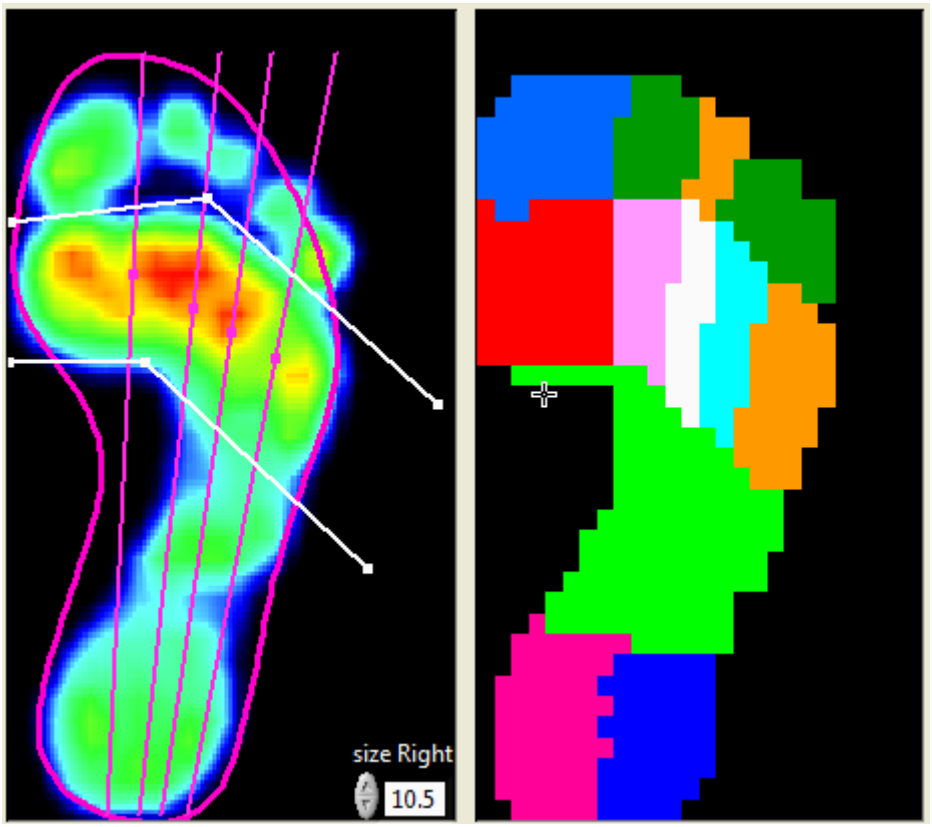

Figure 18: The heat map of pressure distributions overlaid with the mask outline and section lines (right), the final pixel mask for comparison.

The toe length (l_t) was measured from the head of the metatarsal to the point of toe contact with the ground by placing the zero point of a flat metal rule against the underside of the metatarsal head and allowing the participant to stand on it. The point at which the toe touched the ruler was recorded as l_t. To obtain α, a vector from the distal marker to the proximal marker on the metatarsal was calculated and the angle between this vector and the ground throughout stance was obtained.

The simplified bone geometry for the model was calculated using ImageJ (ImageJ 1.50i, Wayne Rasband, National Institutes of Health, U.S.A.). To calculate the radii r_1 and r_2, an image slice was selected in the sagittal plane in the centre of the bone, in which the distal epiphysis was completely visible. The circle fitting function was used whereby a number of points were marked along the edge of the bone in the image and a circle fitted to them. Metatarsal length, l_m, was

calculated in the sagittal plane on three consecutive slices in which the bone was completely in view and taking mean of the three lengths.

Cross sectional information was calculated using a custom MATLAB script (Kenny et al., 2019). The image of the cross section from 50% of the length of the second metatarsal was imported and the brightness adjusted to make the cortical and trabecular bone areas more distinct from the background. A canny edge detection algorithm was used to find the edges of the bone and the area of the cortical bone was divided into a series of triangles from which the cross-sectional area and area moment of inertia could be calculated (Figures 19 and 20). This method is similar mathematically to that used by Nunns et al. (2017). Analysis of the method noted that the error in both the area moment of inertia and cross-sectional area dreased with increasing numbers of triangles. 96 triangles represents an error of approximately 1% in the area moment of inertia and 0.3% in the cross-sectional area. All slices used contained approximately 100 triangles. Cross-sectional area and area moment of inertia values were input into equations 17 and 18 to calculate stress at the midshaft.

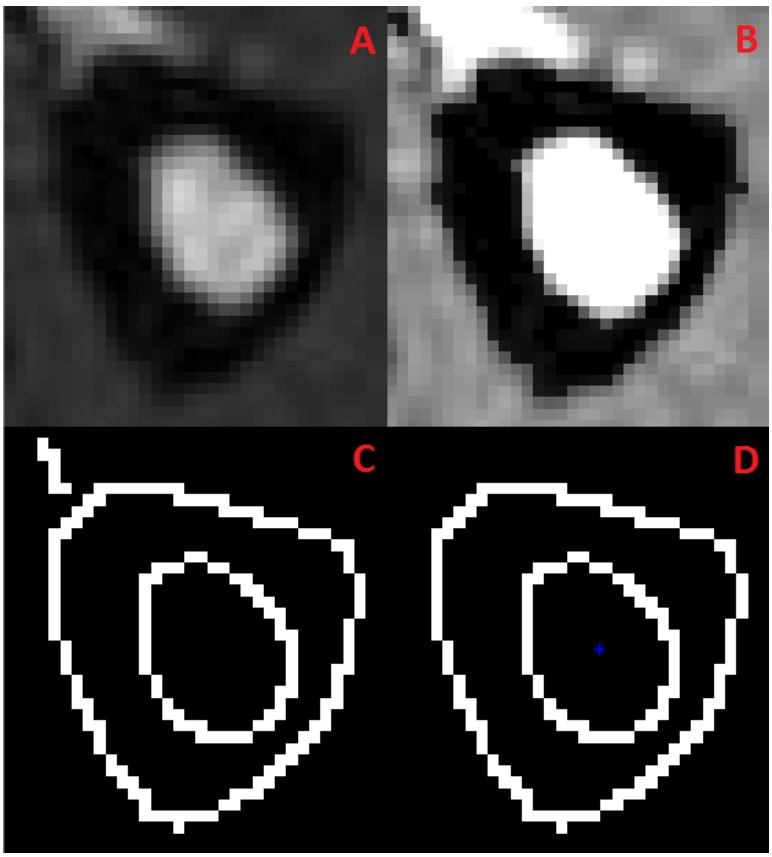

Figure 19: A: Original image of cross section, B: Image with altered contrast, C: Initial edge detection, D: Final edges with centroid plotted in blue.

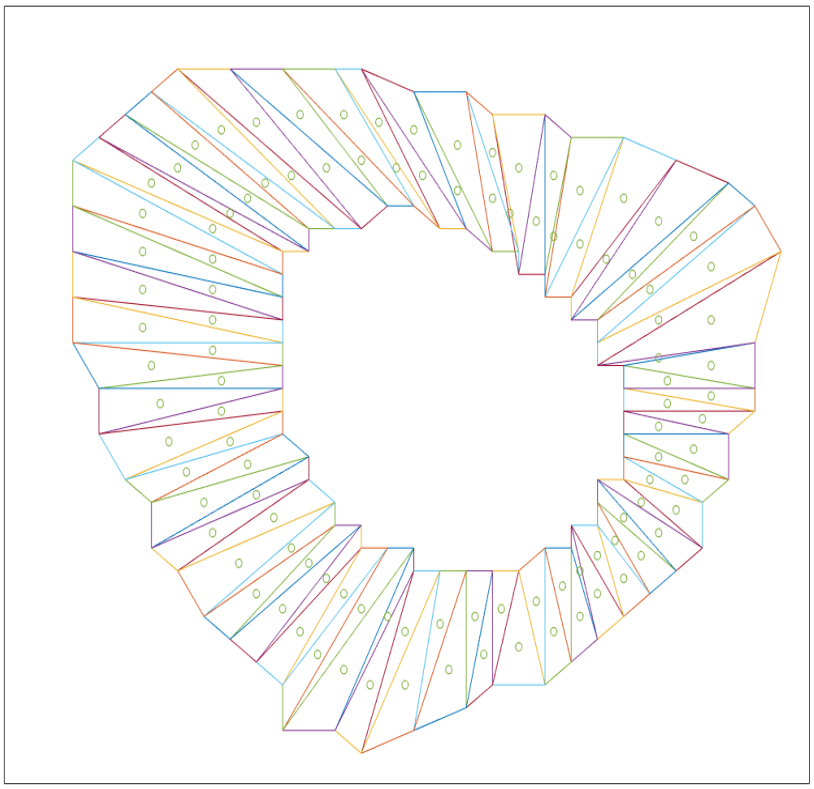

Figure 20: Outline of cross section divided into triangles, with the centroid of each triangle plotted as circles.

Peak values were calculated for the vertical ground reaction force (vGRF) under the second metatarsal head (F_{mz}), the axial force acting on the metatarsal (F_{ax}), the shear force acting on the metatarsal (F_{sh}), the bending moment acting at 50% of the metatarsal length (M_{be}), plantar stress acting at 50% of the metatarsal length (σ_p) and dorsal stress acting at 50% of the metatarsal length (σ_d) and averaged over the ten trials for each participant. Two participants (one RF, one NRF) had additional sites along the metatarsal assessed at 10% intervals between 30% and 80% of the metatarsal length, from proximal to distal in order to examine how stresses changed along the length of the bone. This range effectively contains the diaphysis of the metatarsal but excludes the epiphysis.

The stresses calculated at these points were interpolated and are displayed as a surface.

4.2 Analysis

In order to evaluate the model a sensitivity analysis was conducted. A single trial from a single participant was manipulated to individually increase input variables by 10% and the effects on output variables was observed. Furthermore, the model outputs were computed using the walking data collected from a single participant. This and the running data were compared with other literature models and strain gauge studies for both walking and running.

Statistical analysis to compare the two groups of participants was carried out both in SPSS (Version 24.0, SPSS Inc., Chicago, IL, USA) (discrete variables) and in Matlab using open source statistical parametric mapping (SPM) scripts (http://www.spm1d.org (Pataky et al., 2016)), with a significance level of $P \leq 0.05$. Discrete variables were examined using a Shapiro-Wilk test to confirm normality ($P \geq 0.05$). Means were compared using an independent T-Test (normally distributed variables) or a Mann-Whitney-U test (non-normally distributed variables). Effect sizes were calculated using Cohen's d (Cohen, 1988) for all variables where $P \leq 0.05$.

4.3 Results

4.3.1 Sensitivity Analysis

Results of the sensitivity analysis assessing the influence of manipulating input variables on peak values are presented in Table 02. For most input variables an increase of 10% did not increase output variables by more than a few percentage points.

Table 2: The percentage change in output variables given a 10% increase in individual input variables

Input	M_{be} (%)	σ_d (%)	σ_p (%)
r1	0.2	0.1	0.4
r2	-1.0	-1.0	-1.1
ε	0.1	0.0	0.2
β	-0.3	-0.3	-0.4
l_m	11.0	10.4	11.7
l_t	-0.3	-0.1	-0.6
CSA	0.0	-0.5	0.6
r	0.0	9.5	10.6
I	0.0	-8.6	-9.7
F_{mz}	8.9	8.9	9.2
F_{my}	0.6	0.6	0.7
F_{tz}	0.3	0.5	0.1
F_{ty}	0.1	0.0	0.1
α	-6.2	-5.5	-7.0

4.3.2 Discrete Analysis

Peak stresses are presented in Table 3. There was greater axial force, bending moments and vGRF under the second metatarsal in non-rearfoot strikers compared to rearfoot strikers. However there was no difference in stresses between foot strikes. Peak dorsal stress values for each individual against body weight are presented in Figure 21. Peak bending stress was found to contribute 96.3% (±4.39%) of the peak compressive stress on average, with no difference between groups. Time of peak stress was also reported for descriptive purposes.

Table 3: Peak variables Compared between foot strike modalities

Variable	Mean (SD)		P	d
	RF	NRF		
Midshaft Dorsal Stress (MPa)	-210.18 (89.66)	-244.73 (36.09)	0.249	0.5
Midshaft Plantar Stress (MPa)	196.16 (84.62)	223.14 (35.73)	0.341	0.4
Axial Force (N)	**263.60 (89.41)**	**427.79 (63.57)**	**<0.001***	2.1
Shear Force (N)	294.27 (58.80)	342.04 (33.39)	0.053	0.9
Midshaft Bending Moments (N.m)	**9.35 (1.90)**	**11.63 (1.97)**	**0.019***	1.2
vGRF under MT2 Head (N)	**309.01 (63.76)**	**381.98 (57.23)**	**0.018***	1.2
Time of Peak Dorsal Stress (% stance)	58.7 (3.7)	56.6 (3.6)	0.243	0.5
Time of Peak Plantar Stress (% stance)	58.5 (3.8)	56.6 (3.4)	0.275	0.5
Cross-sectional area (m^2)	3.7×10^{-5} (6.6×10^{-6})	3.8×10^{-5} (5.4×10^{-6})	0.853	0.1
Area moment of inertia (m^4)	2.1×10^{-10} (9.1×10^{-11})	2.1×10^{-10} (7.4×10^{-11})	0.997	0.0
Radial distance from bone centre to surface (m)	3.8×10^{-3} (3.5×10^{-4})	3.9×10^{-3} (2.5×10^{-4})	0.385	0.0

* Significant ($P \leq 0.05$) between groups, negative indicates compressive stress. MT2: second metatarsal.

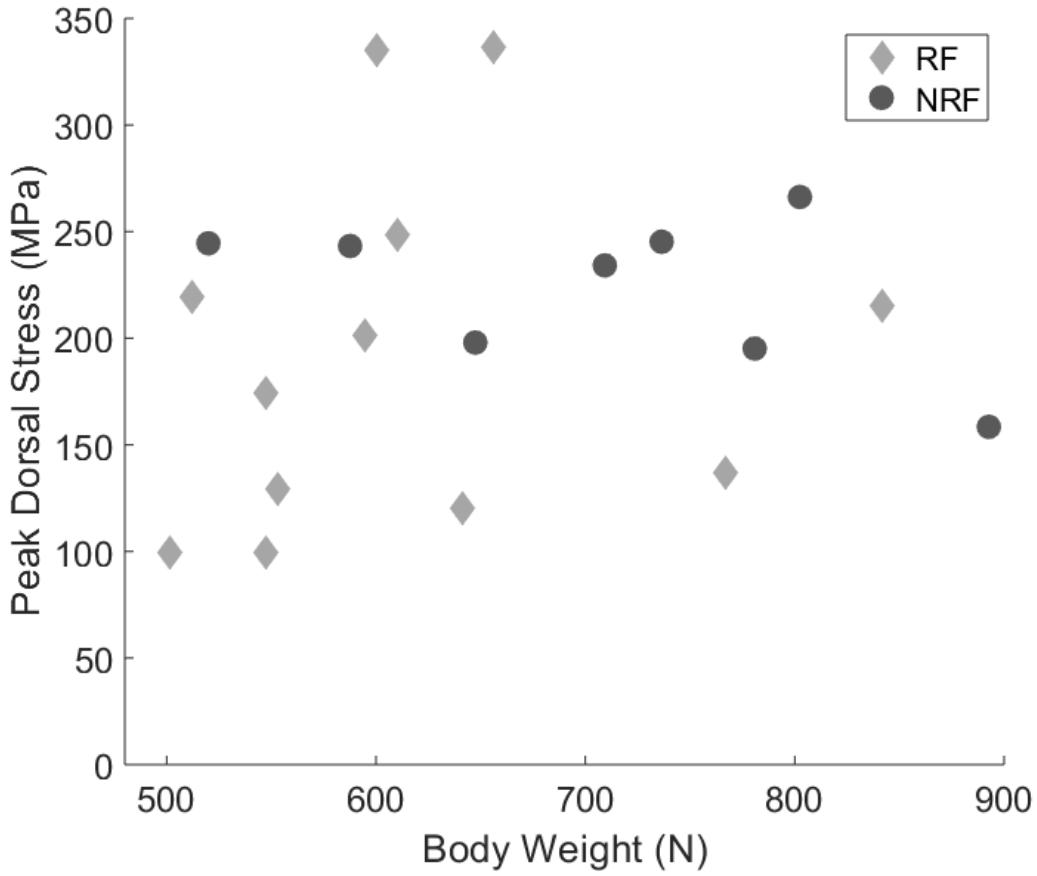

Figure 21: scatter plot displaying individual peak stress values plotted against body weight for rearfoot (RF) and non-rearfoot (NRF) strikers.

4.3.3 SPM Analysis

Comparison of group mean stress time series between foot strikes is shown in Figures 22 and 24. Forefoot strikers showed both greater compressive stress on

the dorsal surface and greater tensile stress on the plantar surface in early stance. The t value throughout stance for both comparisons is shown in figures 23 and 25.

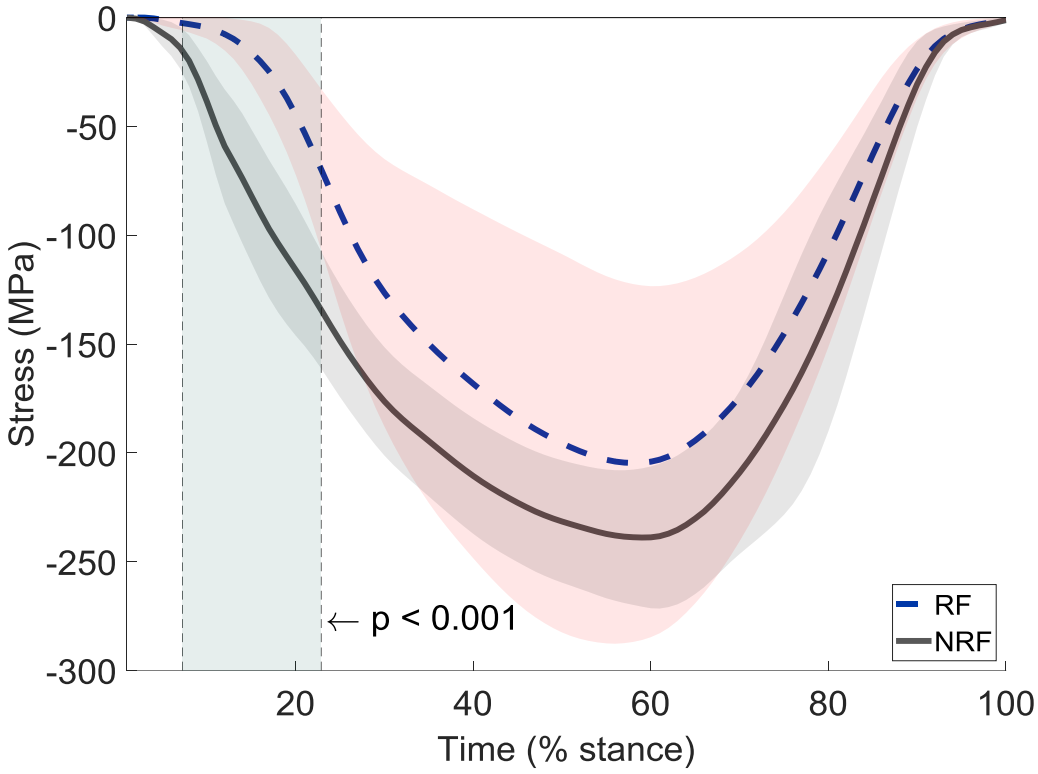

Figure 22: Comparison of dorsal stress between foot strike types. Negative values represent compression. Vertical shaded area shows areas of significant differences.

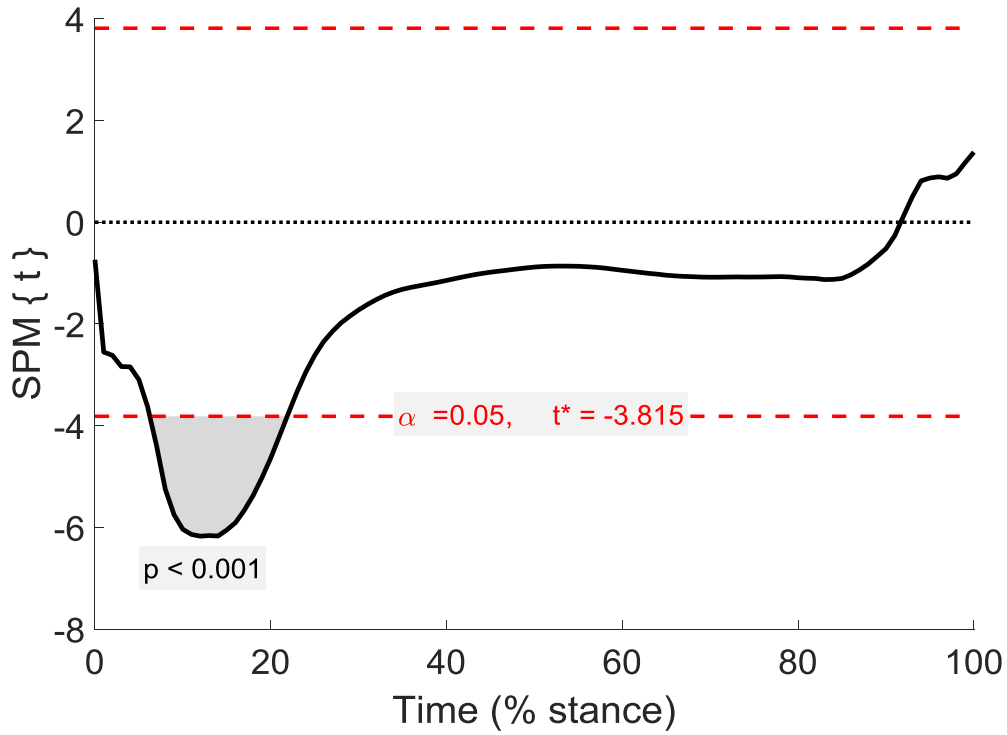

Figure 23: t values for a comparison of dorsal stress between foot strike types across the whole of stance. Area below the alpha line is significant.

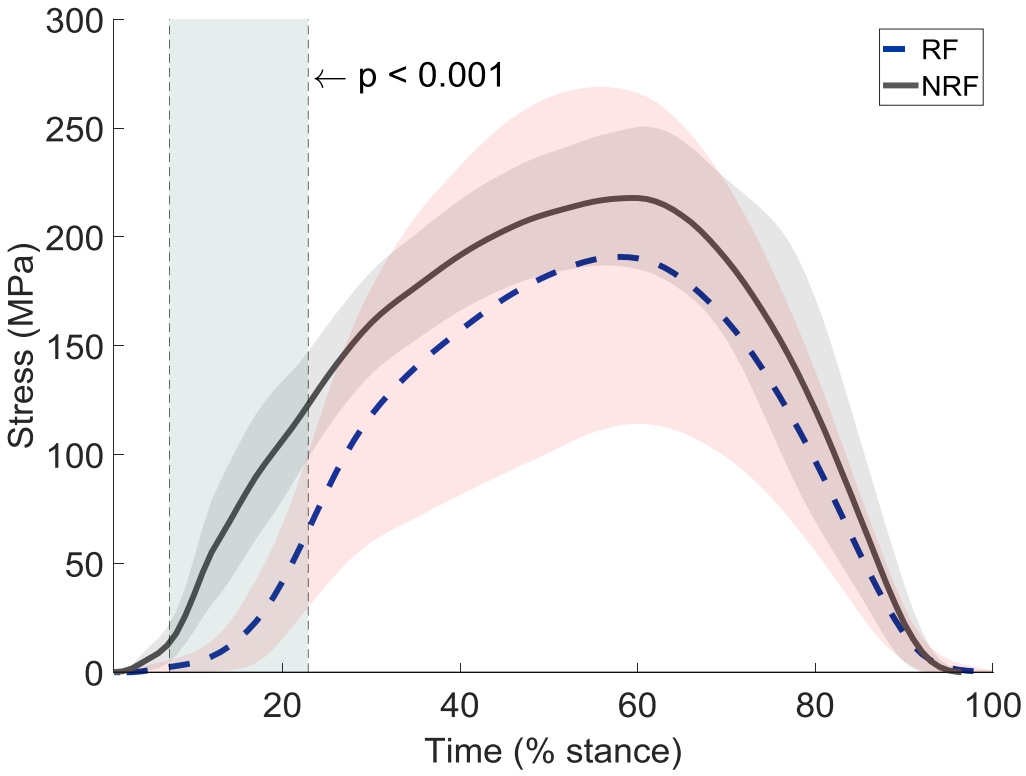

Figure 24: Comparison of plantar stress between foot strike types. Negative values represent compression. Vertical shaded area shows areas of significant differences.

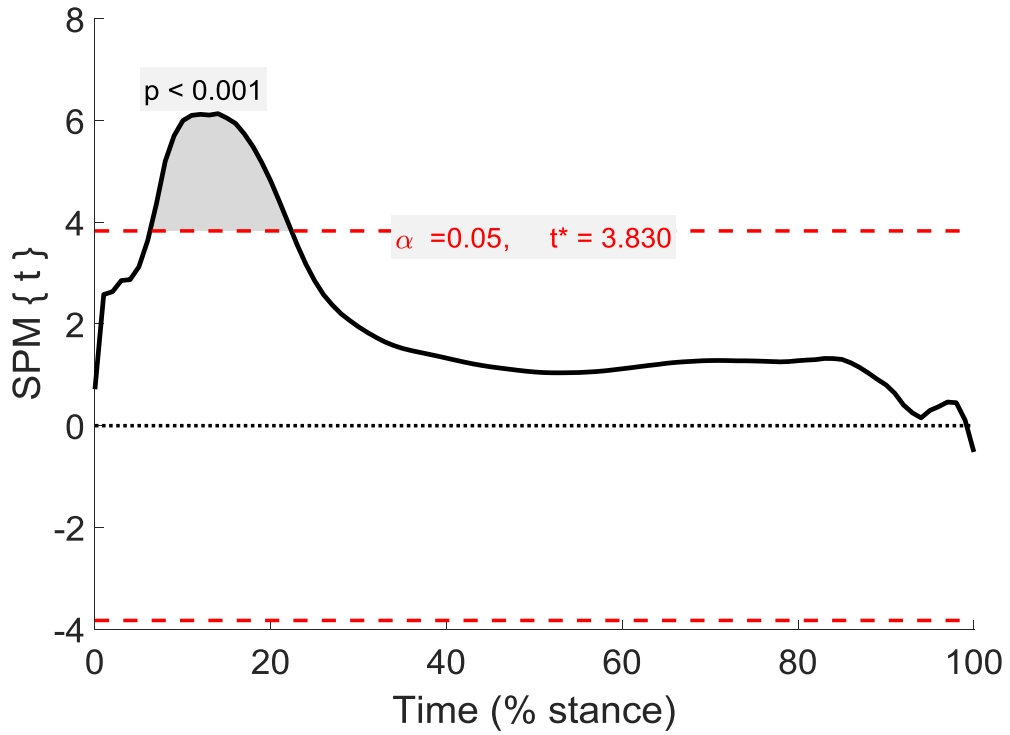

Figure 25: t values for a comparison of dorsal stress between foot strike types across the whole of stance. Area above the alpha line is significant.

4.3.4 Analysis of Additional Points along the Metatarsal Shaft

Figures 26 to 29 show interpolated surfaces of peak metatarsal stress at 10% intervals along the metatarsal shaft. The stress magnitudes are dependent on the participant-specific inertial and cross sectional data. Notably, some areas of the bone show lower stresses despite higher bending moments.

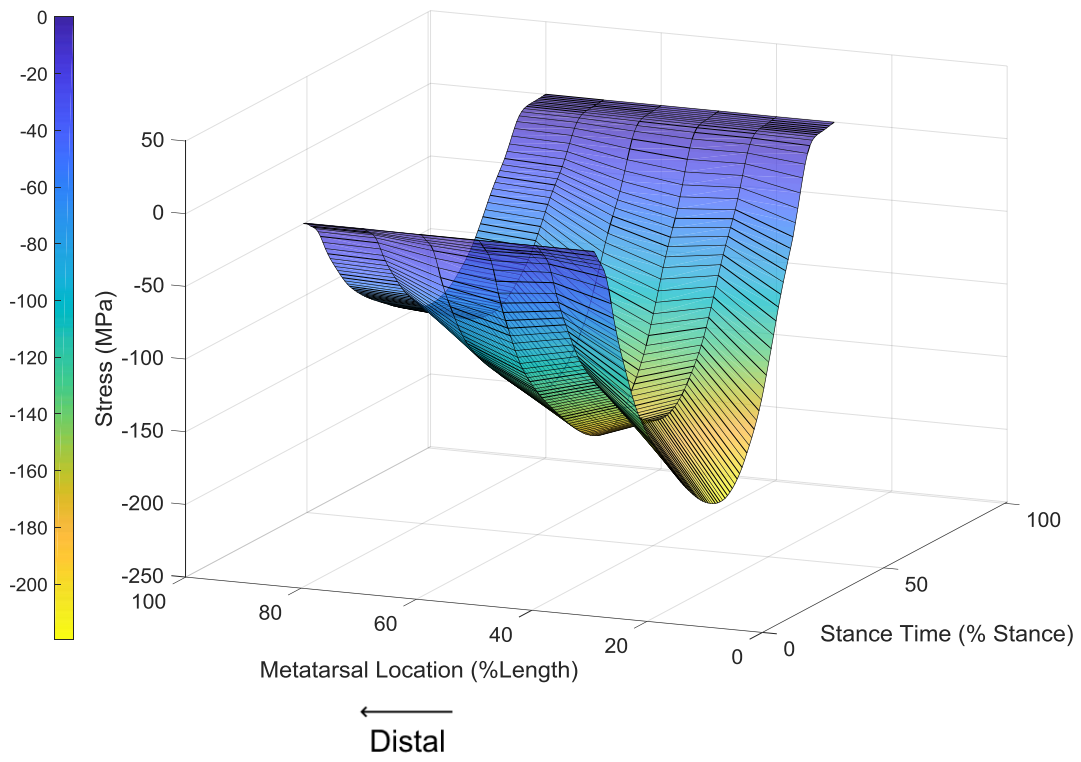

Figure 26: Dorsal stress surface for the single NRF participant. 100% of the metatarsal axis represents the most distal location. Negative values for stress represent compression and positive values represent tension.

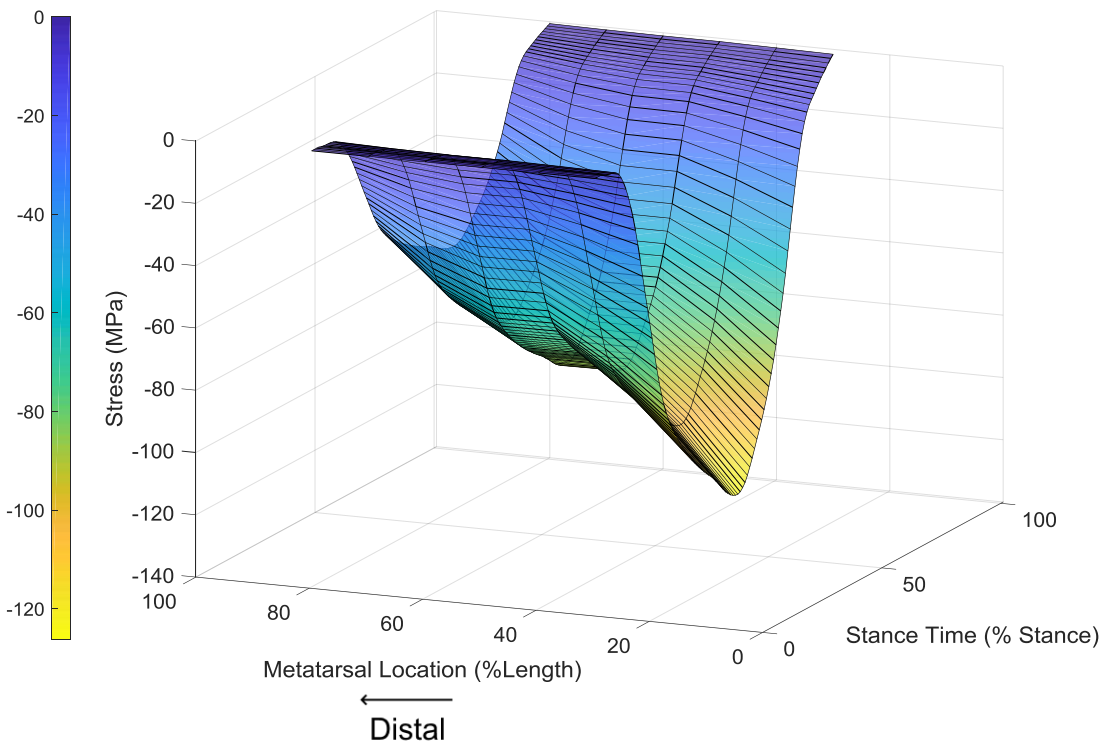

Figure 27: Dorsal stress surface for the single RF participant. 100% of the metatarsal axis represents the most distal location. Negative values for stress represent compression and positive values represent tension.

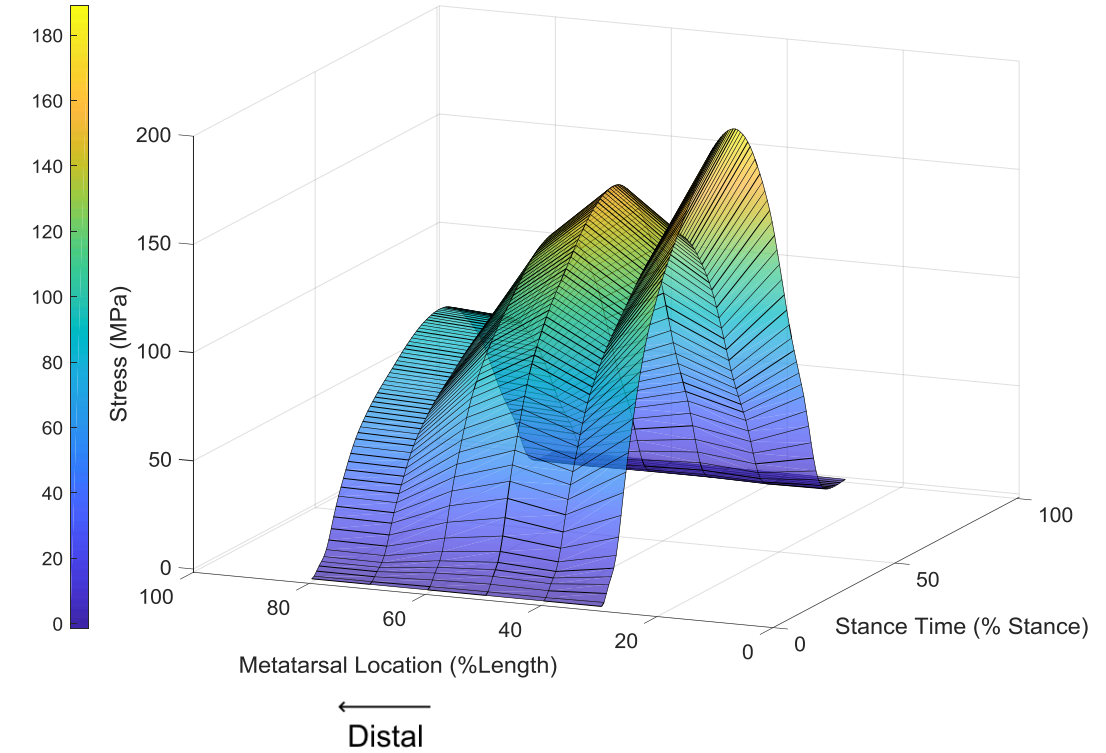

Figure 28: Plantar stress surface for the single NRF participant. 100% of the metatarsal axis represents the most distal location. Negative values for stress represent compression and positive values represent tension.

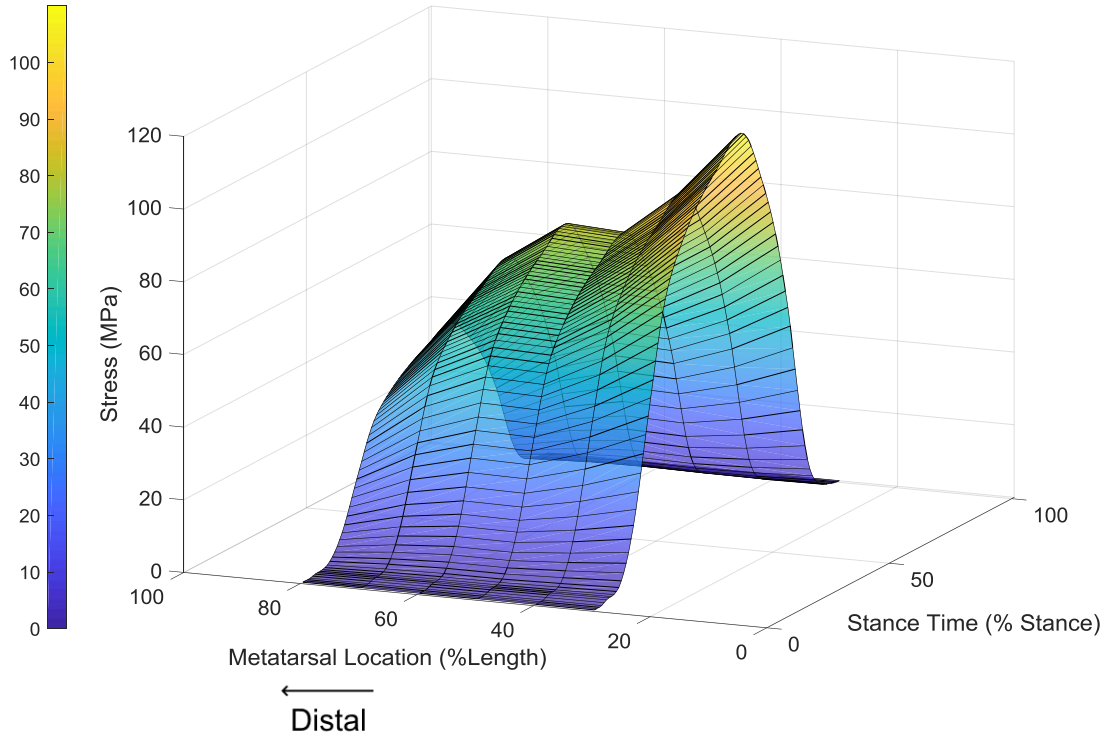

Figure 29: Plantar stress surface for the single RF participant. 100% of the metatarsal axis represents the most distal location. Negative values for stress represent compression and positive values represent tension.

4.4 Discussion

This study developed a novel approach to estimating metatarsal stress during running, adapted from previous beam theory models and with the addition of accurate, participant-specific bone geometry. This new model was then used to compare forces and stresses acting on the second metatarsal during running between runners with different habitual foot strike patterns.

4.4.1 Evaluation

4.4.1a Input Sensitivity Analyses

Results from the input sensitivity analysis give confidence that the model is robust to small errors in measured values. The model is sensitive to changes in variables that are changeable between participants, such as ground reaction forces and

the pitch angle the metatarsal makes with the floor. This suggests that it would be able to detect differences in stresses caused by changes in kinetic or kinematic variables between groups. However the model is also sensitive to small changes in metatarsal length, with an increase of 10% resulting in 19.96 MPa change to stress variables, due to its impact on bending moments. Whilst the model is not sensitive to changes in the cross-sectional area of the metatarsal, it is highly sensitive to the radius of cross-section and inertial inputs, with a 10% increase in either giving a 16.47 or 18.11 MPa increase respectively. These sensitivities again give confidence that the model could identify stress differences caused by geometrical differences between groups. Whilst an increase of 16.47 MPa seems large, it is approximately a 9% increase, consistent with the percentage increase in the input value. Therefore, confidence is required in the reliability of the methods of measurement of geometry values, and participant-specific measurements are necessary to gain a true understanding of stresses when using this model.

4.4.1b Comparison of Running and Walking Results with Existing Studies

For all runners, the dorsal surface of the metatarsal was under compression throughout stance whereas the plantar surface was under tension, with similar magnitudes of stress observed on each surface. Peak pressure acting under the second metatarsal in the present study (RF: 412 kPa NRF: 572 kPa) was similar to that reported by Nunns et al. (2013) (RF: 442 kPa NRF: 464 kPa). Average peak compressive stress across the entire group of runners was 224 MPa in the present study. Gross and Bunch (1989) used a similar modelling approach during shod running to estimate second metatarsal strain, but modelled the cross section as a hollow ellipse. Converting their reported strain value to stress using their reported Young's Modulus (17 GPa) reveals stresses of 113 MPa, far lower than

in the present study. Both models derived stress from midshaft bending moments which were similar between studies (9.35 N.m for rearfoot strikers in the present study compared with 7.71 N.m reported by Gross and Bunch). This suggests the difference in stress magnitudes between studies is predominantly influenced by the difference in metatarsal geometry. There was a large range of area moment of inertia values in the present study (8.15×10^{-11}- 3.83×10^{-10} m^4). When modelling the metatarsals in the present study as a hollow ellipse for comparison with Gross and Bunch the average area moment of inertia was 1.7×10^{-10} m^4, 35 times smaller than the value reported by Gross and Bunch (5.8 e^{-9} m^4), contributing to greater bending stress values despite similar bending moment values. This substantial difference in the inertial properties measured between the two studies is likely to result from the number of estimations made in the study by Gross and Bunch. Firstly, they modelled the bone as a hollow ellipse, which assumes evenly distributed mass about the central axis, and secondly, they used scaled cadaveric data from literature sources for lengths and diameters. Furthermore, the metatarsal stress reported by Gross and Bunch did not include the contribution due to axial compression, although in this study, axial compressive stress contributed only 3.7% on average to total stress and there is no reason to believe any contributions calculated by the methods of Gross and Bunch would not be similarly small.

In-vivo strain estimates obtained during barefoot treadmill running (3.1 $m.s^{-1}$) from two participants were 1891 με and 5315 με (Milgrom et al., 2002). Using the same Young's Modulus of 17 GPa, this equates to 32 MPa and 90 MPa respectively, also lower than the values calculated both in the present study and the value calculated by Gross and Bunch. The average peak stress reported in the present study is higher than reported values for the failure point of cortical bone (e.g. 195

MPa, (Martin et al., 2015)) however, the reported value for the ultimate stress of cortical bone varies greatly depending on the sample site and testing method used (Wolfram and Schwiedrzik, 2016). The disparity between stress values reported in the present study and those reported throughout the literature suggests that relative rather than absolute values are most useful in understanding the influence of different conditions on metatarsal loading.

Table 4 shows Peak output variables for one participant when running and when walking. Stokes et al. (1979) provided detailed results for metatarsals during walking in their study, including time history figures for all outcome variables. Therefore the results of walking data from this study were compared to that of Stokes et al. (1979). It should be noted that whilst the current study assumed an equal division of force between the plantar flexor muscles, Stokes et al. (1979) does not specify the exact division, stating instead that the short plantar tendon was assumed to carry between zero and half of the force carried by the long plantar tendon, providing an upper and lower bound for the output forces. For comparison an average value of the upper and lower bounds provided by Stokes was used. In addition, Stokes et al. (1979) provided each value as a percentage of the average bodyweight of the participants. This analysis is also included here.

Stokes et al. (1979) found axial forces of 535.5 N or 82.75 %BW, which is greater than the forces found in the current study during walking. Bending moments are similar between the two studies with Stokes et al. (1979) finding moments of 7.95 N.m or 1.2 %BW. Although it should be noted that Stokes et al. (1979) calculated the bending moments at the base of the metatarsal, not at the halfway point as in the current study. The shear forces in this study are higher than that of Stokes et al. (1979) who found 142.5 N or 21.05 %BW. These differences may arise from

the treatment of the toe as a rigid segment attached to the metatarsal, rather than calculating joint contact forces as seen in the present study.

Table 4: Peak output variables between walking and running in a single participant

Gait	F_{ax} (N)	F_{sh} (N)	M_{be} (N.m)	σ_d (MPa)	σ_p (MPa)	F_m (N)
Walking	173.29	205.11	6.36	-75.66	70.71	214.82
Walking (%BW)	31.66	37.47	1.16	-13.82	12.92	39.24
Running	295.63	295.18	9.16	-111.27	99.29	297.13
Running (%BW)	54.01	53.92	1.67	-20.33	18.14	54.28

In addition, the time histories of the three primary outcome variables from Stokes et al. (1979) are compared here with the time histories from this study's walking data (Figures 30 - 32). It can be seen that axial force time history for the present study follows a similar shape to that calculated by Stokes, despite differences in magnitudes. The time histories for shear forces and bending moments are different in shape, with the present study registering zero force during early stance in contrast to the shape calculated by Stokes where both shear forces and bending moments in the second metatarsal rise immediately at the onset of stance. The participant analysed in the current study contacted the ground with the heel first and the forefoot did not make contact until 11% of stance on average. With no forces present under the toe during this time, it is not possible using the presented model to estimate the forces experienced by the second metatarsal at this time, although they are assumed to be close to zero. It is not clear whether the participant presented by Stokes walked with different kinematics to the participant in the present study.

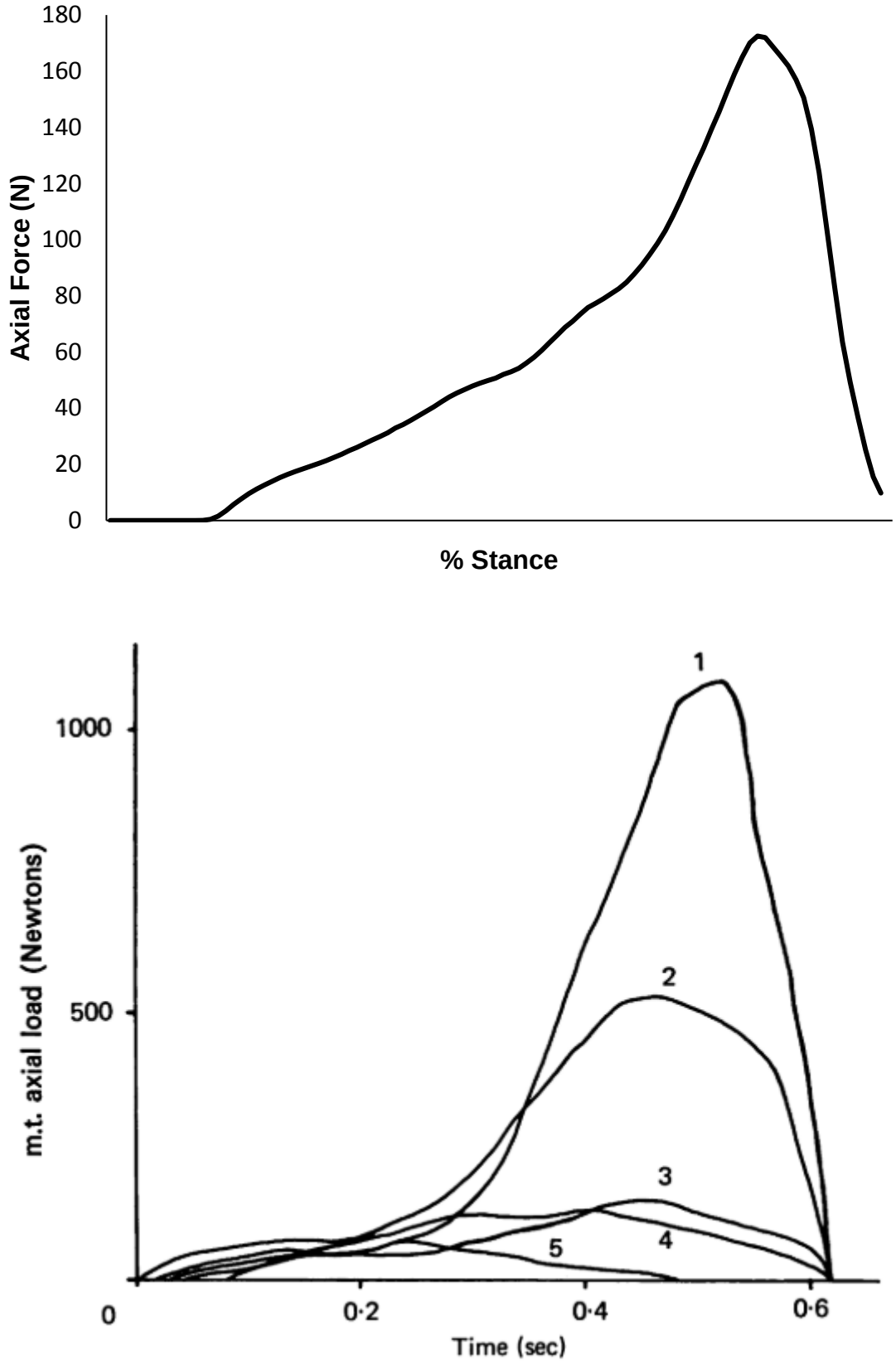

Figure 30: Axial force time history for walking data. Top: Present study, Bottom: Taken from Stokes et al. (1979), line labelled 2 representing the lower bound of second metatarsal forces

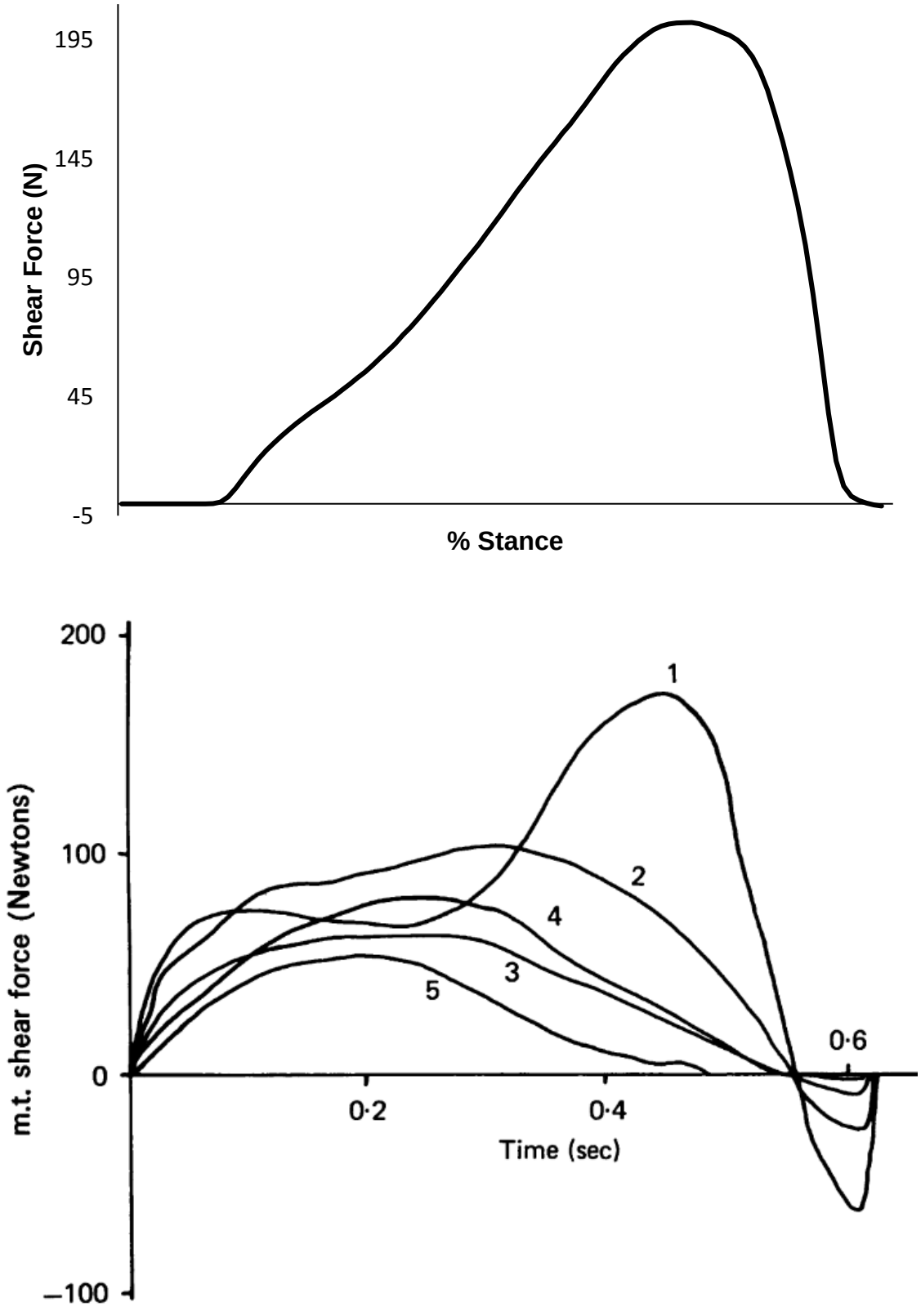

Figure 31: Shear force time history for walking data. Top: Present study, Bottom: Taken from Stokes et al. (1979), line labelled 2 representing the lower bound of second metatarsal forces

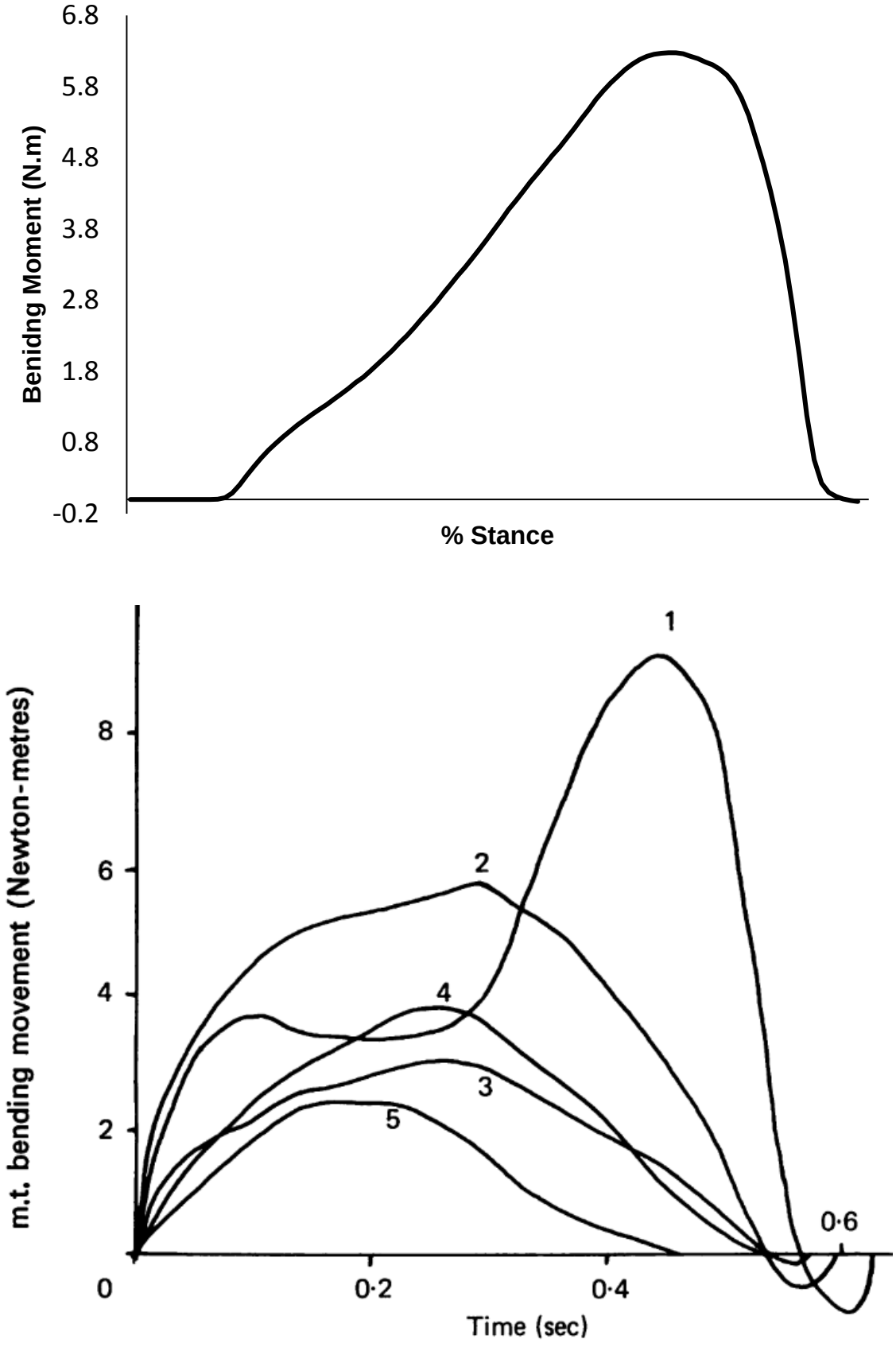

Figure 32: Bending moment time history for walking data. Top: Present study, Bottom: Taken from Stokes et al. (1979), line labelled 2 representing the lower bound of second metatarsal forces

In another mathematical model, Jacob (2001) found that the head of the second metatarsal transfers around 28% BW to the ground, but notes that the range in other studies is 3.3 – 42.4 % BW (Hayafune et al., 1999), and that the forces in the long and short plantar tendons amount to 9% and 13% of bodyweight respectively. In this study, the peak force under the second metatarsal during walking was 39% BW, within the range above. The broad range of values previously reported is indicative of the challenge of validating modelling approaches. In this study the plantar tendons had a peak force of 14 % BW on average between them. This is very similar to the model of Jacob (2001). There are some key differences between the work of Jacob (2001) and the present study, namely the use of cadaveric feet to acquire the data, including direct measurement of geometry. Without knowing the origin and quality of the feet, it is difficult to assess how valid it is to compare the work of Jacob (2001) to the present study where all the feet belonged to healthy, relatively young runners.

Milgrom et al. (2002) reported stains of 2707 με and 2663 με in two participants during barefoot walking with an implanted strain gauge, equivalent to 46.02 MPa and 45.27 MPa respectively using a Young's modulus of 17 GPa. This study reports stresses of 75 MPa, again higher than measured experimentally. The exact location along the shaft of the strain gauges is not noted by (Milgrom et al., 2002), which could affect the magnitude of any strains recorded.

4.4.2 Analysis of Differences between Groups

In contrast to the hypothesis, peak compressive and tensile stresses were not different between non-rearfoot and rearfoot strikers. Both compressive and tensile stresses were greater during early stance in non-rearfoot than rearfoot strikers according to SPM analyses, but no differences were observed at the time of peak stress. Observation of individual peak stress values (Figure 21) supports

this, demonstrating no marked differences in stress magnitudes between groups, influenced in part by a wider range of values in the RF runners. The differences in early stance could be expected based on the more anterior foot contact in non-rearfoot than rearfoot strikers, but it is important to note that the peak stresses occurred at the same point during stance in the two foot strike categories. Therefore the significant differences in stress between these groups only occurred in early stance when the stress magnitudes were lower. The magnitude of bone stress is understood to be important when considering risk of stress fracture, but it is not well-established what magnitudes of peak stress may be detrimental. Therefore these results suggest that foot strike does not influence the magnitude of peak metatarsal stress during running, and therefore may not influence the risk of stress fracture via this mechanism.

The external forces acting under the metatarsal head were significantly greater in the non-rearfoot runners than rearfoot runners, and this was also the case for all calculated variables, other than shear forces, that did not include participant-specific bone geometry (axial force and bending moments). However the stresses - which are influenced by participant-specific bone geometry - are similar between groups. This supports recent research suggesting that external loading measures such as plantar pressures and ground reaction forces may not be a good method of estimating internal loading (Matijevich et al., 2019) as well as research suggesting that geometry is the largest determinant of metatarsal stress magnitude (Nunns et al., 2017). This is further supported by the stress surface plots, displaying areas of lower stress despite larger bending moments, a finding shared with the work of Nunns et al. (2017). It may also support the mechanostat theory that habitual loading leads to bony adaptation in order to better resist that loading (Frost, 1987).

4.4.3 Limitations

The model presented provides a useful tool to allow non-invasive estimates of internal metatarsal loading during barefoot running. However, models require assumptions and these introduce limitations. The model used did not account for surrounding soft tissues in the foot such as the fat pad under the metatarsal heads. This soft tissue plays a role in cushioning and distributing the forces acting at the sole of the foot, in this case the forces measured externally to the foot were assumed to apply directly to the bone, leading to overestimation of stresses. In addition to soft tissue cushioning, several potential soft tissue mechanisms for reducing the strain on the metatarsal bone were not modelled, namely the short and long plantar ligaments, which attach near the base of the metatarsal and act passively to support the tarsometatarsal joints; and the plantar aponeurosis, which acts to support and maintain the longitudinal arch of the foot and has the mechanical effect of reducing the bending in the metatarsal. Modelling of the forces in these tissues, particularly the plantar aponeurosis is likely to reduce the bending moments in the second metatarsal. Modelling the interaction of these soft tissues in the foot would be a beneficial next step in investigating the forces in the metatarsals during different running conditions.

Although the geometry considered was participant-specific, only non-deformable geometry was included and this does not reflect the complex shape of the metatarsal. Additionally, the cross-section was considered to be symmetrical, whereas in reality there are differences in the mass distribution between the dorsal and plantar halves of the metatarsal shaft. It is not clear how much difference an asymmetrical calculation would make to these results, but this would not only be influenced by the geometry of the bone but also the density of the bone. Similarly, the vector angle used to determine the angle between the

metatarsal and the ground does not account for deviation of the foot away from the direction of travel. In addition the cross section of the metatarsal used assumes orientation of the metatarsal to be fixed with regard to the forces acting on it, whereas in reality the change in angle during stance is likely to change the inertial information and the resulting radius. It has already been seen in section 4.3.1 that the modelled stresses are sensitive to changes in *I* and *r* and just a 10% adjustment in either will change the stress values by around 20 MPa. This is a significant limitation that warrant further investigation in subsequent studies. A finite element model would effectively remove this limitation as the geometry of the entire bone is modelled.

This study assessed metatarsal stress during barefoot running, whereas the vast majority of runners wear shoes during running. Previous studies have shown that the choice of footwear can affect external forces differently depending on foot strike modality (Rice et al., 2016). Assessment of metatarsal stress during barefoot running removed the confounding influence of footwear, but does not truly represent the habitual running condition of the participants. Footwear introduces an additional layer of cushioning under the foot, and has an unknown effect on the mechanics of metatarsal bending, therefore it is not clear whether footwear would act to increase or reduce stresses on the metatarsal in both groups, one of the groups or neither. Measuring the motion of individual sections of the foot such as the metatarsals whilst shod is particularly difficult, as the shoe moves independently of the foot and bony land marks are obscured. It is normal practice in this case to modify the shoe by removing material, such that markers can be directly attached to the skin. However, this in itself alters the response of the footwear to the activity being studied (Balsdon and Dombroski, 2018) and for practical purposes, requires shoes that the participants may not be familiar with,

or may not be sized appropriately. In the case of this study the use of barefoot running is acceptable, but future research should build on the results here to include shod running.

Lastly, the group representing non-rearfoot strike runners included both midfoot and forefoot strikers and these groups have different kinetic and kinematic characteristics (Nunns et al., 2013). However, the standard deviations of the peak stress values for this group were smaller than for the rearfoot strike group, providing confidence that this grouping is robust when assessing peak second metatarsal stress.

4.4.4 Conclusions

In conclusion, the model presented here appears to overestimate the stresses present in the second metatarsal, as measured using *in-vivo* strain gauges, particularly during running. However, it compares more favourably with other 2D models, particularly during walking. Other models of running, such as that of Gross and Bunch (1989), produce values for stress that, whilst lower than the values presented here, still overestimate stresses when compared to strain gauge data. Whilst direct measurement using strain gauges is the gold standard, they are associated with numerous limitations and so should be used cautiously. Upon evaluation, the model presented is capable of discerning differences in internal loading between groups displaying differing running characteristics, but should not be used to infer the risk of stress fracture injury as it is not known what magnitude of stress is clinically relevant to the development of a stress fracture and the model appears to overestimate absolute magnitudes of stress. Results from the group comparison indicate that forefoot strikers had greater second metatarsal stress than rearfoot strikers during early stance, but there was no difference between groups in peak stress. Furthermore, it was observed that a

difference in external forces does not necessarily lead to a difference in internal loading. This suggests that measurement of external forces to infer injury risk is flawed, and that either direct measurement or a participant-specific approach to modelling internal forces is necessary.

Overall these results suggest that beam theory models may overestimate stresses in the metatarsals in general, but may be valuable for addressing applied questions in which a between-participant change in stress is of interest. Comparison of beam theory models with alternatives is discussed in Chapter 7.

5. Development of a Three Dimensional Finite Element Model of Metatarsal Stresses during Running

Evaluation of the beam theory model presented in Chapter 4 resulted in the suggestion that a model of metatarsal stresses which incorporates full and deformable geometry would provide valuable information. Furthermore, it was suggested that estimates of the attenuation of forces under the metatarsal head due to the plantar soft tissues warranted inclusion. Therefore the aim of this study was to develop and evaluate a participant-specific finite element model to investigate the magnitudes of forces and stresses acting on the second metatarsal during running. Design of the model was based on the evaluation of the model developed in Chapter 4, aiming to address some of the limitations of the model presented there. Increasing the complexity of the model would inevitably lead to increased computation times. The model developed would remain viable for investigating larger groups of participants by finding the optimum complexity that would provide valuable estimates of metatarsal stresses without requiring the lengthy computation times of models of the entire foot. Due to the longer run times of finite element models compared with the 2D beam theory approach, it was not feasible to simulate every point of stance. Therefore several time points corresponding to important points of stance were simulated.

It was hypothesised that the maximum metatarsal stress estimated by the 3D finite element model would more closely represent previously measured *in-vivo* values than the 2D beam theory model from Chapter 4.

5.1 Model Design

The development of the model began with the mathematical description of internal forces described in section 4.1. The evaluation of the 2D beam theory

model presented in section 4.4 demonstrated that participant-specific geometry was valuable when calculating stresses experienced by the second metatarsal. In a similar approach to the study of Garcia-Aznar et al. (2009), the metatarsal bone was modelled with two layers of bone (cortical and trabecular) that were segmented using MRI. The forces from joint contact with the phalange were applied to the metatarsal directly, similar to (Firminger et al., 2017), whilst the ground reaction force under the metatarsal head were applied via a simulated floor surface and a representation of the plantar soft tissue, similar to (Akrami et al., 2017). This novel approach of modelling the second metatarsal bone with its surrounding soft tissue combined some of the advantages of existing models without the computational expense of a full foot model.

Assumptions of the model were:

1. Forces due to accelerations of the components are negligible (Stokes et al., 1979)
2. Only flexor muscles act to deform the metatarsal during ground contact.
3. The second ray of the foot is independent of other metatarsals and toes (Stokes et al., 1979)
4. Forces and kinematics in the mediolateral direction are negligible

Developing a participant-specific finite element model that can be used to compare between groups of participants requires that the construction of the model is consistent across all participants. Therefore a systematic set of steps was developed, ensuring the reconstruction of tissues and their subsequent assembly into a model was reproducible for each participant. These steps are covered in detail in the following sub chapters.

5.2 Methods

The development of a finite element model from data capture through to calculation follows a well-defined set of steps set out in Morales-Orcajo et al. (2015b) and also in (Akrami et al., 2018). These steps are:

1. Data Collection – the scanning of relevant body parts by appropriate methods, as covered in section 3.4.
2. Reconstruction – the generation of computerised representations of body parts from the scanned data files.
3. Processing – the smoothing and refining of created geometries and the creation of any additional model parts, such as representations of the floor. The assembly of these parts into a 3D representation of the system.
4. Calculation – The meshing of modelled parts using appropriate element shapes, the application of boundary conditions and loads based on measured external loading.
5. Validation – The evaluation of the model by comparison to experimental outcomes.

Steps two, three and four are covered in detail below.

5.2.1 Segmentation of Geometries in Simpleware ScanIP

Segmentation of MR images to create 3D representations of bone and soft tissue was completed in Simpleware ScanIP (Synopsys, CA, USA). 3D geometries of body tissues were reconstructed by segmenting a slice based on the intensity of each pixel. This created a mask representing a 2D slice of the tissue of interest, and was repeated for all slices containing the tissue of interest. ScanIP software has a number of tools and automated procedures that reduce the time required

to segment tissues and increase the accuracy and repeatability of the created masks.

After initial import of raw MR slices in all three planes, the images were smoothed using a recursive Gaussian filter (Figure 33), with a sigma value of 1 pixel. This smoothing procedure homogenises some of the tissue types, such as trabecular bone and makes them more likely to contain a narrower range of pixel intensities, which improves automated thresholding results.

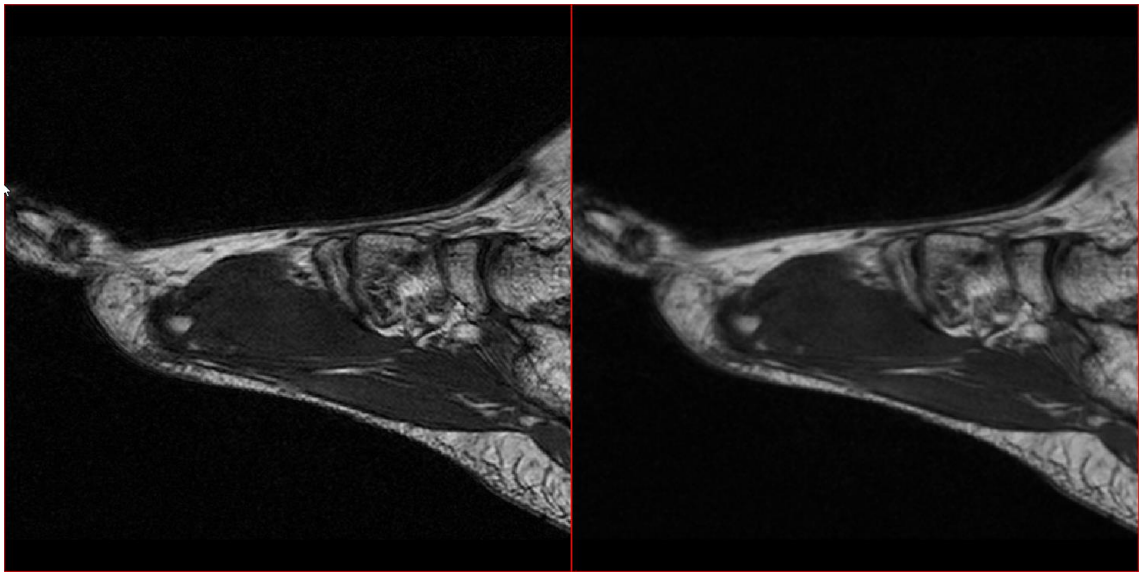

Figure 33: A sagittal plane MRI slice before smoothing (left) and after (right).

The first section segmented was the trabecular bone due to its high visibility and clearly defined boundaries. Initial segmentation was completed in the frontal plane (Figure 34), and the “paint with threshold” tool was used. This allowed the investigator to “paint” a mask over the entire image, but only assigned a mask to those pixels that were within a defined range of intensities. The threshold was set manually based on the view of the entire sagittal plane view of the mid bone. Adjustments were made based on the threshold preview to cover as much trabecular bone as possible without infringing on other tissue types (Figure 34).

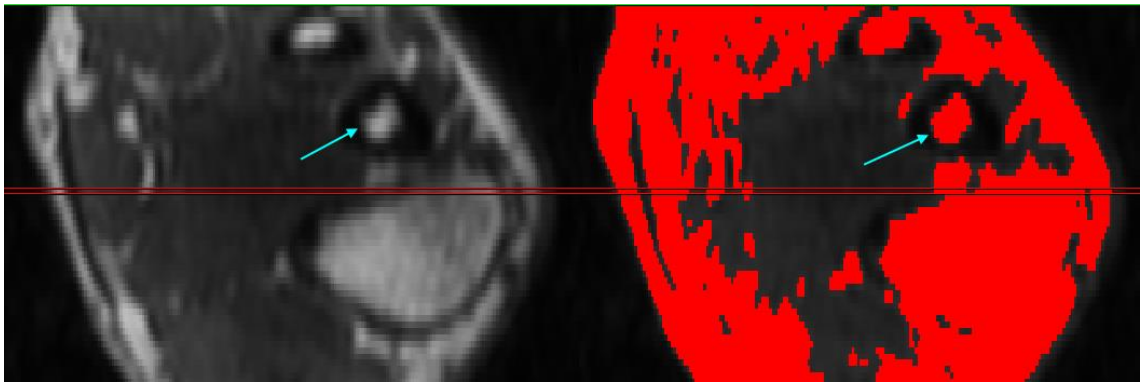

Figure 34: Coronal MRI slice showing 1st, 2nd and 3rd metatarsal cross sections (left). The same slice is shown on the right with thresholding highlighted. The thresholds are selected to cover the maximum area of trabecular bone in the second metatarsal (blue arrows), without infringing on other tissues.

In the frontal plane the slice at mid-shaft was initially painted as this region is a relatively consistent shape between slices. After painting this slice, the propagate slice function constructed the trabecular diaphysis by painting every other slice based on the intensities of the initially painted slice. Each new automated mask shape was checked manually before being propagated to the next slice. At the epiphysis, where bone shape changes rapidly between slices, threshold painting was done manually. In this manner a series of slices were built up representing the outline of the trabecular bone (Figures 35 and 36).

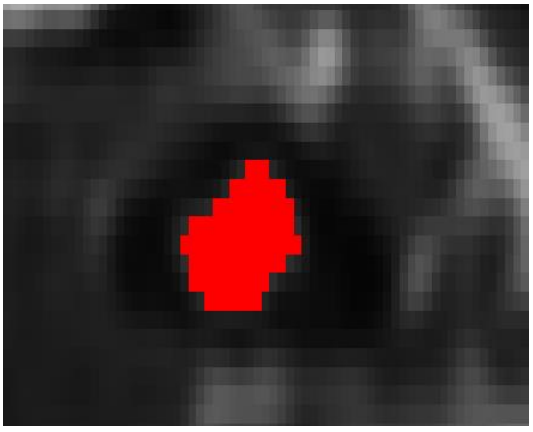

Figure 35: A midshaft slice showing threshold painted mask covering the trabecular bone.

Once the whole bone had been ‘painted’, the thresholding was checked in the sagittal and transverse planes, to ensure a visibly good match to bone geometry

according to the judgement of the investigator. Once this was satisfactory, the slices were interpolated to create a solid shape (Figure 36).

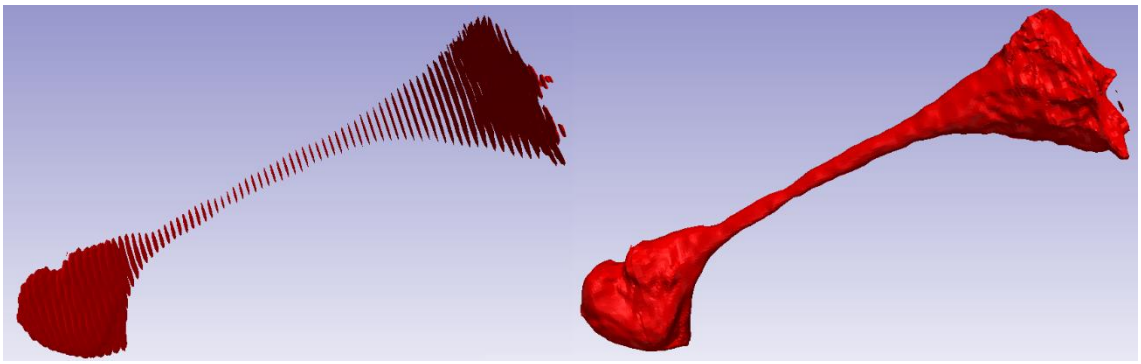

Figure 36: A series of slices are created making up the trabecular bone (left), these are then interpolated to form a solid shape (right).

The shape created via this process is an imperfect representation of the bone geometry, as it is highly faceted, and may contain either cavities inside the geometry or islands of mask unattached to the main shape. These required correction before the geometric mask could be used for other purposes. In order to correct this, firstly a morphological close function was performed on the mask. This is equivalent to dilating the entire 3D region by a set number of pixels and then eroding by that number of pixels. The erode function only applies to edges and the dilate function reduces the number of edges, as small features merge together. This had the effect of removing small holes and edge features whilst preserving the overall shape of the mask. This was refined if necessary. A cavity fill was then used to fill any cavity that was completely enclosed by the mask. Lastly, island removal removed any volume of mask lower than a set threshold. The threshold was set based on the size of pixels in the largest island. Several islands can be seen at the proximal end of the mask in Figure 36. There is no risk of the island removal mask changing the shape of the main mask, therefore it was run repeatedly until all islands were confirmed by the investigator to have been removed.

The final shape was smoothed using a combination of dilate, recursive Gaussian and erode functions. First the mask was dilated by one pixel. It was then smoothed with the recursive Gaussian with a sigma value of 1.5 pixels then the smoothed shape was eroded by one pixel (Figure 37). This was compared to both the unsmoothed shape and the background image in both 3D and 2D views to ensure a good fit according to the judgement of the investigator.

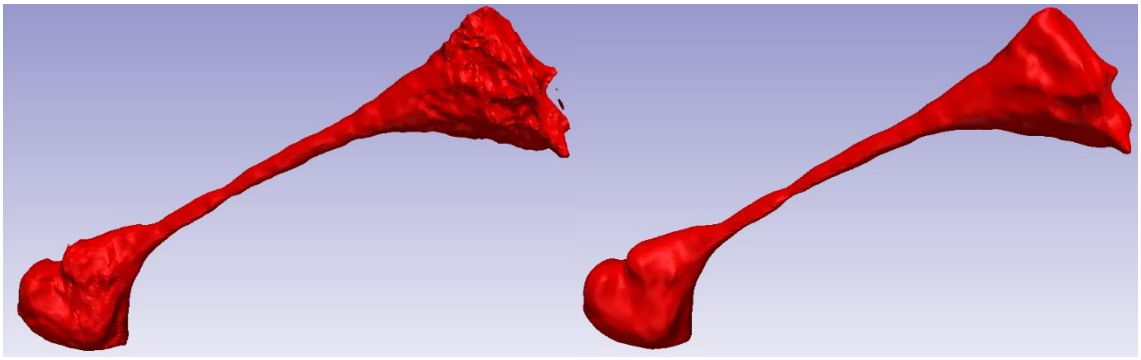

Figure 37: Trabecular mask prior to smoothing, island removal and cavity filling (left) and after (right).

Once the trabecular bone was segmented, the cortical bone was added. The trabecular bone was duplicated and dilated by one pixel to become the basis for the cortical bone. As cortical bone is distinguished by having a very low intensity, the background view was manipulated to display this more clearly. “Paint with threshold” was again used and adjusted manually to best represent the cortical bone. Painting was completed in the sagittal plane, using the duplicated trabecular bone as a guide, and no slices were skipped. All cortical bone segmentation was completed manually. Once masking was complete, the steps outlined above were used to check, improve and smooth the shape (Figure 38)and this was checked in the 3D view against the trabecular bone mask to ensure that the cortical mask had not been excessively eroded and that the trabecular bone mask was completely contained within the cortical bone mask.

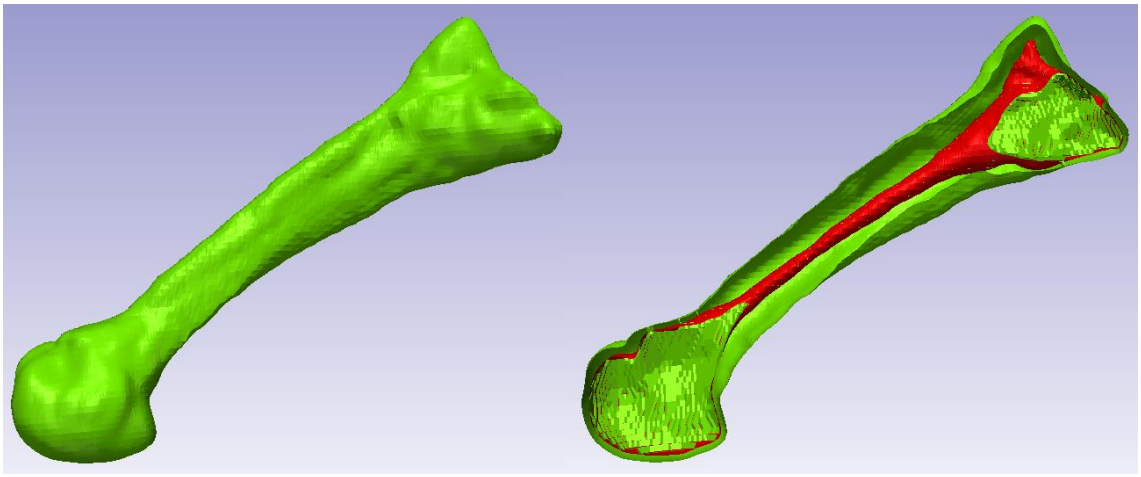

Figure 38: Finalised cortical bone mask (left) and cutaway showing inner trabecular bone (right).

Finally the encapsulating soft tissue was segmented using the intensity of the MR image. Initially, the entire foot section was segmented using a global threshold, which applies a mask to any pixel above a certain intensity range on every slice (Figure 39). This was then smoothed, cavity-filled and islands removed. The fish oil capsules were manually removed from the mask.

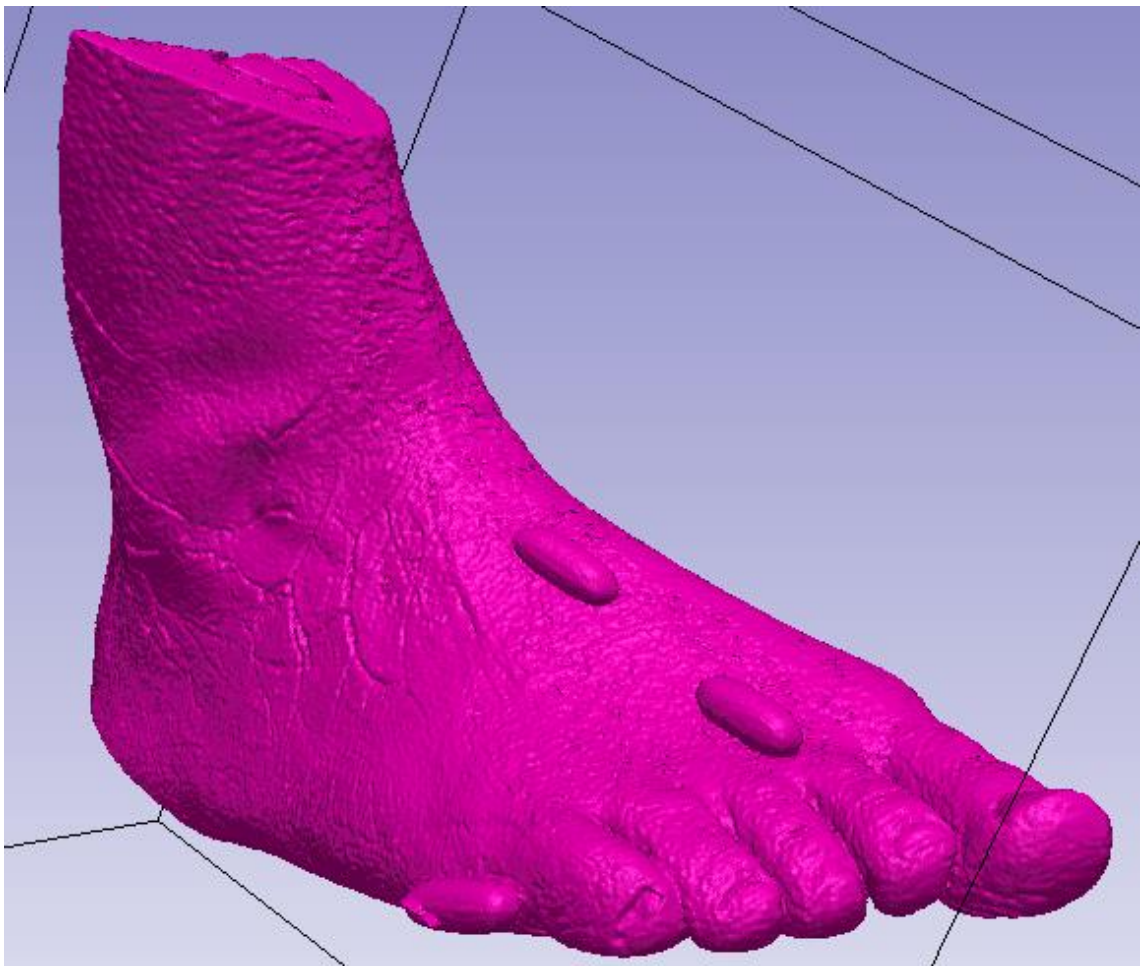

Figure 39: The 3D mask created by thresholding the entire foot, prior to smoothing and filtering operations. Clearly seen are the fish oil capsules which are placed in similar locations to the motion capture markers

In order to isolate the soft tissue surrounding the second metatarsal, the mask was reduced in size such that it only included tissue immediately surrounding the bone and tissues present during floor contact under the metatarsal. This was achieved in a systematic manner, by creating a temporary co-ordinate system with one axis aligned along the longitudinal axis of the bone. This created a new set of slices aligned with this co-ordinate system. Following this the mask was removed from all tissue that was two slices either side of the bone in the sagittal plane. The split region tool isolated this region to leave a 3D volume containing only the tissues surrounding the second metatarsal (Figure 40).

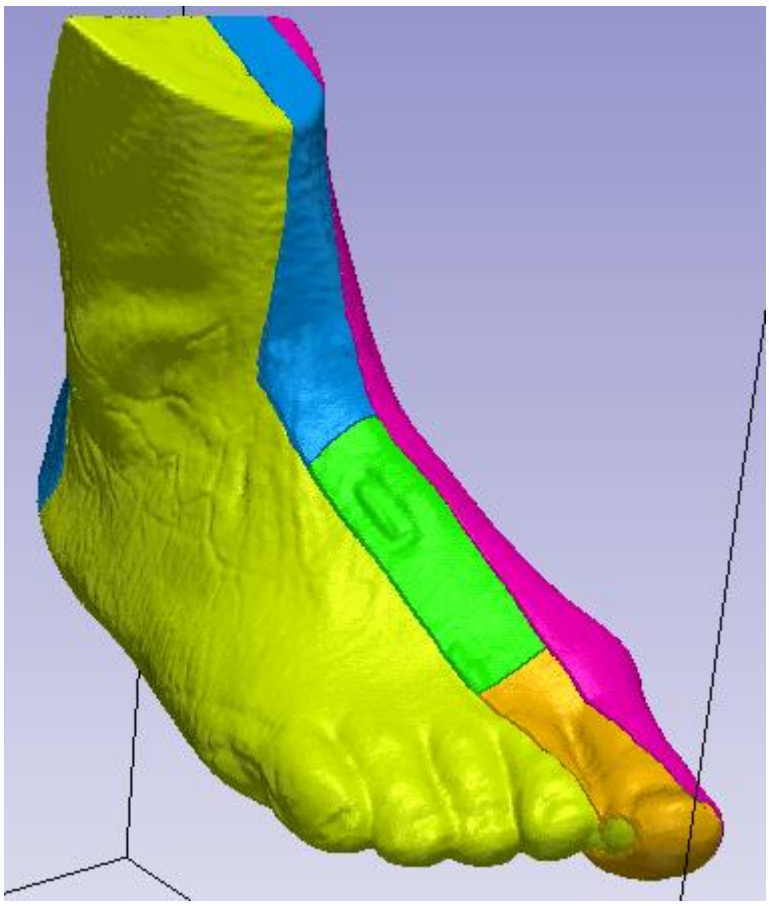

Figure 40: 3D mask representing the whole foot after sectioning to identify the tissues surrounding the second metatarsal (green mask), the indentations left by the fish oil capsules can be seen on the second metatarsal and the head of the fifth metatarsal in this figure.

As in the model presented in Chapter 4, and previously in the literature (Firminger et al., 2017, Gross and Bunch, 1989, Stokes et al., 1979) the metatarsal was to be modelled as a cantilever, fixed proximally. Therefore it was required that the proximal end of the bone was exposed from the soft tissues in order to have boundary conditions applied to it. For this purpose, a section of approximately 14 – 17 slices of soft tissue mask was removed at the proximal end of the metatarsal bone. A temporary co-ordinate system was again used with one axis aligned along the longitudinal axis of the bone, allowing slices to be removed that were perpendicular to this axis. The number of slices removed was adjusted as necessary to ensure that the whole epiphysis was exposed and that a minimal amount of diaphysis was exposed. Further smoothing was conducted after the

sectioning of these areas to remove any artefacts left by the sectioning process (Figure 41).

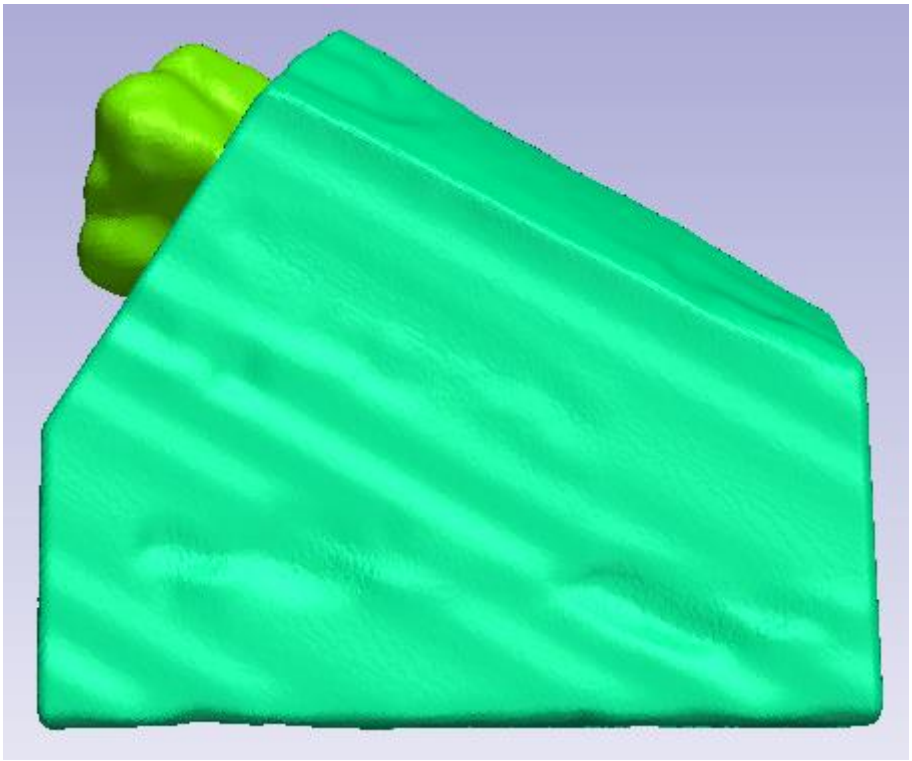

Figure 41: The 3D masks for both the cortical bone and the surrounding soft tissues, showing the extent to which the proximal end of the bone was exposed

Individual masks were imported from ScanIP software as STL surface model files using the global MR coordinate system and millimetres as the scale length. The final model was assembled and calculations carried out using Abaqus software (Simulia, Providence, U.S.A). STL files were converted to STP files, which can be read by the Abaqus software package using CATIA (Dassault Systèmes, USA) which was used to assign boundary surfaces and develop the solid structures of the bone and soft tissue masks.

5.2.2 Importing of Parts to Abaqus

In Abaqus, individual parts were created and assigned individual attributes, such as material properties, or meshes. These were then assembled and interactions between parts, loading conditions and boundary conditions were assigned.

Finally the methods of iterating the model towards a convergent solution were defined and the model was simulated. In this section the various steps of model construction in the Abaqus software suite are discussed.

Initially cortical bone, trabecular bone and soft tissue parts were imported separately and meshed with a coarse mesh to ensure there were no meshing errors due to geometry, where a coarser mesh requires less computation time. If any errors were observed, either in the geometry import or in the meshing process, the part was returned to ScanIP for additional smoothing procedures. The process of smoothing and reimporting to Abaqus is iterative, and often needed several cycles per part before meshing could proceed.

The volume representing both the whole foot and the smaller volume of soft tissue were imported to Abaqus. The whole foot was used to generate reference axes for the assembly. Two axes were created. The first recreated the line between the proximal and distal second metatarsal markers positioned during experimental data collection. Two points were identified on the soft tissue which approximated the centre of the indentations left by the fish oil capsules (Figure 40) which were positioned using the same method of palpation as the 3D motion capture markers. The second axis was created in a similar manner representing the line between markers placed at the distal first and distal fifth metatarsals (Figure 42).

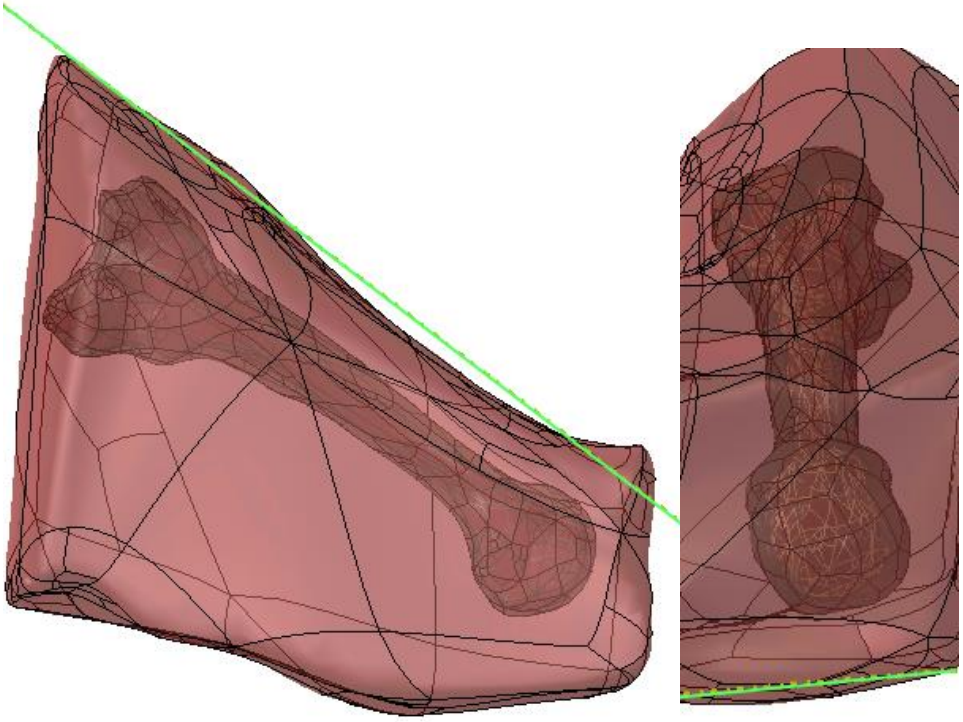

Figure 42: Left – Sagittal plane image of the metatarsal and soft tissue, showing the axis aligned along the metatarsal. Right – Frontal plane image of the metatarsal and soft tissue showing the axis aligned between the fifth and first metatarsal heads. Note the axis has been colour enhanced for clarity in this figure.

Lastly a surface representative of the floor was created using the built in CAD features of the Abaqus software. A volume of 200 mm by 100 mm by 10 mm was extruded for this.

Once the trabecular bone, cortical bone and soft tissues had been imported and meshed with no errors, material properties were assigned to each part (Table 5). The properties of the bony tissues were selected based on Garcia-Aznar et al. (2009), who found these properties to perform better than homogeneous bony tissue in a study of stress in the metatarsals. Encapsulating soft tissue properties were based on Akrami et al. (2017).

Table 5: Model parts and their material properties.

Part	Material Type	Element Type	Young's Modulus (Mpa)	Poisson's ratio
Cortical Bone	Solid, linear elastic	Tetrahedral	17,000	0.3
Trabecular Bone	Solid, linear elastic	Tetrahedral	700	0.3
Encapsulating Soft Tissues	Solid, linear elastic	Tetrahedral	1.15	0.49
Simulated Floor	Solid, linear elastic	Hexahedral	50000	0.1

5.2.3 Assembly

Parts were combined in the assembly module. The co-ordinate systems of each part were equivalent to the global co-ordinate system of the magnetic resonance scans and therefore align in Abaqus with the exact positional information they were created with in ScanIP. For example the trabecular bone was correctly aligned inside the cortical bone and did not require positional adjustment (Figure 43).

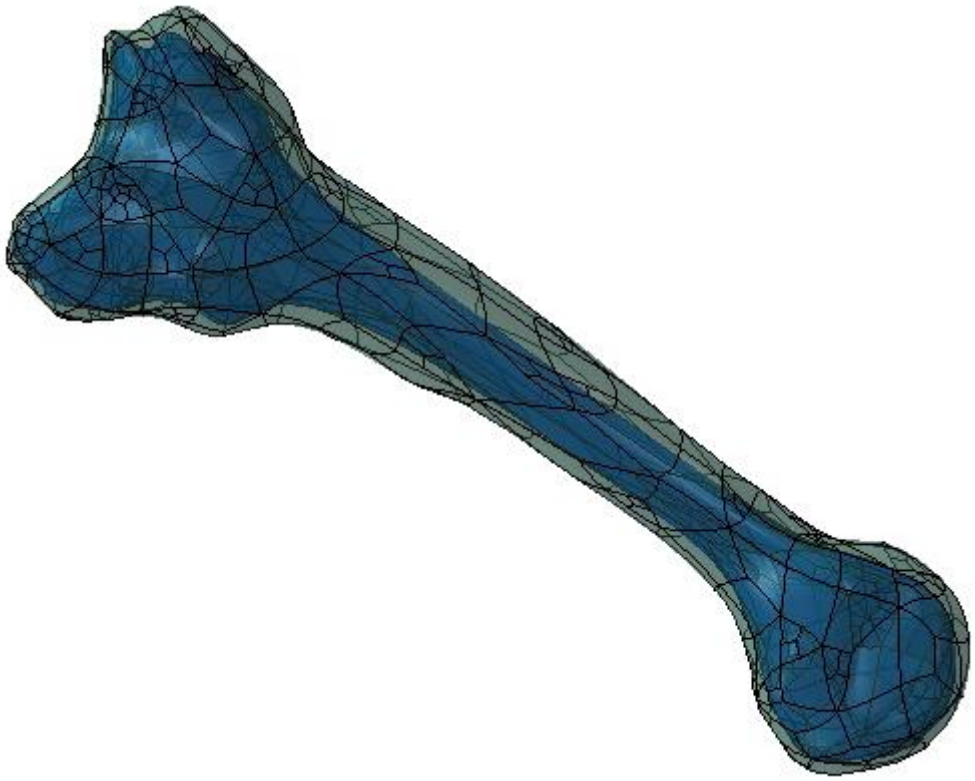

Figure 43: The cortical bone (pale green) showing perfect of alignment of trabecular bone inside it (blue)

The interaction between parts required consideration. It was necessary to remove the soft tissue from where the cortical bone would sit, and this was achieved using a Boolean operation in the assembly module. The trabecular bone was modelled as an embedded region within the cortical bone mask. The defaults for tolerances between the two parts were used, similar to the work of Li et al. (2017). No

movement was allowed at the interface between the cortical bone and soft tissue, and default values for tolerance were again used.

After checking for convergence and errors, a test boundary condition was applied by constraining a single face of the proximal bone using an encastre condition. This allowed no translation or rotations to occur during the analysis of the application of a test load condition of 100 N. This was applied to a single face on the underside of the soft tissue part. In order to minimise computation time for the test analysis, each part was meshed using a coarse mesh with an average element size of 5 mm.

The floor part was added to the assembly and moved to coincide with a node on the lower surface of the soft tissue. Each simulation of the model calculated stresses at a single time point of stance, reflecting different orientations of the metatarsal relative to the ground. In order to represent this the floor was placed in the appropriate orientation for each time point. First, a parallel edge constraint aligned the long edge of the floor with the metatarsal reference axis (Figure 44), and the shorter edge of the floor to be parallel with the mediolateral reference axis.

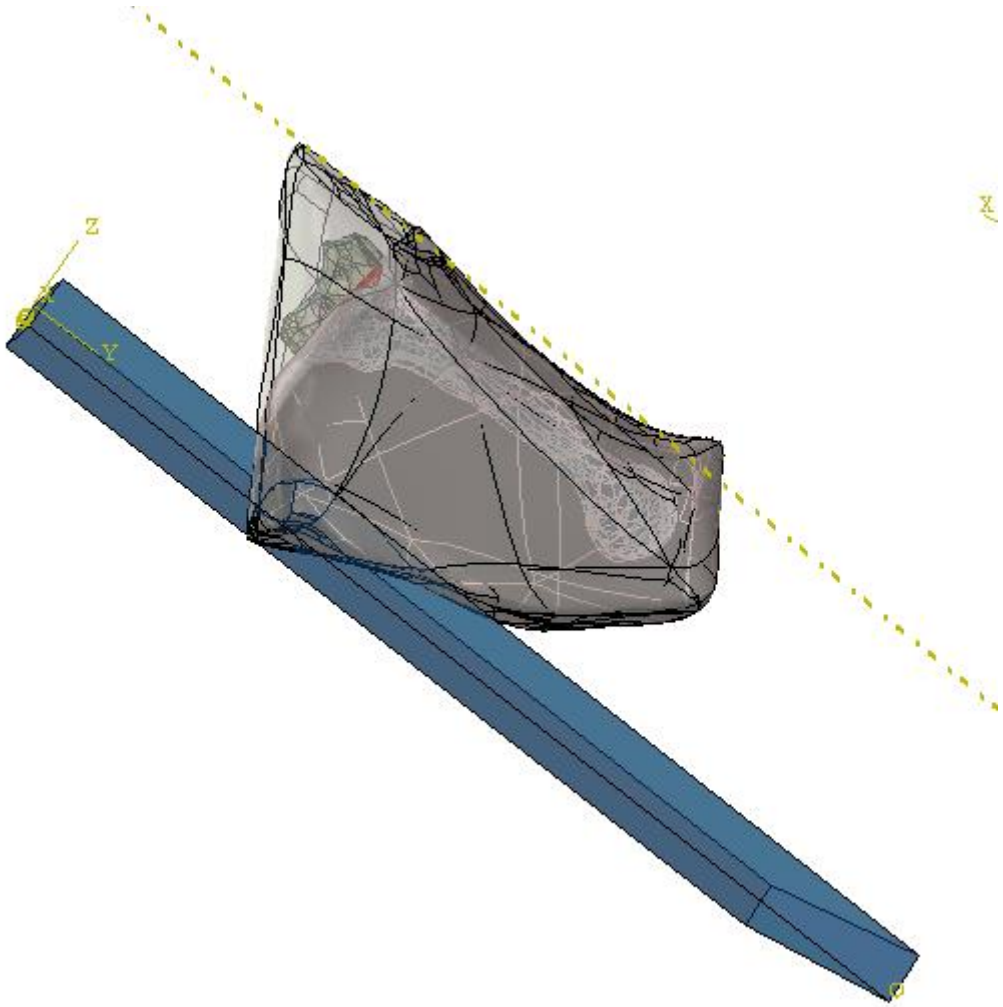

Figure 44: The simulated floor (blue) is moved parallel to the reference axes (yellow dashed line)

The floor was then rotated by the angle between the ground and the metatarsal, in both the sagittal and frontal planes, according to the kinematic data (section 3.2) (Figure 45). A greater sagittal plane angle represents a proximal metatarsal that was higher vertically than the distal metatarsal, and a greater frontal plane angle represents a forefoot in which the fifth metatarsal was higher vertically than the first metatarsal.

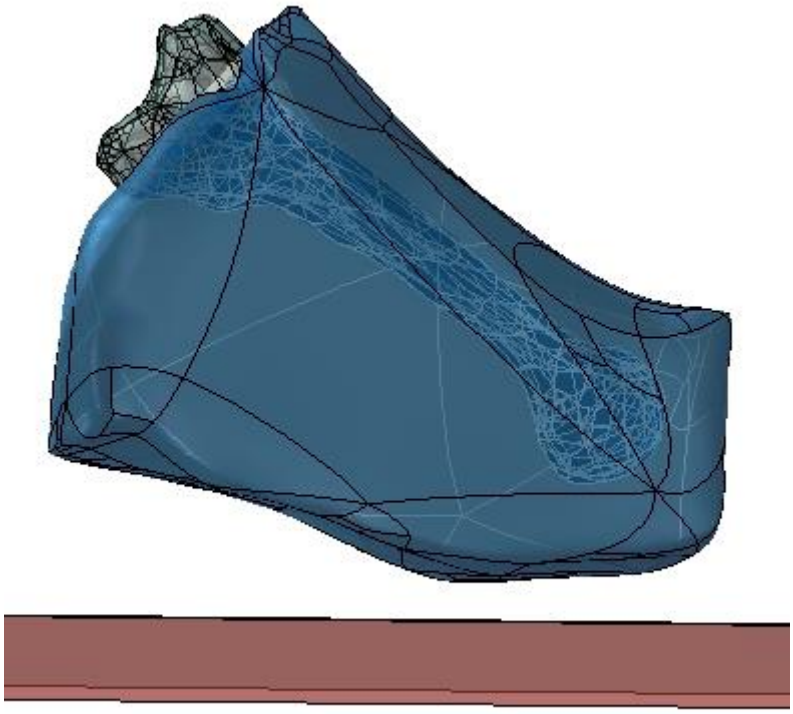

Figure 45: The floor is rotated into the correct inclination with reference to the metatarsal and soft tissues

A contact interaction was set between the floor surface and the underside of the soft tissue part using the surface to surface interaction tool. (Figure 46). Two interaction properties represented the contact in both the normal and tangential directions. In the normal direction “hard contact” was selected, such that the surfaces may not pass through each other. In the tangential direction, a friction penalty was applied using a coefficient of 0.6, based on previous models using experimentally captured data of the friction between the sole of a human foot and the ground (Akrami et al., 2017).

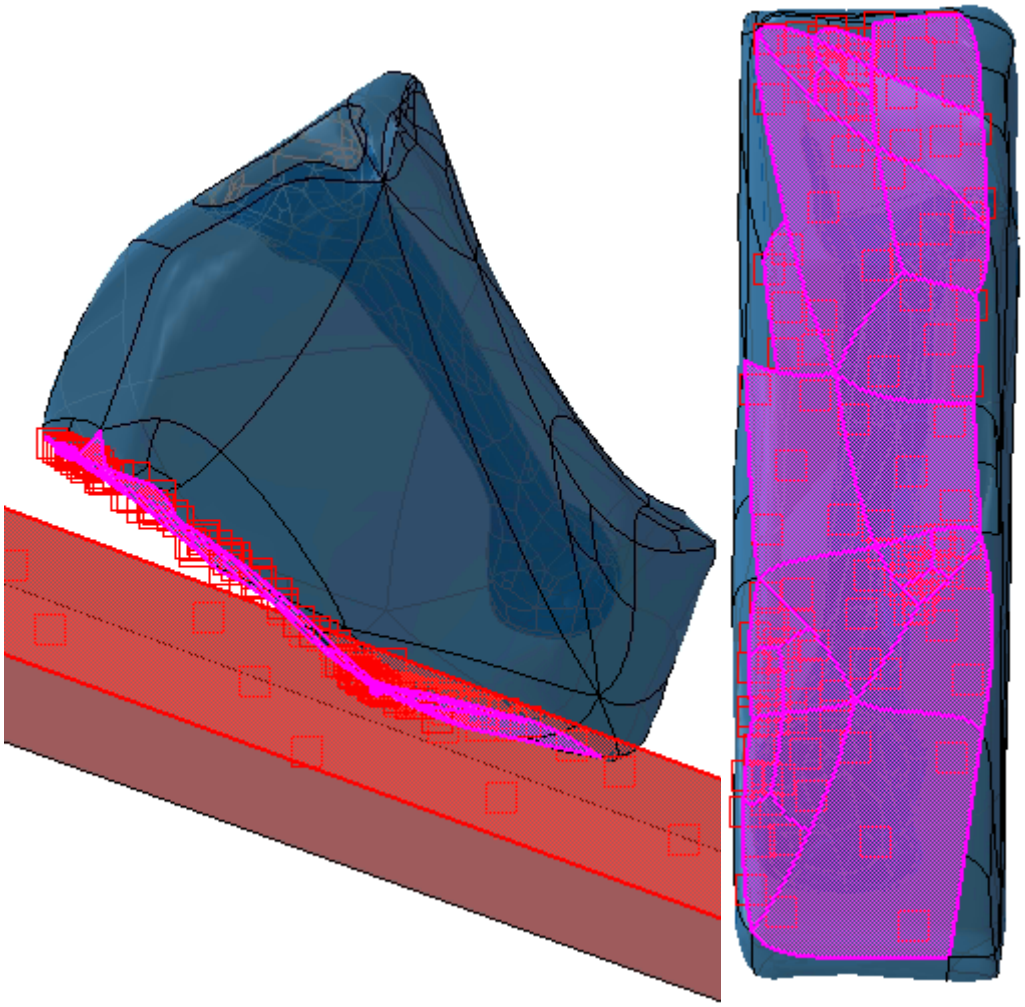

Figure 46: Left – The soft tissue and floor showing the master contact surface (red shaded area) and slave contact surface (purple shaded area). Right – The underside of the soft tissue showing the extend of the slave surface (purple shaded area)

It is a requirement for valid simulation that the floor and soft tissues begin the simulation in contact with each other, but without parts overlapping. The floor surface was translated into perfect contact with the underside of the foot using a vector generated by a custom Matlab script. The current co-ordinates of both the floor and soft tissue were imported into Matlab where the upper surface of the floor was redefined as a plane using two vectors. Each node of the soft tissue was then projected perpendicularly onto this plane and the length of each vector between the soft tissue nodes and the floor surface was calculated. The node with the minimum distance between soft tissue and floor surface was returned

and the floor was translated in Abaqus by this distance perpendicular to the surface of the floor (Figure 47).

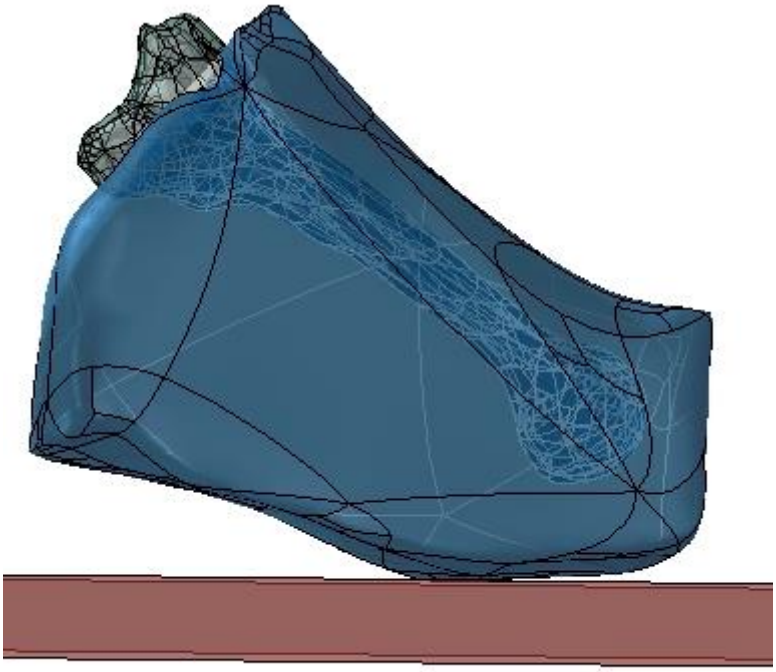

Figure 47: Fully assembled model in contact with the simulated floor surface

5.2.4 Loads and Boundary Conditions

Once assembled the model was loaded using an appropriate approximation of the forces experienced during running or walking. The proximal end of the bone was fixed in place using an encastre condition, whereby the nodes of the mesh were unable to translate or rotate. The remainder of the model was allowed to move freely as determined by the force applied.

The experimentally-determined vertical and anterior-posterior ground reaction forces were applied to the model via the simulated floor surface which allowed the floor to move only in the vertical and anterior-posterior directions respectively. In addition, joint contact forces as calculated in Chapter 4 were applied to the model. These were applied as a force vector to the most anterior 2% of nodes on the bone. This percentage was selected in order to systematically approximate

the contact area between phalange and metatarsal head and was visually similar in proportion and position to the area seen by Flavin et al. (2008) in a simulation of the contact between the first metatarsal and phalange (Figure 48).

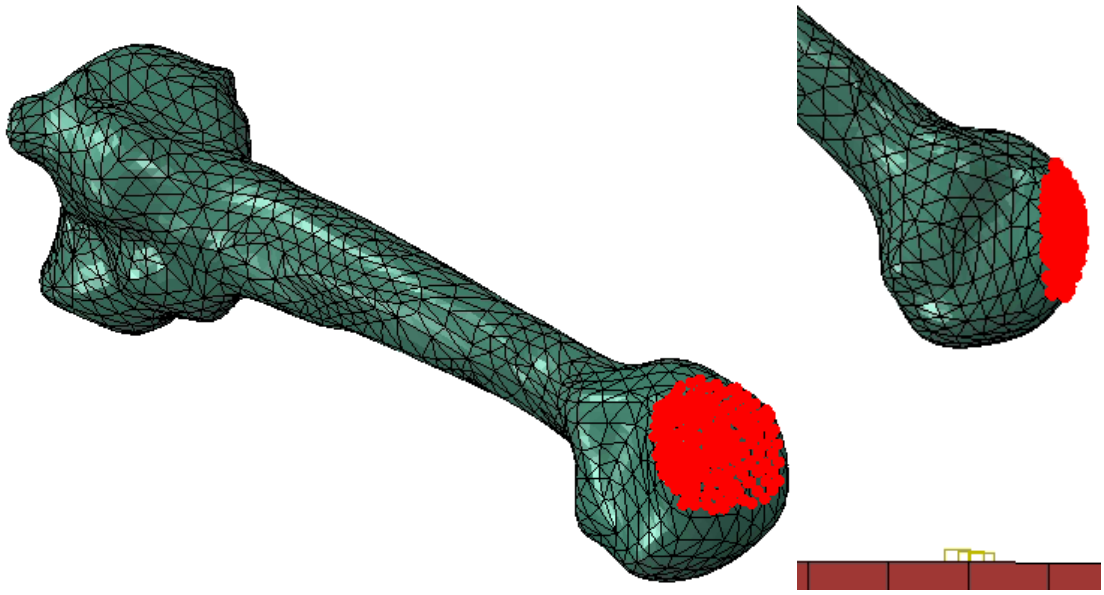

Figure 48: Left – Whole metatarsal view showing the area selected to receive joint contact forces. Right – Sagittal view showing anterior 2% of nodes selected

5.2.5 Mesh Generation and Sensitivity Analysis

Mesh properties have a direct impact on both computation time and result accuracy (Akrami, 2016). Therefore the mesh generated in this study has been assessed for its quality, and the sensitivity to the size of the average element have been computed.

For the purposes of mesh refinement and sensitivity analysis a point of stance representing the time of greatest vertical ground reaction force was investigated in one participant and then evaluated in a second participant to ensure that the mesh properties determined by the refinement process were not unique to one individual participant. The characteristics of the two participants were:

1. female; age: 49 years; mass: 55.8 kg; height: 1.62 m; RF
2. male; age: 19 years; mass: 91 kg; height: 1.85 m; NRF

The average element sizing for each part as determined by the refinement process was used in all other participant models, thus whilst each participant may have differing numbers of elements in each modelled part due to individual geometry and foot size, the sizes of elements making up the mesh were consistent across participants.

Two types of element were used in this study. For the complex tissue geometries of the cortical bone, trabecular bone and soft tissues a quadratic tetrahedral element was used (C3D10). This element type has 10 nodes per element which gives better accuracy compared to a linear element with 4 nodes (Gíslason and Nash, 2012) and is very versatile, enabling it to represent these complex geometries. For the floor surface a simpler element type was used (C3D8R): a linear hexahedral element with 8 nodes, which is suitable for representing regular geometric shapes. Meshing was conducted using a free meshing algorithm, which is fully automated. The initial global element size for each part was selected to be 5 mm.

When a mesh is generated, there are several important properties that affect its ability to produce accurate results in a model: skewness, aspect ratio, smoothness and number of elements. In general a mesh made of a greater number of smaller elements will produce more realistic results, however the greater the number of elements the greater the computation time required to arrive at a solution. Therefore a sensitivity analysis was conducted to determine the optimum mesh element numbers for each part separately. All computations listed here were performed on a machine running the Windows 7 operating system (CPU: Core i5 3470 @ 3.20 GHz, Ram: 8 GB).

Initially all element sizes were large and were then adjusted to produce denser meshes (smaller elements). Each iteration used a mesh density that was approximately double the number of elements of the previous iteration, resulting in reduced average element seed size. The meshes were subject to identical loading conditions and the result of the highest von Mises stress in the cortical bone was used to determine the optimum mesh size for that part. Meshes of other parts were held constant at the initial value whilst the analysis was conducted. Finally, to check for a possible interaction effect between parts, a model was constructed with the optimum mesh sizes in all parts and this was compared to a model with double the element numbers in all parts.

5.2.5a Floor Surface

The floor surface element size varied between 50 and 3750 elements. Initial element size was set at 20 mm, producing 50 elements. This produced a maximum stress of 33.3 MPa on the bone and a maximum contact pressure of 0.2 MPa on the surface of the floor. The pressure changed by 13.3% when increasing the elements in the floor from 50 to 91; 16.2% from 91 to 200 elements; 21.7% from 200 to 406 elements and 4.0% from 406 to 900 elements (Figure 49). Run time increased by seven minutes from simplest to densest mesh. The small change in the contact pressure between 406 and 900 elements indicates that the mesh should not be sensitive to further increases. Maximum stress on the bone increased from 33.3 MPa to 35.4 MPa (+6.0%) from simplest to densest floor mesh. Therefore an element size of 6.66 mm corresponding to 900 elements was selected because despite the relatively fine mesh, the computation time was fast due to the regular geometric shape of the element.

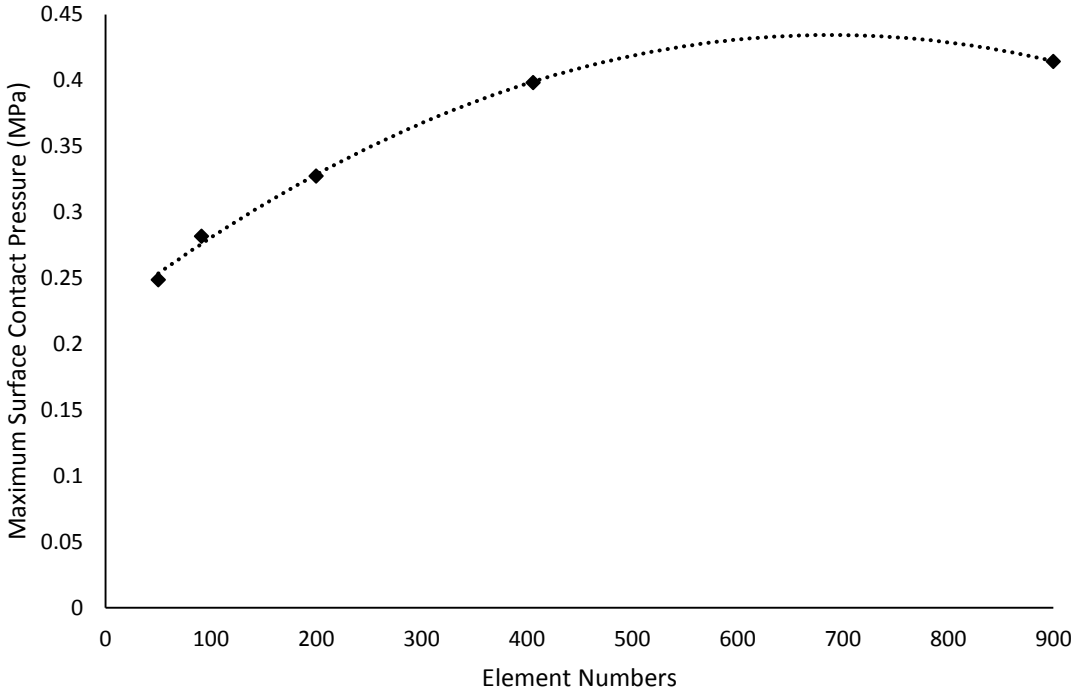

Figure 49: Maximum surface pressure of the floor vs element number

5.2.5b Bone

The mesh of the bone was then subjected to a similar procedure. The initial mesh used an average element size of 10 mm and 5281 elements, as this was the coarsest mesh that could be created. Initial results showed a bone stress of 34.9 MPa. Increasing the element numbers to 10303 gave a stress of 36.7 MPa (+5.1%) and doubled the computation time. A second doubling to 20496 elements gave a maximum stress of 36.4 MPa, a change of only -0.8% but increased the computation time to approximately 27 hours. Therefore 10303 elements was deemed optimal, resulting in an element size of 2.35 mm. The model was highly stable to changes in trabecular bone mesh density. Variation between 8430 elements and 36761 elements yielded only a 0.02 MPa difference in maximum stress on the cortical bone with corresponding computation times of 8430 elements: 29 min; 16726 elements: 37 min; 36761 elements: 45 mins. Based on this 8430 elements were used. Examples of the influence of cortical bone mesh on run time and maximum stress is presented in Figure 50.

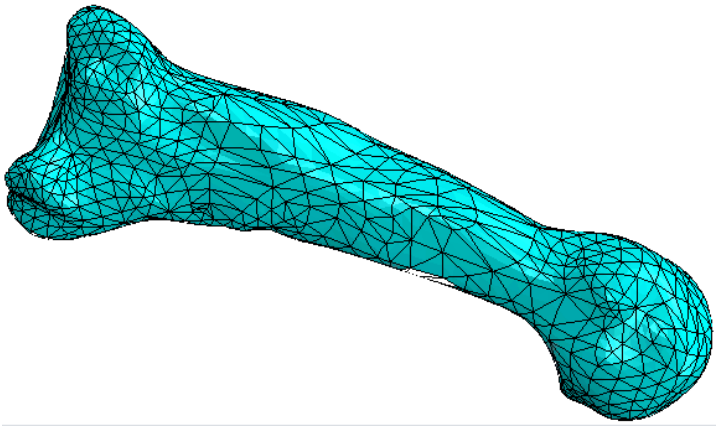

5281 Elements; runtime 35 min; max von Mises stress 34.9 MPa

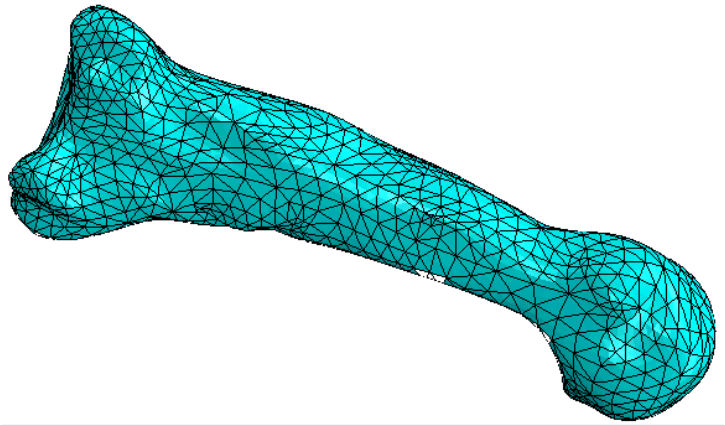

10303 Elements; runtime 57 min; max von Mises stress 36.4 MPa

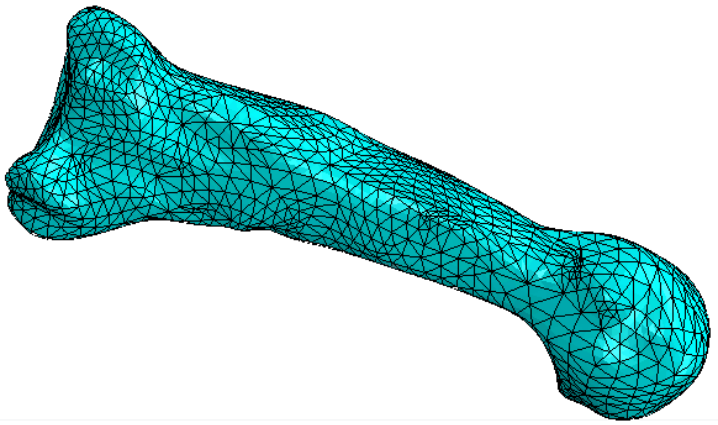

20496 Elements; runtime 27 hours; max von Mises stress 36.37 MPa

Figure 50: A series of images, showing a series of meshes from coarse (top) to fine (bottom). The middle image is representative of the average element size used in the final model

5.2.5c Soft Tissues

The encapsulating soft tissues were given an initial average element size of 20 mm, corresponding to 8279 elements. Maximum stress on the bone was 34.9 MPa and the maximum stress within the soft tissue was 0.6 MPa. Upon increasing the number of elements, the stress within the soft tissue oscillated as seen in Figure 51. However, maximum bone stress only increased by 0.7% across the first two conditions, then decreased by 0.1% over the subsequent conditions. Each condition increased computation time by approximately 20 minutes, until the last condition where computation time substantially increased to approximately 25 hours. As the model was not designed to examine the soft tissue stress and the bone stress appears to be extremely stable to soft tissue element numbers, a global element size of 5.8 mm, corresponding to 16713 elements was chosen.

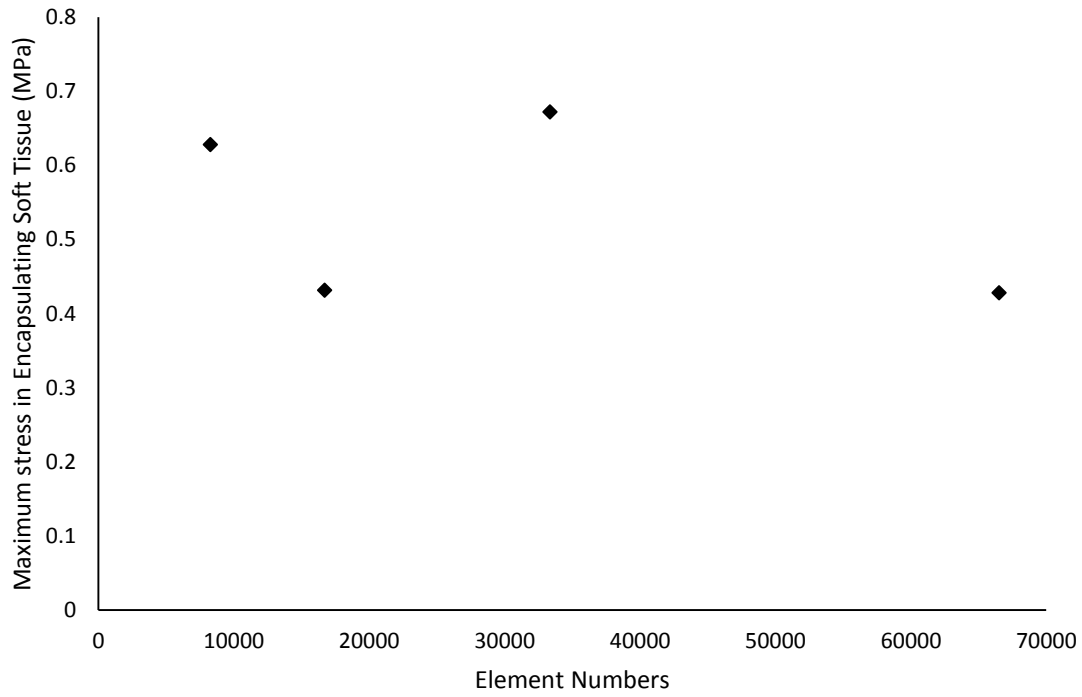

Figure 51: Maximum stress in the encapsulating soft tissue vs element number

Finally a model was constructed with the chosen mesh element numbers (cortical bone – 10303; trabecular bone 8430; soft tissues – 16713; floor surface – 900) and the simulation was run, resulting in a maximum stress on the bone of 36.4 MPa and taking 76 minutes. Element numbers in all meshes were doubled and the simulation was run again, this time producing a maximum bone stress of 35.7 MPa (-1.7%) but run time was increased to 36 hours. This gives assurance that the model results are stable with respect to increasing element numbers and that further increases in element number will cost large amounts of computing time, but will not change the magnitude of bone stress considerably.

For the second participant, exact element numbers could not be replicated due to differences in geometry. Therefore the refinement study was conducted independently of the first participant's data, again starting with a coarse mesh and approximately doubling the element numbers for each condition, but with the inclusion of the exact optimum global element sizes included from the initial participant's refinement study for comparison. In all parts the optimal mesh numbers corresponded closely to the mesh numbers deemed optimal in the first participant. This gives confidence that the selected global element sizes seen in Table 6 can be utilised for all participants.

Table 6: Optimal global element sizes for each part

Part	Global Element Size (mm)
Cortical Bone	2.35
Trabecular Bone	5.00
Encapsulating Soft Tissues	5.75
Floor	6.66

5.2.5d Analysis of Mesh Quality

In addition to the number of elements, mesh quality can be evaluated by assessing the shape of the elements used to make up the mesh, for example

how close to regular they are. A higher quality of mesh is less likely to encounter errors upon simulation and will lead to more realistic results. Once mesh element size was determined, each participant's model was meshed and analysed to evaluate the mesh shape. The parameters used and results are discussed below.

Skewness determines how closely the faces of the element shapes are to being ideal. In this case ideal is represented by either equilateral or equiangular faces. Skewness is important as the algorithm for calculating the forces in a mesh will assume that the faces are close to ideal. Skewness can be calculated using either the volume of a cell made up of elements (for example the tetrahedrons making up the cortical bone) or the angles at which its elements meet. In Abaqus, the shape factor is a function that indicates the skewness of a set of elements. It is calculated using Equation 13, where the optimal volume is the volume of a shape made of regular polygons (i.e. a tetrahedron made of equilateral triangles), with the circumradius equal to the length of the elements making up the volume. In this equation a value of one would indicate an optimal shape and zero indicates a completely degenerate shape where the faces are essentially collinear. Table 7 shows the acceptability of mesh elements based on their skewness (Bakkar, 2012).

Table 7: Skewness values vs the quality of cell

Value of Skewness	Cell Quality
0	degenerate
< 0.02	bad (sliver)
0.02 - 0.25	poor
0.25 - 0.5	fair
0.5 - 0.75	good
0.75 - 1	excellent
1	equilateral

$$Shape\ Factor = \frac{Element\ Volume}{Optimal\ Element\ Volume}$$

Equation 13: Shape factor as defined by the Abaqus software suite.

It is not possible to make a complex geometry from elements with a shape factor of one only, instead it is expected that the geometry will contain a mix of shape factor elements. Therefore the average element shape factor was used here to represent the shape factor of the whole mesh. The average shape factor across all participants for each model part can be found in Table 8 as well as the highest and lowest result. The shape factor cannot be calculated for hexahedral elements, and therefore the floor is not represented here. Based on Table 7, the average cells in the meshes seen here are of good quality.

Table 8: Average and ranges of shape factors by part

	Average Shape Factor	**Shape Factor Range**
Cortical Bone	0.62	0.57 – 0.64
Trabecular Bone	0.56	0.51 – 0.61
Encapsulating Soft Tissue	0.56	0.53 – 0.60
Floor	N/A	N/A

The aspect ratio of a cell is the ratio between the longest and shortest element. Ideally it should be close to one, however, as with the shape factor, an average aspect ratio of one is impossible to achieve in practice. The Abaqus manual (Dassault Systèmes Simulia Corp., 2013) suggests that an aspect ratio of less than 10 is acceptable. The aspect ratios of the parts of the model are presented in Table 9 showing all average aspect ratios are small.

Table 9: Average and ranges of aspect ratios by part

	Average Aspect Ratio	Aspect Ratio Range
Cortical Bone	1.75	1.70 – 1.87
Trabecular Bone	1.95	1.80 – 2.09
Encapsulating Soft Tissue	1.92	1.81 – 2.01
Floor	1.33	N/A

5.3 Model Evaluation

For the purposes of evaluating the model's performance, simulation was conducted at three time points during the stance phase of running for one participant: time of maximum vertical ground reaction force; time of maximum braking force (maximum posterior force); and time of maximum propulsion (maximum anterior force). This was repeated for the same participant during walking.

Similarly to the 2D model discussed in Chapter 4 this model was tested to examine its sensitivity to input variables using the same single participant. The six input variables (vertical and horizontal ground reaction forces, calculated vertical and horizontal joint contact forces, and sagittal and frontal plane angles) were adjusted independently and their effect on maximum von Mises bone stress was observed. These simulations were conducted at the time of maximum propulsion during running as at this time point the vertical ground reaction forces and joint contact forces were most similar in magnitude. Therefore when manipulating the input forces systematically by a percentage of the original input force, the absolute change in ground reaction force and joint contact force magnitudes were similar.

In order to examine the effect of the inclusion of the soft tissue on maximum bone stress, the model was simulated both with and without its inclusion, and maximum

von Mises stresses were compared. When the soft tissue was removed the floor surface was placed in direct contact with the head of the metatarsal. Simulation of this condition resulted in a high localised stress at the point where the bone contacts the floor surface in addition to the stress distribution across the shaft of the bone. The results presented consider only the stresses on the shaft of the metatarsal. To examine the effect of joint contact forces, the model was also simulated with and without these included, and maximum von Mises stresses were compared. These simulations were conducted on a single participant's data at all three time points during running and walking.

For comparison with the 2D model presented in Chapter 4, additional analyses were performed at 10% intervals between 10% and 80% of running stance for this participant and one additional non-rearfoot striker. At times greater than 80% of stance the sagittal plane angle of the metatarsal approached 90° which, coupled with the very low force values at these times, would lead to less valid results.

5.4 Results

5.4.1 Sensitivity Analysis

The sensitivity of the model to changes in the six input variables can be found in Figures 52 and 53. The results of the sensitivity analysis suggest a linear relationship between input forces or pitch angle and maximum bone stresses in the model, with the model being most sensitive to pitch angle (Figure 53) and vertical joint contact forces (Figure 52B). A change of one degree in the pitch of the metatarsal corresponds to approximately one MPa change in maximum bone stress, with a steeper angle producing less stress. A change of one Newton in vertical joint contact force represents approximately a 0.2 MPa change in bone

stress. The model is less sensitive to ground reaction forces, with one Newton changes in the vertical and horizontal forces representing 0.04 MPa and 0.03 MPa changes in the bone stress respectively.

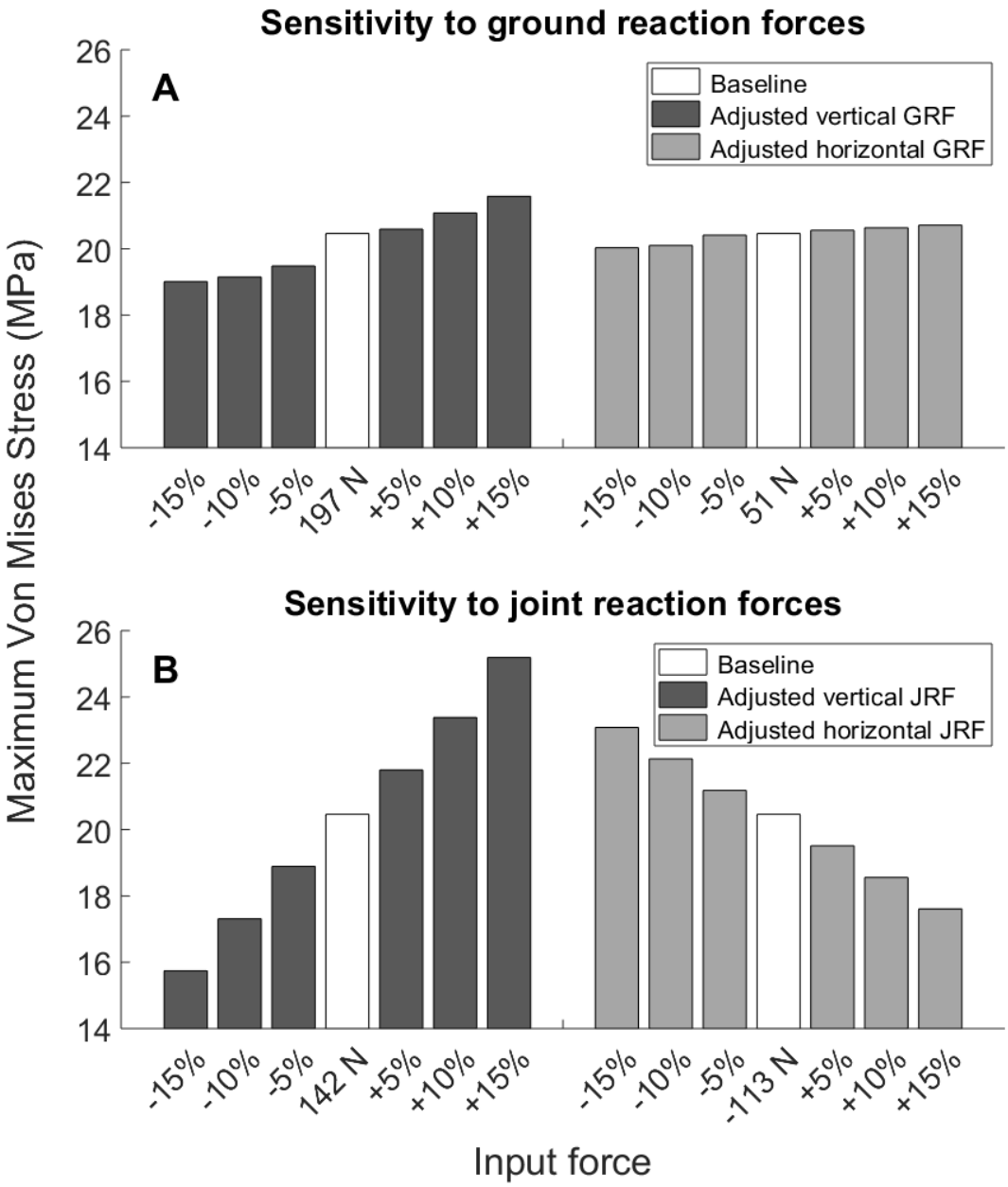

Figure 52: Model sensitivity to changes in input ground reaction forces (A) and joint contact forces (B).

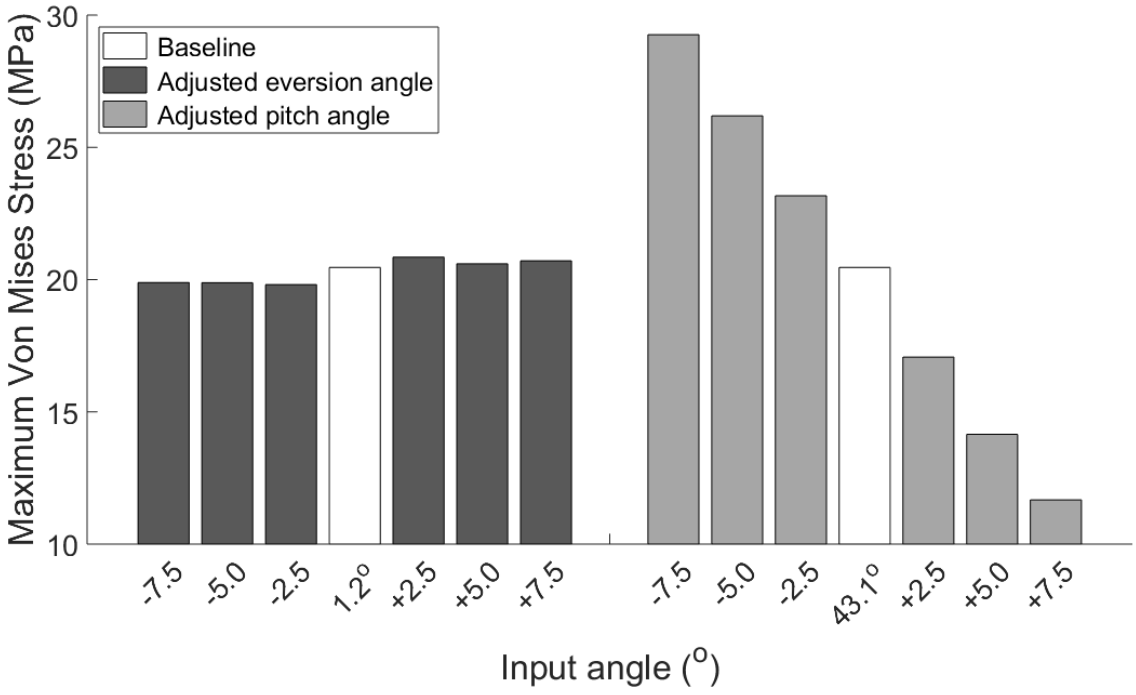

Figure 53: Model sensitivity to changes in input angle.

5.4.2 Comparison without Joint Contact Forces or Soft Tissues

The influence of soft tissue and joint contact forces on maximum bone stress is shown in Figure 54. Removing the soft tissues increased maximum stress in the shaft of the metatarsal greatly, particularly at the time of maximum propulsion. Exclusion of the joint contact forces reduced the maximum stress, particularly at the time of maximum propulsion.

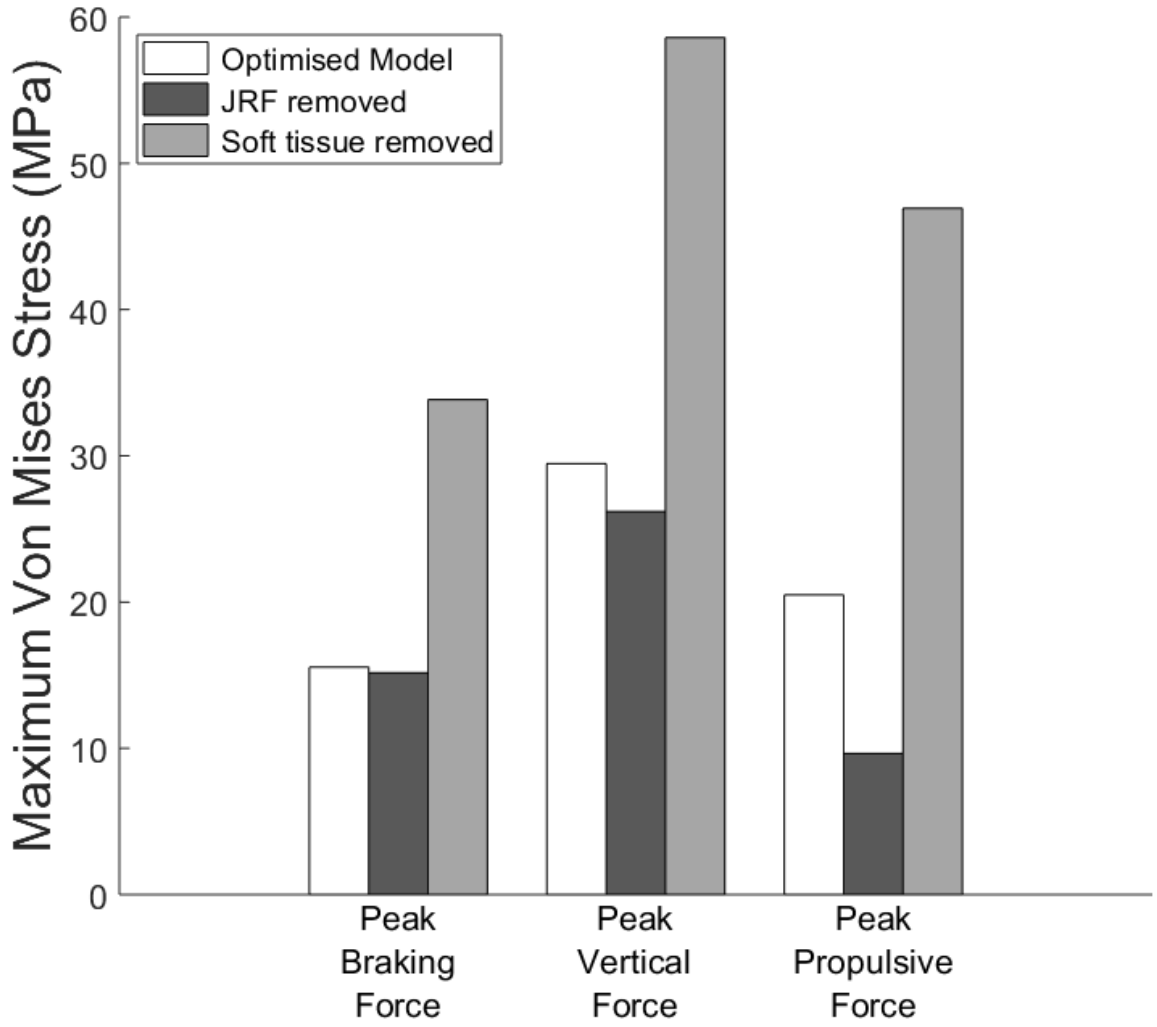

Figure 54: Model sensitivity to the inclusion of the joint contact forces (JRF) and the soft tissue throughout stance.

5.4.3 Evaluation of Maximum Bone Stress during Walking and Running

The maximum von Mises stress on the bone during the three points of stance for walking and running in the single rearfoot participant are displayed in Table 10. The dorsal metatarsal was under compression whereas the plantar surface was under tension throughout stance. The point of stance corresponding to the maximum vertical ground reaction force had the highest bone stresses in both walking and running, with maximum braking representing the lowest stress on the bone of the three stance points investigated. Angles were similar during walking and running, whilst forces were larger during running than walking, as expected. In this participant the maximum stress was on the dorsal surface at the distal end

of the shaft at time of maximum propulsive force whereas it was located at the plantar midshaft at the time of both the maximum braking force and maximum vertical force. Figure 55 shows the loading on the bone as a stress heat map for running data for a single participant, with the points of maximum stress indicated.

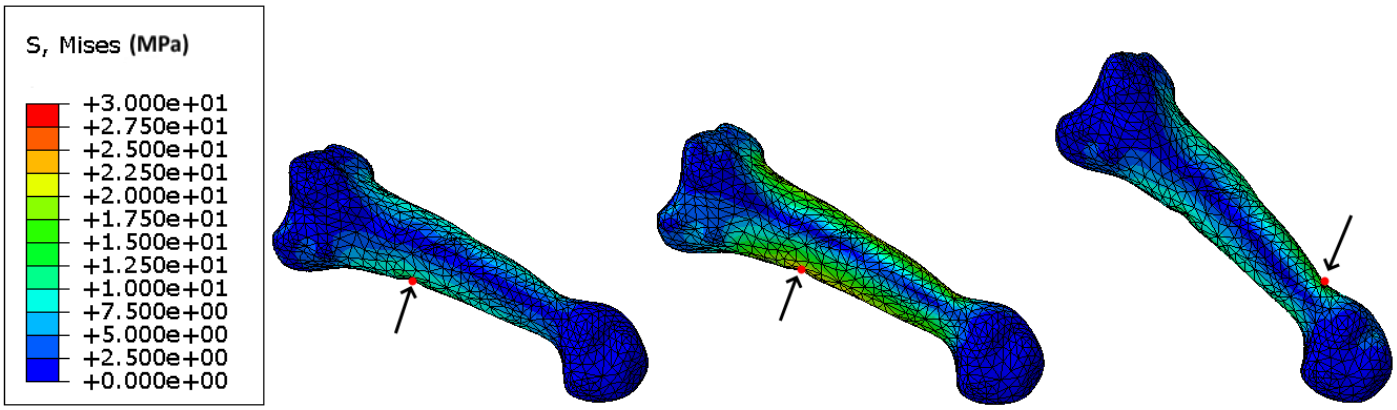

Figure 55: Results from three points of running stance for a single participant, left to right: maximum braking, maximum vertical GRF, maximum propulsive force. Red dots represent location of maximum stress at each time point.

Table 10: A comparison of walking and running data for one participant

Stance Phase	Gait	Vertical GRF (N)	Horizontal GRF (N)	Vertical JRF (N)	Horizontal JRF (N)	Pitch Angle (deg)	Eversion Angle (deg)	Maximum Stress (MPa)
Max Braking	Walking	74.15	-3.74	0.04	-0.07	22.01	1.77	4.04
	Running	194.83	-30.91	15.35	25.77	22.67	2.11	15.55
Max Vertical GRF	Walking	211.26	18.67	15.31	-21.56	26.35	2.03	19.50
	Running	291.35	21.71	91.30	122.41	27.99	2.07	29.46
Max Propulsion	Walking	179.57	33.01	63.67	60.37	38.38	0.80	13.51
	Running	197.40	51.02	141.52	113.44	43.13	1.29	20.46

5.4.4 Comparison of Results with a Beam Theory Approach

The analysis of multiple time points conducted on two participants can be compared to the time series of stress data from the same participants using the 2D model. In this case, the stresses output by each model were normalised by dividing by the peak stress of that model. Results of this are seen in figures 56 and 57.

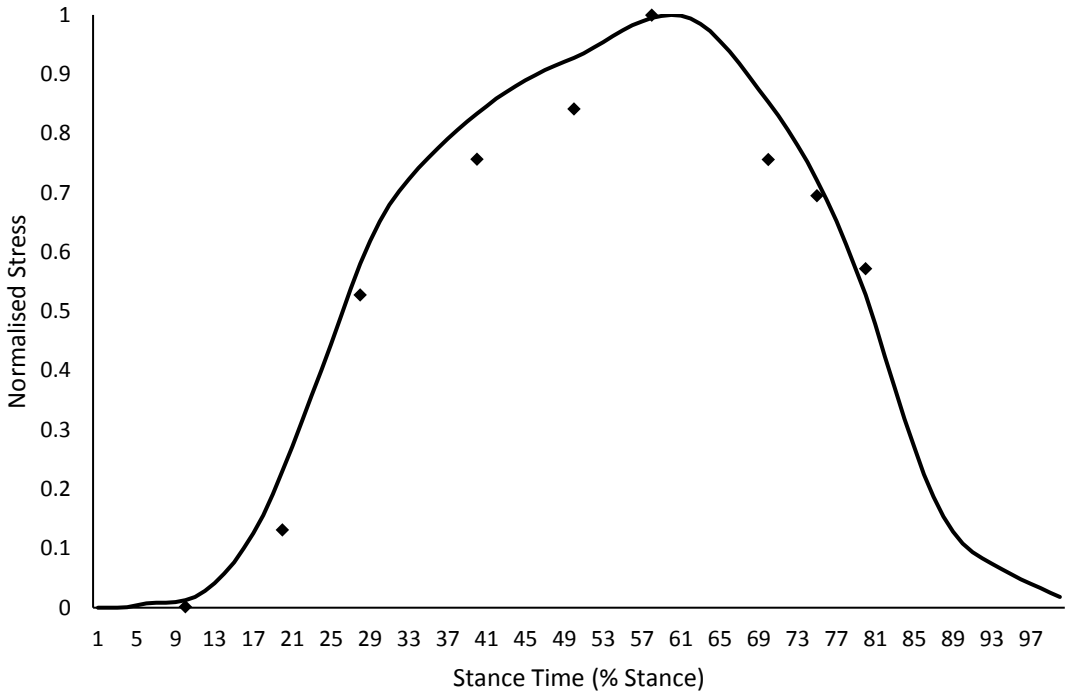

Figure 56: Comparison of stresses output by the beam theory model (line) and finite element model (diamonds) for a single RF participant

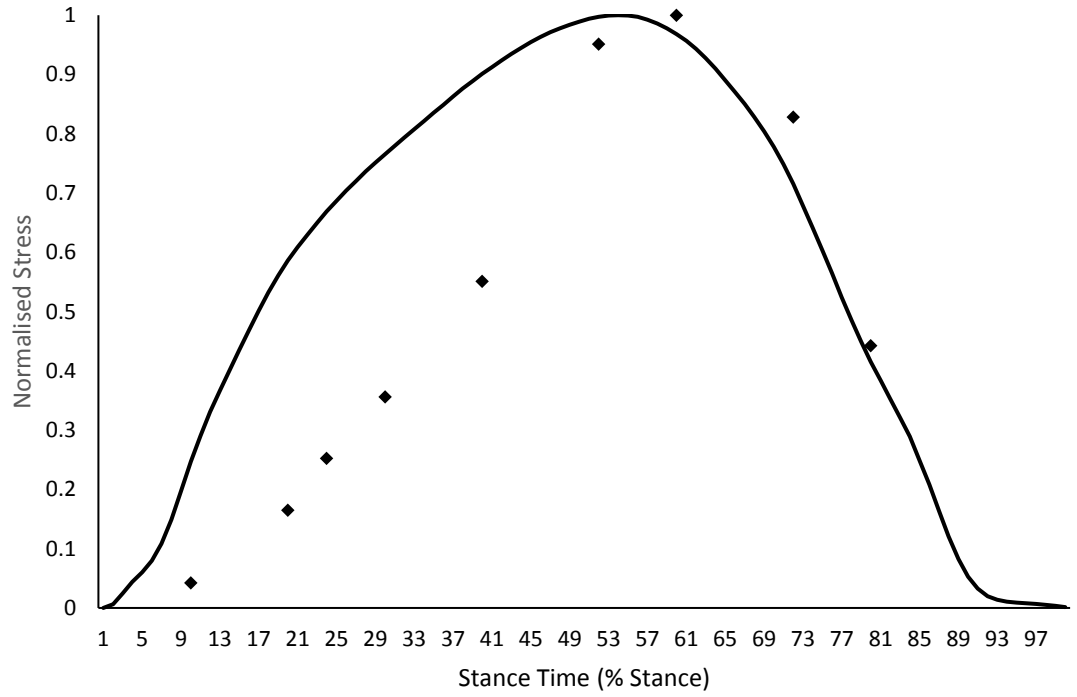

Figure 57: Comparison of stresses output by the beam theory model (line) and finite element model (diamonds) for a single NRF participant

For both participants the times of peak stresses coincide well, and the stresses match closely at stance times after the time of peak stress. However, the stresses

match less well at earlier times in stance for the non-rearfoot participant, but match closely for the rearfoot participant. It should also be noted that the stresses from the beam theory model come only from the point of dorsal mid-shaft, whereas the maximum stress in the finite element model can be anywhere along the shaft of the metatarsal.

5.5 Discussion

This study developed a novel, participant-specific finite element model to quantify metatarsal stresses during running, and evaluated the influence of model parameters and independent input variables on maximum bone stress. The model simulation time was approximately 35 minutes, making this approach feasible for assessing stresses in the metatarsals with a sample size similar to those seen in typical applied biomechanics studies.

5.5.1 Evaluation during Walking

During walking, the maximum stress on the bone was 19.50 MPa at the time of greatest vertical ground reaction force, which coincides approximately with mid-stance. This is equivalent to a strain of 1147 με. Finite element models of the entire foot have reported von Mises stresses in the second metatarsal of ~4.00 MPa (Chen et al., 2001b), 6.65 MPa (Gu et al., 2010) and 6.80 MPa (Akrami, 2016) during walking at mid-stance. *In-vivo* measurements of strain on the metatarsals using implanted strain gauges have reported 1534 με during barefoot walking (Arndt et al., 2002) and an average of 1144 με during shod walking (Milgrom et al., 2002). The current model, whilst simplistic compared to the whole foot models listed above, compares better with bone staple strain gauge data. However, it should be noted that strain gauges in *in-vivo* studies may not be positioned at the location of maximum stress on the bone. When using complex whole foot models such as that of Akrami et al. (2017), the alignment of individual

parts of the model is not always changed between points of stance. For example, during stance the angle between the phalanges and metatarsals changes, however in the model of Akrami et al. (2017) the toes were considered to lie in a neutral position throughout stance. This may lead to differences in the distribution of forces in the model. By considering just a single bone with joint reaction forces applied to it, the interaction between the toe and the phalange is accounted for without having to model its change in position during stance. This suggests that whilst the additional complexity of a whole foot model may seem to make the simulation more realistic, in some case more assumptions are required regarding the interactions of different parts, leading to the potential for more error in results.

5.5.2 Evaluation during Running

During running, the maximum stress on the bone was 29.46 MPa at the time of greatest vertical ground reaction force, equating to a strain value of 1732 με. Other recent finite element models of the second metatarsal during shod running have reported strains of 1393 με (typical running shoe) and 1937 με (minimally cushioned shoe) (Firminger et al., 2017), with which the values in the present study compare well. *In-vivo* strain gauge studies have reported strains of 1468 με during shod jogging and an average of 3603 με during barefoot jogging (Milgrom et al., 2002). These values were an average of two participants' values which differed considerably (5315 με and 1891 με), highlighting the need for participant-specific modelling approaches that permit sufficient sample sizes to be obtained. Whilst it is not feasible to directly validate the model, comparisons with previously reported values and the differences in magnitude between walking and running indicate that this model can be used to address applied questions. Whilst the maximum stress during running occurred on the dorsal midshaft of the metatarsal, the magnitude of von Mises stress at the corresponding position on

the plantar surface was very similar. This suggests that microdamage to the bone is likely to occur at both dorsal and plantar surfaces, consistent with studies showing a wide range of locations of stress fractures on the second metatarsal (Orava, 1980). From a modelling perspective this also gives assurance that the metatarsal cross-section may be considered to be symmetrical for the purposes of any 2D analyses.

5.5.3 Sensitivity to Model Inputs

The high sensitivity of the model to pitch angle suggests that kinematics of the foot during running are an important consideration when investigating loading on the metatarsal bones and injury risk. With a smaller pitch angle the metatarsal is closer to parallel to the ground and therefore the relatively large vertical ground reaction force under the metatarsal head can produce a greater amount of bending in the metatarsal compared with later stance when the metatarsal is more vertical (i.e. increased pitch angle). When conducting input sensitivity analyses in the present study, the original vertical ground reaction force and the joint contact force inputs were comparable in magnitude during late stance. This is not the case during other points of stance, such as early stance, when the joint contact force is very low compared to the ground reaction forces under the metatarsal head, limiting its ability to influence bone stress. It should also be noted that whilst directly increasing the forces under the metatarsal head did not provide the greatest increases in bone stresses, the ground reaction forces under the toe contribute greatly to the joint contact forces, which the model is sensitive to. This supports recent work suggesting that direct external measurements do not correlate well to internal forces (Matijevich et al., 2019). The lack of sensitivity to the eversion angle is likely influenced by the fact that the angles measured are very small. Furthermore, due to the anatomy of the foot, there is little ability for

the individual metatarsals to rotate along their longitudinal axes. The frontal plane position of the foot may be likely to influence the ratio of loading under the five metatarsals rather than change the line of action of the forces in a way that would affect the stresses seen on the bone. It should be noted that the sensitivity analyses provide a useful understanding of how external factors independently influence metatarsal stress, yet the manipulations may not be physiologically realistic. Furthermore, it is unlikely that any of the individual input variables would change without a concurrent change in the other input variables.

5.5.4 Sensitivity to the Inclusion of Joint Contact Forces and Soft Tissues

Excluding the joint contact forces from the simulation provided insight into the influence of muscular action and toe forces on metatarsal stresses. At all three time points during stance, exclusion of joint contact forces decreased the maximum stress on the bone. Its influence was greatest during late stance, likely due to the position of the foot at push off when the ground reaction forces are lower under the metatarsal head and higher under the toe. From the free body diagrams in Chapter 4 it can be seen that higher ground reaction forces under the toe lead to increased tension in the tendons and through that higher joint contact forces. This allows the forces from the toe to be a major contributor to metatarsal stresses when the toe force is high. This also supports previous literature showing that the metatarsophalangeal joint moment is largest in late stance (Day and Hahn, 2019), suggesting muscular contributions to bone stresses may also peak at this time.

The novel inclusion of soft tissue surrounding the metatarsal in the present study was shown to considerably influence maximum bone stress. The maximum stresses seen in the metatarsal shaft approximately double when soft tissue is not present and forces are transferred directly from floor to bone. The model of

Firminger et al. (2017) obtained results that compared well with strain gauge studies without the use of soft tissues. However, it should be noted that there were a number of other differences between these two models, such as the use of computed tomography and apparent density to define bone properties, and the methods of application of forces to the bone that may account for this. The mesh sensitivity analysis revealed that stresses within the encapsulating soft tissues oscillated considerably with different mesh densities, yet bone stresses remained extremely stable throughout these manipulations. The variation in the soft tissues is likely due to the choice of a linearly elastic soft tissue, which is undergoing large strains. This suggests that if the stresses within the soft tissues themselves are important outcome variables, a non-linear material should be chosen, such as those used by Morales-Orcajo et al. (2018). However, if the soft tissue stresses are unimportant, as in the present study where the model is designed to quantify bone stress, the large strains are acceptable and the use of a linearly elastic soft tissue saves considerable computational time whilst allowing for the distribution of ground reaction forces across the bone and also the attenuation of forces between the ground interface and the head of the metatarsal.

5.5.5 Limitations

All models have limitations, as they are simplified representations of real systems. In this case the system modelled consisted of a large number of bones and soft tissues, with forces acting under all five rays of the foot. This model consists of just one bone, assuming no interactions between neighbouring parts of the foot at the distal end and a fixed proximal end. Proximally, the second metatarsal bone is attached to the midfoot via three other bones, forming a reasonably stiff joint with little room for extension or flexion, and several models have used a fixed cantilever to model the metatarsal in the past (Lemmon et al., 1997b, Gross and

Bunch, 1989, Stokes et al., 1979, Fung et al., 2017). At the distal end, the metatarsal heads are connected via the transverse metatarsal ligaments, limiting their independent motion. It is not clear to what extent this would affect the sharing of loading from external forces. The deformation of the arch is not accounted for here, nor is the possible reduction in bending from its supporting tissues, such as the plantar aponeurosis and the long and short plantar ligaments. Models that do include representations of these tissues have far lower stresses on the second metatarsal (Chen et al., 2001b, Akrami, 2016, Gu et al., 2010), but do not represent the high strains reported using *in-vivo* strain gauges (Arndt et al., 2002, Milgrom et al., 2002).The effect of these tissues on the distribution of internal loading in the foot is unclear.

5.6 Conclusions

In conclusion the model presented here has been evaluated against recent studies of metatarsal stresses and *in-vivo* measurements of stress during both walking and running, and been deemed to provide representative values. It appears to perform better than more complex whole foot finite element models when investigating walking. The model shows sensitivities to the pitch angle of the metatarsal and the joint contact forces, but less sensitivity to ground reaction forces under the metatarsal head. This suggests that measurement of external ground reaction forces does not correlate well to internal loading. The inclusion of joint reaction forces and soft tissue effects have been shown to be influential on the magnitude of peak stress in this model.

6. Using the 3D Finite Element Model to Assess the Stress in the Second Metatarsal in Rearfoot and Non-Rearfoot Runners

Having developed and evaluated a 3D participant-specific finite element model in Chapter 5, metatarsal stresses in rearfoot and non-rearfoot runners could now be compared. The data set was the same used in Chapter 4. However upon assembly, data from one rearfoot participant was found to be unsuitable for use in the model, as the kinematic data matched poorly to the MR data, likely due to poor placement of fish oil capsules during the MR scan. Therefore the present study included 11 rearfoot strikers (6 Female; age 27 ± 11 years; mass 63.6 ± 10.3 kg; height 1.65 ± 0.07 m) and 8 non-rearfoot strikers (3 Female; age 20 ± 3 years; mass 72.3 ± 12.3 kg; height 1.73 ± 0.09 m). As with the earlier analysis of 20 participants, no differences in mass or age between groups were found, and in addition there was now no difference in heights.

It has been determined that the magnitudes of stresses acting on bony tissues play an important role in the development of stress fractures, whether directly or via the activation of a remodelling process. Furthermore, it is unclear what effect, if any, foot strike modality has on metatarsal stresses and their location during running. This study aimed to use the evaluated 3D participant-specific finite element model from Chapter 5 to explore differences in internal loading between those who land on their heel during running and those who do not.

It was hypothesised that non-rearfoot strikers would experience both greater external and internal second metatarsal loading than rearfoot strikers during running.

6.1 Analysis

The model was simulated at three points of stance for each participant. The three time points of interest during the stance phase were the time of maximum braking force (minimum horizontal ground reaction force); time of maximum vertical ground reaction force; and time of maximum propulsive force (maximum horizontal ground reaction force). An individual model assembly was created for each participant at each investigated stance point based on the procedures outlined in section 5.2. These were simulated and the peak von Mises stress on the cortical bone was obtained for each participant at each of the three stance phases. Group mean comparisons were made on the six input variables (horizontal and vertical ground reaction forces, horizontal and vertical joint contact forces and the pitch and frontal plane angles) and the peak von Mises stress at each time point. Variables were examined using a Shapiro-Wilk test to confirm normality ($P \geq 0.05$). Means were compared using an independent T-Test (normally distributed variables) and a Mann-Whitney-U test (non-normally distributed variables) with a significance level of $P \leq 0.05$. Peak stresses at each time point are also presented for the whole group for comparison with literature values of stress estimation. Additionally, graphical representations of all 19 metatarsal bones, loaded at the point of peak ground reaction force are presented. A qualitative and descriptive analysis of bone shape and the location of peak stresses is given. The position of maximum stress in these figures was defined by whether maximum stress occurs on the dorsal or plantar aspect of the bone and also by the location along the shaft, where proximal shaft refers approximately to the proximal third, mid-shaft refers to the middle third and distal shaft refers to the most distal third. Similar graphical representations of each

participant at the points of maximum braking and maximum propulsion can be found in Appendix 3.

Based on the findings of Nunns et al. (2017) regarding the importance of geometry in determining the stresses experienced by the metatarsal, the volumes of the cortical, trabecular and combined bone were correlated with the peak stress using a Pearson's correlation coefficient.

6.2 Results

6.2.1 Whole Sample Stress Data

Mean inputs and stresses for each stance time point during running across the entire group can be found in Table 11. Maximum stress occurred at the time of maximum vertical ground reaction force, with the lowest stress occurring at the time of maximum braking forces.

Table 11: Mean input and outcome variables for the entire running sample

Stance Phase	Vertical GRF (N)	Horizontal GRF (N)	Vertical JRF (N)	Horizontal JRF (N)	Pitch Angle (deg)	Eversion Angle (deg)	Maximum Stress (MPa)
Max Braking	221.54 (60.41)	-42.12 (13.16)	28.26 (26.37)	-44.98 (44.46)	27.67 (3.80)	2.08 (5.99)	19.81 (9.64)
Max Vertical GRF	339.86 (65.75)	16.89 (13.37)	105.02 (49.53)	-128.69 (62.56)	32.26 (5.10)	2.64 (3.91)	44.99 (13.16)
Max Propulsion	239.44 (58.33)	64.27 (16.71)	123.71 (52.76)	-80.76 (35.66)	49.27 (6.48)	4.20 (3.56)	33.54 (16.67)

6.2.2 Discrete Analysis of Running Data

There was no difference in maximum stress values at the time of maximum braking (Table *12*), maximum vertical ground reaction force (Table *13*) or maximum propulsion (Table 14). Pitch and eversion angles were similar between groups at all times. Vertical ground reaction forces were significantly greater in the non-rearfoot runners than the rearfoot runners at all stance points. Horizontal ground reaction forces were significantly greater in the non-rearfoot group at the

points of maximum braking and maximum propulsion, but were similar at the time of greatest vertical ground reaction force. Both vertical and horizontal joint contact forces were greater in the non-rearfoot group at the time of maximum braking and maximum vertical ground reaction forces, but were similar at the point of maximum propulsive force.

Table 12: Comparison of input and outcome variables between foot strike modalities at the point of maximum braking

Variable	Foot strike Modality		P value	d
	RF	NRF		
Maximum von Mises Stress (MPa)	17.30 (8.35)	23.25 (10.76)	0.215	0.6
Vertical GRF (N)	**190.17 (51.51)**	**264.67 (43.85)**	**0.004***	**1.5**
Horizontal GRF (N)	**-36.43 (12.05)**	**-49.96 (10.78)**	**0.02***	**1.2**
Vertical JRF (N)	**14.57 (14.52)**	**47.07 (28.07)**	**0.012***	**1.5**
Horizontal JRF (N)	**-22.07 (22.07)**	**-76.48 (49.26)**	**0.016***	**1.5**
Pitch Angle (deg)	27.11 (2.61)	28.45 (5.12)	0.513	0.3
Eversion Angle (deg)	1.06 (5.51)	3.49 (6.70)	0.778	0.4

* Significant (P ≤ 0.05) between groups, negative indicates compressive stress

Table 13: Comparison of input and outcome variables between foot strike modalities at the point of maximum vertical ground reaction force

Variable	Foot strike Modality		P value	d
	RF	NRF		
Maximum von Mises Stress (MPa)	39.92 (10.82)	51.97 (13.50)	0.057	1.0
Vertical GRF (N)	**314.84 (62.71)**	**374.26 (56.26)**	**0.046***	**0.9**
Horizontal GRF (N)	14.67 (8.66)	19.94 (18.29)	0.469	0.3
Vertical JRF (N)	**81.28 (38.22)**	**137.67 (46.03)**	**0.014***	**1.4**
Horizontal JRF (N)	**-99.01 (51.09)**	**-169.50 (55.20)**	**0.013***	**1.3**
Pitch Angle (deg)	31.00 (3.20)	34.00 (6.80)	0.276	0.6
Eversion Angle (deg)	2.13 (3.40)	3.33 (4.67)	0.55	0.3

* Significant (P ≤ 0.05) between groups, negative indicates compressive stress

Table 14: Comparison of input and outcome variables between foot strike modalities at the point of maximum propulsive force

Variable	Foot strike Modality		P value	d
	RF	NRF		
Maximum von Mises Stress (MPa)	27.04 (8.20)	42.47 (21.47)	0.051	1.0
Vertical GRF (N)	**212.28 (53.36)**	**276.78 (43.93)**	**0.01***	**1.3**
Horizontal GRF (N)	**55.23 (12.89)**	**76.71 (13.26)**	**0.003***	**1.6**
Vertical JRF (N)	106.04 (46.96)	148.01 (53.30)	0.097	0.8
Horizontal JRF (N)	-70.46 (33.93)	-94.95 (35.05)	0.148	0.7
Pitch Angle (deg)	47.08 (5.72)	52.28 (6.59)	0.095	0.9
Eversion Angle (deg)	3.46 (3.09)	5.22 (4.10)	0.325	0.5

* Significant (P ≤ 0.05) between groups, negative indicates compressive stress

6.2.3 Qualitative Analysis of Bone Stresses

There was a large range of maximum stresses, ranging from 28.12 to 79.02 MPa. Group mean peak stresses were 19.81 MPa, 44.99 MPa and 33.54 MPa at the times of maximum braking, maximum vertical ground reaction force and maximum propulsive force respectively. Maximum stress at the time of maximum ground reaction force was located within the diaphysis in all cases (Figure 58). This was not the case in later stance, where examples of maximum stresses close to the epiphysis were observed (Appendix 3). For each participant, at all three simulated time points, the maximum stress magnitude at the dorsal surface was similar to the maximum stress magnitudes at the plantar surface.

In all cases maximum stresses were clearly located within the diaphysis, but in some cases at the point of maximum propulsion this stress was located close to or at the point where the bone transitions between epiphysis and diaphysis. At all stance points maximum stress magnitudes at the dorsal surface were similar to the maximum stress magnitude at the plantar surface.

Importantly, there were differences in both the shapes and proportions of the metatarsals in the present study, with some much more slender relative to their length than others.

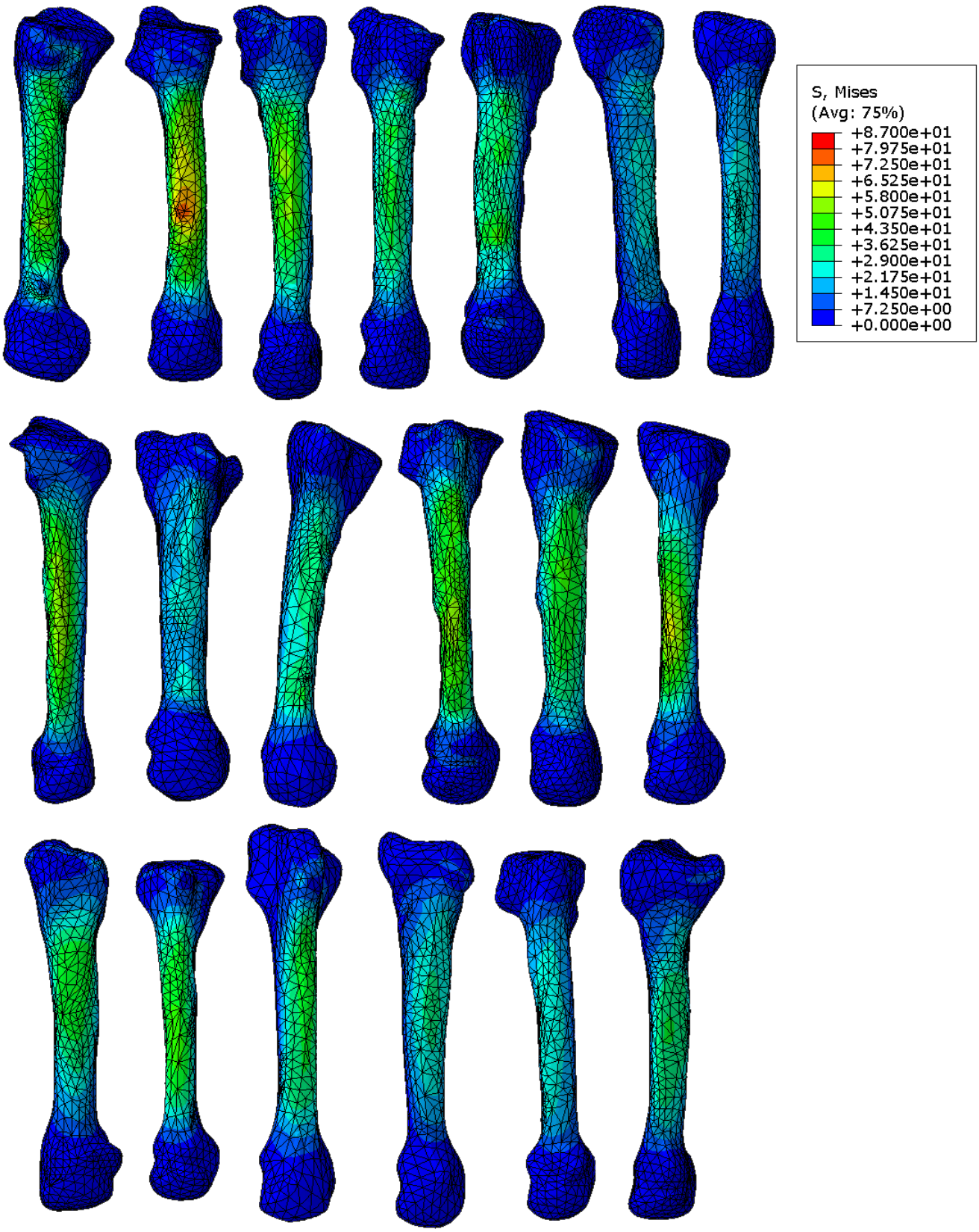

Figure 58: von Mises stress distribution across the metatarsal dorsal aspect for all participants' metatarsals at the point of greatest vertical ground reaction forces. Note: the bones are scaled to appear approximately the same length in the figure for presentation purposes only.

Maximum stresses were more likely to be located on the dorsal surface than the plantar surface, with 70%, 58% and 94% of participants experiencing peak

stresses on the dorsal surface at the points of maximum braking, vertical ground reaction force and propulsion respectively. Maximum stresses were also more likely to be located at approximately mid-shaft with 64%, 70% and 82% of participants experiencing the maximum stress in the mid-shaft at the points of maximum braking, vertical ground reaction force and propulsion respectively. Only one participant experienced the maximum stress in the distal shaft at the point of maximum braking and a single different participant experienced maximum stress in the distal shaft at maximum propulsion. No participants displayed maximum stresses in the distal shaft at the point of maximum vertical ground reaction forces, which was the time of overall maximum stress of the three time points analysed in all but one participant. The stress distribution for all the participants in this study is visually similar to that seen in Firminger et al. (2017), with the stresses concentrated at the mid-shaft in the dorsal and plantar regions whereas the region at the medial and lateral aspects of each metatarsal had very low stresses.

Table 15 shows the volume of each participant's metatarsal bone, with a further breakdown by cortical and trabecular bone types. Examination using a Pearson's correlation coefficient reveals that total bone stress was not associated with total bone volume nor with trabecular or cortical bone volume (P=0.596 Cortical vs. Stress; P=0.308 Trabecular vs. Stress; P=0.699 Whole Bone vs. Stress).

Table 15: Average bone volumes for each group along with the stress reported at the point of maximum ground reaction force

Group	Whole Bone Volume (mm^3)	Cortical Volume (mm^3)	Trabecular Volume (mm^3)	Stress at maximum vGRF (MPa)
Total	9225.5 (1892.6)	4691.4 (980.4)	4534.2 (1132.6)	44.99 (13.16)
RF	8758.8 (1477.5)	4643.6 (1096.0)	4115.17 (618.2)	39.92 (10.82)
NRF	9867.2 (2297.6)	4756.9 (864.3)	5110.3 (1448.3)	51.97 (13.50)

6.3 Discussion

This study used the evaluated model from Chapter 5 to compare peak second metatarsal stresses between rearfoot and non-rearfoot runners at three points of stance. It also provided a qualitative analysis of bone geometries and stress locations over the combined group of participants.

6.3.1 Discrete Comparison of Groups

Firminger et al. (2017) reported median strains of 1393 με (typical running shoe) and 1937 με (minimally cushioned shoe), lower than the current study. However *in-vivo* strain gauge studies have reported strains ranging between 1891 με and 5315 με (Milgrom et al., 2002). Firminger et al. (2017) also reported the 95th percentile strains for their shoe types and found 3110 με (typical running shoe) and 4341 με (minimally cushioned shoe). The wide range of values reported in these earlier studies may reflect the sensitivity of the measurement or true physiological variability. The results from the current study are within the range of previously reported strain magnitudes. The highest strain during the time of maximum ground reaction forces reported by any participant was 4648 με and the lowest strain was 1654 με.

Regarding the discrete analysis of stresses between groups, the results here support the results from the beam theory model, finding that whilst input forces, in particular the vertical ground reaction forces under the metatarsal head, were significantly greater at all investigated time points, the output peak stresses were not significantly different. This supports work by Matijevich et al. (2019) who found that greater ground reaction force metrics did not correlate to greater tibial forces, and suggests that externally measured forces may not be the most valid method for inferring internal loading, and therefore injury risk. However at the points of maximum vertical ground reaction forces and maximum propulsive forces, the

level of significance for the von Mises stress is very close to 0.05, which, in combination with the large effect size of 1.0, suggests a trend of greater stresses for NRF runners. As observed using a 2D beam theory approach, the results of the present study suggest that foot strike does not influence the magnitude of peak metatarsal stress during running, and therefore may not influence the risk of stress fracture via this mechanism. However the large effect sizes suggest there is a trend for increased stresses in NRF striker runners, but this is considerably less marked than the differences in external forces observed between groups.

Bone geometry has previously been noted as an important determinant of bone stress (Nunns et al. (2017) and this may partly explain why difference in external forces between groups did not equate to differences in internal forces. The fact that no association between total volume of the bone and maximum stress was observed in the present study suggests that some aspect of the shape rather than size *per se* may influence stress magnitude. However, there are numerous ways to quantify bone geometry and the geometry may influence peak stress differently according to the phase of stance. There is evidence that bone geometry may adapt over time through habitual loading, for example elite runners show thickened cortical bone and reduced trabecular bone compared to recreational runners (Hart et al., 2017). However, it is not known what magnitude of force or number of cycles induces these levels of adaptation. All of the participants in the present study were recreational runners, reporting similar levels of activity, so it was assumed that the level of adaptation between participants would be equal unless influenced by their habitual foot strike. It is also possible that the geometry of the soft tissues may mitigate the forces more in some participants than others For example if the distance between the most plantar aspects of the metatarsal

head and the sole of the foot is greater (i.e. soft tissue is thicker) it can be assumed there would be more cushioning and that forces may be damped more than with less soft tissue.

6.3.2 Qualitative Analysis

The stress distribution on the metatarsal bones in the present study visually match those of recent models such as Firminger et al. (2017). This pattern is influenced in part by the nature of modelling the metatarsal as a cantilever with no mediolateral or torsional forces. The shape of the metatarsals highlights the variability of individual geometry, and is one potential explanation for the lack of statistical difference between groups, despite there being no correlation between bone volume and stress. For example, some bones are slender and long, whilst others are wider and shorter. This difference would result in potentially similar volumes, but two very different mechanical responses to the input forces.

The magnitudes of peak stresses on the plantar and dorsal surfaces for each simulation were similar which means that identifying whether the maximum stress occurred on the plantar or dorsal surface is of relatively low importance, whereas it may be important to identify the proximal-distal location of peak stress.

However, it should be noted that whilst the magnitudes were similar between the dorsal and plantar surfaces, the dorsal surface is under compression whilst the plantar surface is under tension. Bone is known to have different mechanical responses to compression vs. tension (Martin et al., 2015), being stronger in compression. Therefore a magnitude of stress on the dorsal surface may not induce either the same level of microdamage, or the same level of remodelling response as the same magnitude of stress on the plantar surface, and stress fracture may be more likely on the plantar surface.

6.3.3 Limitations

The limitations of this study are similar to the limitations of Chapter 4 and Chapter 5 and are discussed in greater detail in those sections. From chapter 4, the limitation of running barefoot when most populations would run in shoes and the limitation of grouping midfoot, forefoot and toe runners together in a single group apply here. From chapter 5, the limitation of reducing the foot to a single bone modelled as a fixed cantilever and the lack of modelling of a deformable arch and other plantar tissues such as the long and short plantar ligaments apply here.

6.3.3 Conclusions

In conclusion, the magnitudes of stresses for the whole group of runners fall within the ranges of stress reported by both *in-vivo* and previous finite element approaches. Vertical ground reaction force under the metatarsal head was significantly greater in the non-rearfoot runners than the rearfoot runners, but stress magnitudes did not differ between groups. This suggests that the external forces do not represent the internal forces experienced by the metatarsal and further suggests that foot strike modality may not influence the risk of stress fracture development through increased stress magnitudes.

7. General Discussion and Comparison of Modelling Methods

This section assesses the degree to which the studies described in this thesis have achieved the aims set out in section 2.6. There are suggested areas for future development of the modelling techniques used and a discussion of possible future studies to assess the risk of stress fracture in runners.

The strengths and weaknesses of the 2D beam theory model and the 3D finite element model presented in this thesis are considered, as well as their best use in the context of answering specific research questions. Finally, the question of whether running with a rearfoot or non-rearfoot strike influences metatarsal stress is addressed.

7.1 Advantages and Disadvantages of using a 2D Beam Theory or 3D Finite Element Model

Both models presented in this thesis use the same input kinetic and kinematic data, treated in an identical fashion. The main differences between model inputs are the treatment of geometrical data from the body tissues and the simulation types and assumptions. These are listed in Table 16 before a discussion of their implications.

Table 16: Examples of similarities and differences in model properties

Model Element	Beam Theory	Finite Element
Geometry Used	Single Cross-section	Whole Bone
Deformable Geometry		x
Fixed Cantilever	x	x
Vertical and Horizontal GRF	x	x
Joint Contact Forces	x	x
Action of Forces	Point	Distributed
Soft Tissue Effects		x
Analysis of Stance	Whole Stance	Single Time Points

The finite element method has distinct advantages when considering the quality and nature of the output data. The model considers all points along the metatarsal and stress is computed at every node. This allows the peak stress and its location to be easily identifiable and it is therefore relatively easy to perform a qualitative assessment of the data. The beam theory method uses only individual slices of MR data to determine participant-specific parameters, which whilst less time consuming to segment, provides much less detailed information. The results from the finite element model show that the peak stress can be located differently for any given time point of stance, with only 70% of participants showing a peak stress in the mid-shaft at the time of peak vertical force. The 2D beam theory model cannot provide this information and only the peak dorsal and plantar stresses at the selected cross-section are obtained. Conversely the beam theory model can easily compute the stress across the whole of stance, allowing analyses such as SPM to be used (Chapter 4). This allows for detailed information about differences in stress magnitudes at different stance points with more detail than the finite element model. However, in the context of understanding injury risk, it is believed that the magnitude of peak stress is important, and therefore stresses throughout stance that are submaximal may not be highly important.

The presented models show large differences in the magnitudes of stresses calculated, for example the 2D beam theory model calculated a mean peak stress of 224 MPa across all participants compared with 44.99 MPa calculated using the finite element model. In vitro testing suggests that 224 MPa is above or very close to the failure load of bone (Wolfram and Schwiedrzik, 2016), whereas 44.99 MPa falls within the range measured using *in-vivo* strain gauges during barefoot jogging (Milgrom et al., 2002). Other 2D beam theory studies do also report high

stresses compared with *in-vivo* measures. For example, 113 MPa was reported by Gross and Bunch (1989) in the second metatarsal and 114 MPa was reported by Nunns et al. (2017) in the third metatarsal during running. Whilst the differences in magnitudes between the current study and these previous studies was discussed in more detail in section 4.4 it should be noted that all reported beam theory results are greater than *in-vivo* measurements, which reported only 90 MPa in the participant with the greatest measured stress. Based on this it seems likely that the simplicity of beam theory models leads them to overestimate stresses, whereas finite element models produce more similar magnitudes to actual measured results. This overestimation is likely due to a number of factors, such as the application of ground reaction forces directly to a single point on the bone and the non-deformable geometry.

Despite the differences in absolute stress magnitudes obtained by the two models in this thesis, the relative differences were preserved between methods. Both studies found no differences in peak metatarsal stresses at the time of peak input forces. The SPM analysis of the 2D time series data did find a difference between 7 % and 23% of stance, whereas the finite element model required the selection of discrete stance time points for analysis. The time of maximum braking was the earliest time point selected and this occurred on average at 27% of stance, later than where differences were observed using the 2D beam theory approach.

Whilst it should be noted that the overestimation of the stresses by the beam theory model is a limitation to the interpretations of its results, there is currently no well-defined figure for a stress magnitude that will induce the formation of a stress fracture over a fixed number of cycles. Therefore, either model could be used to investigate differences between groupings of participants, but neither can discern if the stress estimated might lead to a stress fracture.

Figure 59 shows a plot of how each model ranked each participant in terms of stress magnitude, with the lowest ranking representing the participant with the highest stress. A root mean square calculation was carried out on the differences in ranking and found that on average each participant was five out of 19 places away from their ranking in one model compared to another. There may be a number of reasons for the differences in rankings, for example the finite element model can estimate stresses anywhere on the bone and may find a higher stress away from the mid-shaft. However these differences do not represent an advantage in one model over another, merely represent the difference in calculation methods used to estimate the peak stresses.

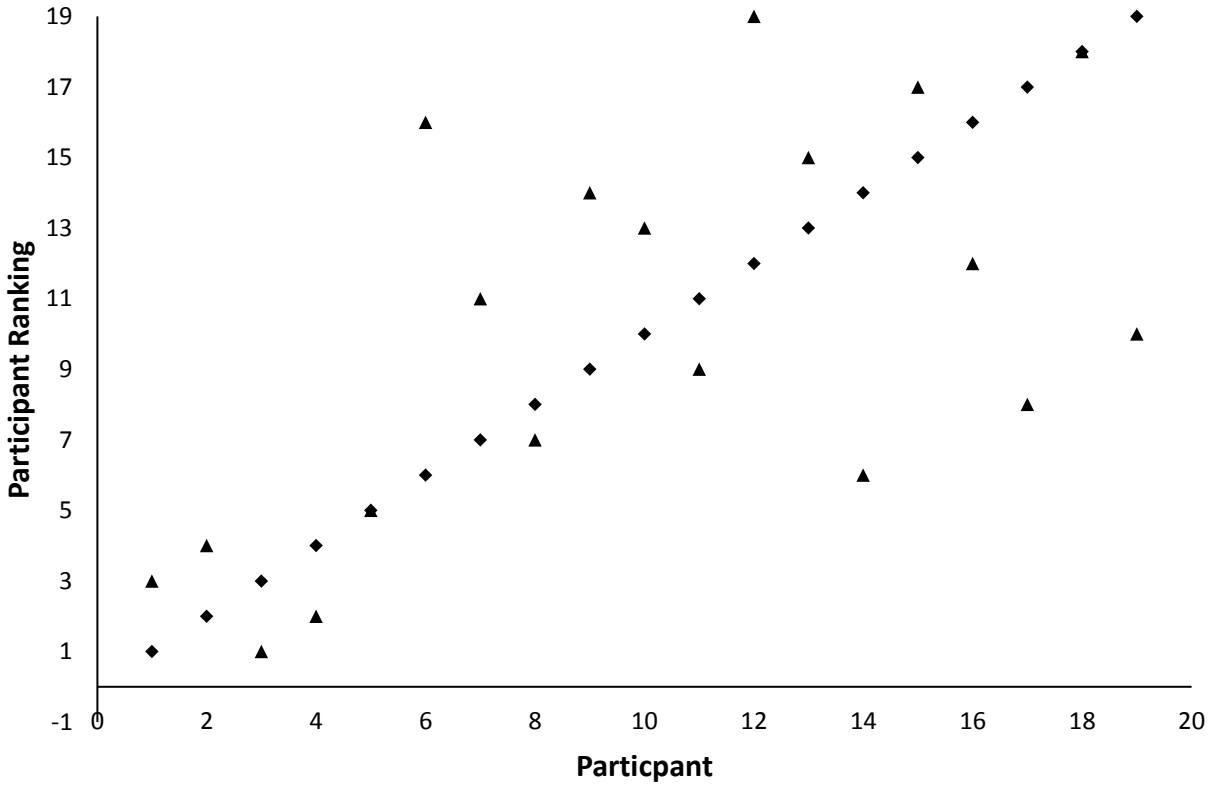

Figure 59: Figure showing the participants ranked by stress magnitude. Diamonds represent the 2D model ranking and are in order. Triangles represent the corresponding ranking for the 3D model. If the two models presented relative stress magnitudes that were very similar between models, it would be expected that each participant's diamond and triangle would be close together.

This section will compare the design of the two modelling approaches presented in this thesis. The limitations for each model have been discussed in detail in

Chapters 4 and 5. The main differences mathematically between the two modelling approaches is the addition of encapsulating soft tissues in the finite element model and the different methods of applying the forces to the metatarsal. In the beam theory model, forces are applied at a single point, at the centre of the head of the metatarsal. This means that the forces from the ground are applied directly to the bone and are not distributed at all. In reality, the forces that are calculated as input to the model come from plantar pressure data where it is distributed over an area of several square centimetres. These forces then have to pass through the soft tissues of the foot which act both as a mechanism to distribute the force but also to dissipate energy as they act in a viscoelastic manner. Whilst the soft tissue modelled in in this thesis did not utilise non-linear elastic properties, it allowed for the forces at the floor to be passed to the bone in a more realistic manner than a direct application on the bone. Similarly the joint contact forces are applied as point loads to the metatarsal in the beam theory model, whereas they are distributed over the anterior 2% of nodes in the finite element model. This distribution of forces is coupled with the ability for the finite element model to deform as forces are applied, which the beam theory model cannot reproduce. This effect subtly changes the lines of action of the forces as they are being applied, leading to more realistic estimations of stresses compared with a rigid rod.

A consideration of the development time and computational expense is warranted. The finite element model is more time consuming in all aspects of its development, but not so time consuming that larger groups of participants than studied here could not be analysed. However, given that both models have provided similar findings when comparing two groups, the ultimate choice of model should depend on the level of detail required by the research questions.

For example, if comparison of time histories is required then the 2D model allows for SPM analysis to be conducted and the timing of any differences between groups or interventions can be discerned. If on the other hand an examination of the location of peak stresses is required, then the finite element model is best suited to this task. It remains unclear how the models would compare when assessing within-participant differences, and whether any relative differences would be similar between modelling approaches.

Finally, when considering the results of both these models the reliability of the input data should be examined to ensure confidence in the outcome variables. Both models are sensitive to the pitch of the metatarsal, which was calculated from two markers on the metatarsal. The markers' spatial locations were measured using Coda CX1 units with a stated error of less than 0.05 mm in any direction. A simple geometry calculation reveals that if each marker were reported with the maximum error, the angle would be changed by 0.12 degrees. Marker placement can also be subject to human error. The research in this thesis involved a marker set based on the Oxford Foot model (Carson et al., 2001), and was applied to each participant's foot in the order and manner specified in their training materials. Previous work investigating the reliability of this marker set has found a possible change of 3.14 ° in sagittal plane angles between marker sessions in adults during walking (Wright et al., 2011). This could have been compounded by alignment of MR data with the experimental coordinate system in the finite element model. Whilst all care was taken to reduce this variability in marker placement, the finite element model shows approximately one MPa difference in peak stress for each degree of pitch. This suggests the magnitudes of peak stress reported from the 3D model in this thesis may have inaccuracies of ± 3 MPa.

The pitch angle used in this thesis was calculated as a vector angle between the floor and the metatarsal markers, and therefore does not account for any movement of the foot away from the laboratory defined anterior-posterior axis that may have occurred during running. Both models therefore make the assumption that the anterior-posterior ground reaction forces act along the plane formed by the longitudinal axis of the bone and the floor rather than at an angle to it. Adjustment to include this would involve scaling the anterior-posterior ground reaction forces and inclusion of a component of the medio-lateral ground reaction forces. However, neither model is sensitive to the horizontal forces with a one Newton difference leading only to 0.03 MPa difference in stress in the finite element model. In the beam theory model a change of 10% in horizontal force under the metatarsal head leads only to a 0.6% change in dorsal stress. The movement of the markers out of the anterior-posterior plane may also adjust the pitch angle of the metatarsal, to which the model is shown to be sensitive. Cavanagh (1987) suggests that an abduction angle of approximately 5.1° is typical during running at a moderate speeds. Using a sample of data from the present study, an adjustment of one marker out of plane by this angle would change the pitch angle by approximately 0.2°.

The models were found to be reasonably sensitive to force input data. A 10% change in vertical ground reaction force yields a change of 8.9% in the peak dorsal compressive stress for the beam theory model, whilst the finite element model was found to be sensitive to the joint contact forces calculated from forces under the toe. These data were calculated from both force plates and pressure plates. Low and Dixon (2010) conducted a study using pressure insoles, finding that the reliability generally excellent (Intra Class Correlation>0.75). Although this is for pressure insoles rather than a pressure plate, the technology used in the

equipment for this study is similar and the results of Low and Dixon (2010) are included here as indicators of reliability. A further study by Ferber et al. (2002) shows good reliability for ground reaction forces and sagittal plane kinematic variables in both between session and between day correlations (Intra Class Correlation>0.88). Both these studies give assurance of the reliability of the data used for input into both models presented in this thesis.

7.2 Does Habitual Foot Strike Pattern Affect the Magnitudes of Stresses Experienced by the Second Metatarsal Bone during Running?

This thesis presents two different modelling approaches to answer the same research question using a single data set. Both models produced similar outcomes and the conclusions from both are the same.

The beam theory model looked only at stresses in the mid-shaft of the metatarsal but assessed stress across the whole of stance. The reported peak stress was the maximum stress calculated at any stance point. Conversely the finite element model assessed stresses across the whole of the bone, but only at three stance points. The point of maximum vertical ground reaction forces gave the greatest stress in all but one participant when using the finite element model and the beam theory model reported peak stress at approximately mid-stance in all participants. The time of peak vertical ground reaction forces were approximately mid-stance (mean 56% stance) in all cases. This suggests that regardless of the modelling approached used, the magnitude of metatarsal stresses at approximately midstance are the most important.

It was hypothesised that the non-rearfoot group would run with greater loading under the metatarsals due to the nature of landing with the centre of pressure in a more anterior location on the foot than the rearfoot group and dispersing the

forces over a smaller area. It was further hypothesised that this greater external loading would lead to significantly greater peak stress in the non-rearfoot group.

In both models the input forces and angles came from the same data set, and statistical comparison of the means of the two groups found that at the times of peak vertical ground reaction force, forces were significantly greater in the non-rearfoot group compared to the rearfoot group, supporting the hypothesis. However, neither model demonstrated a significant difference in peak stresses between groups (beam theory model: NRF 244.73 MPa vs. RF 210.18 MPa P=0.249; finite element model: NRF 51.97 MPa vs. 40.62 MPa P=0.114) in contrast to the hypothesis.

Effect sizes from the two studies were medium to large (Cohen, 1988). The beam theory model reported medium effect sizes of 0.5 and 0.4 for dorsal and plantar stress differences respectively whilst the finite element model reported larger effect sizes of 0.6, 1.0 and 1.0 at the times of maximum braking, maximum vertical ground reaction force and maximum propulsion respectively. These effect sizes indicate that whilst non-significant, there was a trend for bone stress to be greater in NRF runners than RF runners. Therefore, from the perspective of second metatarsal stress fracture injury risk, RF runners cannot be recommended to transition to a NRF strike.

The participants included in this study were well habituated to their running technique and were all training on a regular basis with no reported injuries affecting their training frequency or duration, or which may have forced them to change their foot strike modality. These results suggest that whilst non-rearfoot runners do indeed experience higher forces under the metatarsal heads, this is unlikely to translate to meaningfully greater loading on the bone itself. It is likely

that a number of factors interact synergistically in order to produce this effect. In particular, there are slight non-significant differences in the angle of the bone at the point of peak stress, with non-rearfoot runners tending to have an angle that is three degrees steeper on average. From the sensitivity analysis conducted on the finite element model, it has been shown that an increase of 2.5° in the pitch angle of the bone can reduce the stress by several MPa, with similar results in the beam theory model.

7.3 Modelling Conclusions

Based on the outcomes of the statistical tests, both models provide similar answers to the research question “how does foot strike modality affect the magnitudes of stresses in the second metatarsal?” Given the similarity of results, both modelling methods should be considered useful tools for the estimation of internal metatarsal loading. However, given the large differences in stress magnitudes estimated by the models, care should be taken when comparing the results of either model to previous literature or to directly measured strains. This thesis used comparison with all three estimation methods in order to evaluate the models presented, concluding that both are valid methods for estimation of metatarsal stress, particularly when comparing two sets of values. However, neither can be used to determine the exact magnitude of stress with confidence. This is acceptable given that there is no known ‘threshold’ value for a stress magnitude that will trigger a bone remodelling response or the development of a stress fracture.

7.4 Implications for Future Modelling Research

Future research may seek to improve the bio-realism of the models and reduce their limitations. Although it is not possible to incorporate the full effects of soft tissues into a beam theory model, it should be possible to adjust the distribution

of loading from a point load at the metatarsal head to a distributed load, whereby some percentage of the forces act further up the metatarsal shaft. This could be done based on the plantar pressure distribution under the whole metatarsal. The benefit of this more complicated method for calculating bone stresses would be the output of more accurate bending moments as some forces would be applied closer to the fixed proximal end of the bone.

For the finite element model, an additional layer of material could be added with the geometry and properties of a running shoe, allowing studies to be conducted with shod participants, which is more realistic for the running populations studied. This would allow the interaction of foot strike modality and footwear types to be investigated.

Another area of interest for these models is the training of a machine learning algorithm to estimate the outcome stresses based purely on certain inputs. Despite the increased technical expertise required for the development of such a model, its usability once developed would make it an accessible tool for researchers with limited technical knowledge of finite element modelling or machine learning. Whilst the training of such an algorithm is time consuming, requiring many data points in order to be robust, once training is complete, further computations are very fast. A similar modelling study has been performed by Halloran et al. (2009) with success.

7.5 Implications for Training

This thesis studied participants assumed to be well-habituated to their shod foot strike who were assessed whilst running barefoot. Several participants changed foot strike when running barefoot, which may indicate that these participants were less well habituated than those who did not change between shod and barefoot

running. In the wider context there is a growing trend for runners to transition from one foot strike to another, and this may mean running populations are not always well habituated to the foot strike they are using. In particular transitioning from RF to NRF has increased in popularity recently (Hamill and Gruber, 2017), potentially influenced by suggestions that this is a more “natural” way to run. Confounding this, minimalist shoes and barefoot running are also more popular, in part due to popular running books such as “Born to Run” by Christopher McDougall and research suggesting that barefoot running is what humans were “designed” to do (e.g. Lieberman, 2012). Studies have associated the effects of transitioning to minimalist shoes on stress fractures of the metatarsals in several case studies (Cauthon et al., 2013, Salzler et al., 2012). However it is not clear whether this is due to the lack of cushioning or a transition to a more anterior landing pattern commonly reported when using these shoes (Firminger and Edwards, 2016). The research in this thesis does confirm that landing using a non-rearfoot modality leads to greater loading under the metatarsals, but in the well-habituated population studied, this does not translate to a significantly greater bone stress.

Aside from stress fracture injuries, transitioning to a NRF strike has other reported benefits, such as reduced force loading rates (Futrell et al., 2020), which has been suggested to help to resolve some injuries, for example patellofemoral pain (Davis et al., 2020). However, gait retraining is a process that requires a significant time commitment, and sufficient feedback to ensure the new movement pattern is not in itself problematic. Specific programs used by clinicians may have a phase of learning the new movement (around 4 – 6 weeks) followed by several months of incremental increases in mileage and running intensity (Davis et al., 2020). This habituation time is important as it allows for the tissues of the body to adapt to new loads that may be placed on them by new

movements. This includes the remodelling process of bone. The results of this study are clear that by using a NRF strike, runners place more force under the metatarsal heads compared to RF runners. Less clearly, there is a moderate to large effect size for increased bone stresses in NRF runners compared to RF runners, but no statistically significant difference. In the case of changing from a RF to a NRF strike where the runner is not a non-habituated to the loading experienced, these increased forces could lead to clinically relevant increased bone stresses and via this mechanism increase the risk of metatarsal stress fracture. It is unclear whether differences in metatarsal loading would exist in a RF runner who transitions to a NRF strike. It has previously been suggested that when changing foot strike pattern, the characteristics of the new pattern are exaggerated by the runner in the short term (Boyer et al., 2014, Rice and Patel, 2017). Running with an exaggerated NRF strike, whilst unaccustomed to this mode of loading, may increase the risk of metatarsal stress fracture. Therefore transitioning from one footstrike to another cannot be recommended based on this research.

Both models appear sensitive to the pitch angle of the metatarsal, which implies that the orientation of the foot is important to the development of stresses in the bone when forces are applied via the ground. The finite element model was also sensitive to the joint contact forces applied to it, which may partly explain why measurement of external forces alone is not a useful indicator of the internal loading. The contact forces were calculated using a quasi-static method and incorporated the plantar tendon forces, therefore these forces should also be considered important to the magnitude of stresses experienced by the metatarsal. The fact that multiple factors influence metatarsal stress magnitudes can go some way to explaining the variation in location on the bone that stress

fractures are observed (Orava, 1980). In addition the metatarsals examined in this thesis showed variation in their geometry, and in the beam theory model geometry was shown to influence the areas of greatest stress. Although it remains unknown what magnitude of stress should be considered high enough to cause a stress fracture in any particular person, greater loading is still held to be the general mechanism by which the bone is subjected to microdamage, which may lead to stress fracture. Based on this research it is unlikely that the development of high stress magnitudes in the second metatarsal during running is due to only one training factor, but may be a combination of factors which need researching and addressing independently. The findings presented in this thesis suggest that foot strike modality alone does not influence the maximum stress magnitude during running.

7.6 Implications for Future Research

This thesis has developed two models for estimating stresses in the metatarsals during running for use in applied studies. In this thesis it was shown that greater externally-measured forces do not always correspond to greater internal loading. This suggests that future research investigating internal loading and inferring injury risk from this should not assume that differences in externally measured forces will correlate to differences in internal forces. Future research should make use of participant-specific methods of estimating internal loads from external measures, of which the models presented here are examples.

It has been established that when examining the effects of foot strike during running it is often confounded by factors such as footwear and level of habituation. It may be beneficial for future work in this area to improve understanding of how these factors influence the magnitudes and distributions of stresses in the metatarsals independently. For example, a study utilising in-shoe

pressure measurement insoles and the inclusion of a shoe sole layer in the finite element model would be useful in understanding the role of differences in cushioning in shoes on peak metatarsal stress. A second example would be to investigate the stress magnitudes of poorly habituated participants, such as asking a group to run with several different modalities and comparing the effect on modelled stresses. Finally, future research to provide an indicator of the ecological validity of the modelling approach, without necessarily validating the absolute magnitudes would be valuable. This could be achieved by assessing peak stress in runners at the start of a lengthy training programme and quantifying bone oedema pre- and post-. This would provide an indicator of the remodelling response and could be associated with baseline stress magnitudes. Future work in this area is important to ensure an understanding of the development of stress fractures, and ultimately to give the best possible advice to allow more people to run injury free and increase their overall health and wellbeing.

7.7 Conclusions

This thesis has used two differing modelling approaches to investigating second metatarsal stresses in habitual rearfoot and non-rearfoot runners. The main conclusions drawn from the work are as follows:

1. External force measurements under the second metatarsal head are not representative of stress magnitudes on the second metatarsal and therefore should not be used in isolation to infer stress fracture injury risk.

2. Habitual rearfoot strikers and habitual non-rearfoot strikers experience similar second metatarsal stress magnitudes during running despite non-rearfoot strikers experiencing greater vertical ground reaction forces under the metatarsal head.

3. The 2D beam theory model and the 3D finite element models presented in this thesis are both useful tools for investigating second metatarsal stresses and led to similar conclusions when comparing rearfoot and non-rearfoot runners. However, both models are best suited to investigating differences in stresses between- or within-groups rather than quantifying absolute stress magnitudes.

References

ACTIS, R. L., VENTURA, L. B., LOTT, D. J., SMITH, K. E., COMMEAN, P. K., HASTINGS, M. K. & MUELLER, M. J. 2008. Multi-plug insole design to reduce peak plantar pressure on the diabetic foot during walking. *Med Biol Eng Comput,* 46**,** 363-71.

ACTIS, R. L., VENTURA, L. B., SMITH, K. E., COMMEAN, P. K., LOTT, D. J., PILGRAM, T. K. & MUELLER, M. J. 2006. Numerical simulation of the plantar pressure distribution in the diabetic foot during the push-off stance. *Med Biol Eng Comput,* 44**,** 653-63.

AHN, A. N., BRAYTON, C., BHATIA, T. & MARTIN, P. 2014. Muscle activity and kinematics of forefoot and rearfoot strike runners. *Journal of Sport and Health Science,* 3**,** 102-112.

AKRAMI, M. 2016. *A Large-Scale Subject-Specific Three-Dimensional Finite Element Model of the Human Foot Musculoskeletal Complex.* PhD, University of Manchester.

AKRAMI, M., CRAIG, K., DIBAJ, M., JAVADI, A. A. & BENATTAYALLAH, A. 2018. A three-dimensional finite element analysis of the human hip. *Journal of Medical Engineering & Technology,* 42**,** 546-552.

AKRAMI, M., QIAN, Z., ZOU, Z., HOWARD, D., NESTER, C. J. & REN, L. 2017. Subject-specific finite element modelling of the human foot complex during walking: sensitivity analysis of material properties, boundary and loading conditions. *Biomechanics and modeling in mechanobiology,* 17**,** 559-576.

ALEXANDER, R. M. 1990. Optimum take-off techniques for high and long jumps. *Philos Trans R Soc Lond B Biol Sci,* 329**,** 3-10.

ALLEN, S. J., KING, M. A. & YEADON, M. R. 2010. Is a single or double arm technique more advantageous in triple jumping? *J Biomech,* 43**,** 3156-3161.

ALLEN, S. J., KING, M. A. & YEADON, M. R. 2012. Models incorporating pin joints are suitable for simulating performance but unsuitable for simulating internal loading. *Journal of Biomechanics,* 45**,** 1430-1436.

ANTUNES, P. J., DIAS, G. R., COELHO, A. T., REBELO, F. & PEREIRA, T. 2008. Non-Linear Finite Element Modelling of Anatomically Detailed 3D Foot Model. *Report Paper*.

ARNDT, A., EKENMAN, I., WESTBLAD, P. & LUNDBERG, A. 2002. Effects of fatigue and load variation on metatarsal deformation measured in vivo during barefoot walking. *J Biomech,* 35**,** 621-628.

ARNDT, A., WESTBLAD, P., EKENMAN, I. & LUNDBERG, A. 2003. A comparison of external plantar loading and in vivo local metatarsal deformation wearing two different military boots. *Gait & Posture,* 18**,** 20-26.

BAKKAR, A. 2012. *Meshing Lecture 7* [Online]. Available: http://www.bakker.org/dartmouth06/engs150/07-mesh.pdf [Accessed 18 February 2020].

BALSDON, M. E. R. & DOMBROSKI, C. E. 2018. Reliability of a multi-segment foot model in a neutral cushioning shoe during treadmill walking. *Journal of Foot and Ankle Research,* 11**,** 60.

BENNELL, K. L., MALCOLM, S. A., BRUKNER, P. D., GREEN, R. M., HOPPER, J. L., WARK, J. D. & EBELING, P. R. 1998. A 12-month prospective study of the relationship between stress fractures and bone turnover in athletes. *Calcif Tissue Int,* 63**,** 80-85.

BENNELL, K. L., MALCOLM, S. A., THOMAS, S. A., WARK, J. D. & BRUKNER, P. D. 1996. The Incidence and Distribution of Stress Fractures in Competitive Track and Field Athletes. *The American Journal of Sports Medicine,* 24**,** 211-217.

BOYER, E. R., ROONEY, B. D. & DERRICK, T. R. 2014. Rearfoot and Midfoot or Forefoot Impacts in Habitually Shod Runners. *Medicine & Science in Sports & Exercise,* 46**,** 1384-1391.

BRILAKIS, E., KASELOURIS, E., XYPNITOS, F., PROVATIDIS, C. G. & EFSTATHOPOULOS, N. 2012. Effects of foot posture on fifth metatarsal fracture healing: a finite element study. *J Foot Ankle Surg,* 51**,** 720-728.

BUDHABHATTI, S. P., ERDEMIR, A., PETRE, M., SFERRA, J., DONLEY, B. & CAVANAGH, P. R. 2007. Finite element modeling of the first ray of the foot: a tool for the design of interventions. *J Biomech Eng,* 129**,** 750-756.

BURR, D. B. 1997. Bone, exercise, and stress fractures. *Exerc Sport Sci Rev,* 25**,** 171-194.

CAMACHO, D. L., LEDOUX, W. R., ROHR, E. S., SANGEORZAN, B. J. & CHING, R. P. 2002. A three-dimensional, anatomically detailed foot model: a foundation for a finite element simulation and means of quantifying foot-bone position. *Journal of rehabilitation research and development,* 39**,** 401-410.

CARSON, M. C., HARRINGTON, M. E., THOMPSON, N., O'CONNOR, J. J. & THEOLOGIS, T. N. 2001. Kinematic analysis of a multi-segment foot model for research and clinical applications: a repeatability analysis. *J Biomech,* 34**,** 1299-1307.

CARTER, D. R., CALER, W. E., SPENGLER, D. M. & FRANKEL, V. H. 1981. Fatigue behavior of adult cortical bone: the influence of mean strain and strain range. *Acta Orthop Scand,* 52**,** 481-490.

CAUTHON, D. J., LANGER, P. & CONIGLIONE, T. C. 2013. Minimalist shoe injuries: Three case reports. *The Foot,* 23**,** 100-103.

CAVANAGH, P. R. 1987. The Biomechanics of Lower Extremity Action in Distance Running. *Foot & Ankle,* 7**,** 197-217.

CAVANAGH, P. R. & LAFORTUNE, M. A. 1980. Ground reaction forces in distance running. *J Biomech,* 13**,** 397-406.

CHAKRAVARTY, E. F., HUBERT, H. B., LINGALA, V. B. & FRIES, J. F. 2008. Reduced Disability and Mortality among Aging Runners: a 21-year Longitudinal Study. *Archives of internal medicine,* 168**,** 1638-1646.

CHEN, W.-P., TANG, F.-T. & JU, C.-W. 2001a. Stress distribution of the foot during mid-stance to push-off in barefoot gait: a 3-D finite element analysis. *Clinical Biomechanics,* 16**,** 614-620.

CHEN, W. M., LEE, S. J. & LEE, P. V. 2015a. Plantar pressure relief under the metatarsal heads: therapeutic insole design using three-dimensional finite element model of the foot. *J Biomech,* 48**,** 659-665.

CHEN, W. M., LEE, T., LEE, P. V., LEE, J. W. & LEE, S. J. 2010. Effects of internal stress concentrations in plantar soft-tissue--A preliminary three-dimensional finite element analysis. *Med Eng Phys,* 32**,** 324-331.

CHEN, W. M., PARK, J., PARK, S. B., SHIM, V. P. & LEE, T. 2012. Role of gastrocnemius-soleus muscle in forefoot force transmission at heel rise - A 3D finite element analysis. *J Biomech,* 45**,** 1783-1789.

CHEN, W. P., TANG, F. T. & JU, C. W. 2001b. Stress distribution of the foot during mid-stance to push-off in barefoot gait: a 3-D finite element analysis. *Clin Biomech (Bristol, Avon),* 16**,** 614-620.

CHEN, Y. N., CHANG, C. W., LI, C. T., CHANG, C. H. & LIN, C. F. 2015b. Finite element analysis of plantar fascia during walking: a quasi-static simulation. *Foot Ankle Int,* 36**,** 90-97.

CHENG, H. Y., LIN, C. L., WANG, H. W. & CHOU, S. W. 2008. Finite element analysis of plantar fascia under stretch-the relative contribution of windlass mechanism and Achilles tendon force. *J Biomech,* 41**,** 1937-1944.

CHEUNG, J. T., AN, K. N. & ZHANG, M. 2006. Consequences of partial and total plantar fascia release: a finite element study. *Foot Ankle Int,* 27**,** 125-132.

CHEUNG, J. T., ZHANG, M. & AN, K. N. 2004. Effects of plantar fascia stiffness on the biomechanical responses of the ankle-foot complex. *Clin Biomech (Bristol, Avon),* 19**,** 839-846.

CHEUNG, J. T., ZHANG, M., LEUNG, A. K. & FAN, Y. B. 2005. Three-dimensional finite element analysis of the foot during standing--a material sensitivity study. *J Biomech,* 38**,** 1045-1054.

CHEUNG, R. T. H. & DAVIS, I. S. 2011. Landing Pattern Modification to Improve Patellofemoral Pain in Runners: A Case Series. *Journal of Orthopaedic & Sports Physical Therapy,* 41**,** 914-919.

CHUCKPAIWONG, B., COOK, C., PIETROBON, R. & NUNLEY, J. A. 2007. Second metatarsal stress fracture in sport: comparative risk factors between proximal and non-proximal locations. *British journal of sports medicine,* 41**,** 510-514.

COHEN, J. 1988. The Analysis of Variance. *Statistical Power Analysis for the Behavioral Sciences (Second Edition).* Lawrence Erlbaum Associates.

DASSAULT SYSTÈMES SIMULIA CORP. 2013. *Abaqus 6.13 Documentation* [Online]. Available: http://dsk.ippt.pan.pl/docs/abaqus/v6.13/index.html [Accessed 09/02/2020 2020].

DAVIS, I. S., TENFORDE, A. S., NEAL, B. S., ROPER, J. L. & WILLY, R. W. 2020. Gait Retraining as an Intervention for Patellofemoral Pain. *Current Reviews in Musculoskeletal Medicine,* 13**,** 103-114.

DAY, E. M. & HAHN, M. E. 2019. A comparison of metatarsophalangeal joint center locations on estimated joint moments during running. *Journal of Biomechanics,* 86**,** 64-70.

DEMPSTER, W. T. 1955. *Space requirements of the seated operator: geometrical, kinematic, and mechanical aspects of the body with special reference to the limbs,* Wright-Patterson Air Force Base, Ohio, Wright Air Development Center.

DIEBAL, M. A. R., GREGORY, R., ALITZ, C. C. & GERBER, C. J. P. 2012. Forefoot Running Improves Pain and Disability Associated With Chronic Exertional Compartment Syndrome. *The American Journal of Sports Medicine,* 40**,** 1060-1067.

DIXON, S., NUNNS, M., HOUSE, C., RICE, H., MOSTAZIR, M., STILES, V., DAVEY, T., FALLOWFIELD, J. & ALLSOPP, A. 2019. Prospective study of biomechanical risk factors for second and third metatarsal stress fractures in military recruits. *Journal of Science and Medicine in Sport,* 22**,** 135-139.

DIXON, S. J., CREABY, M. W. & ALLSOPP, A. J. 2006. Comparison of static and dynamic biomechanical measures in military recruits with and without a history of third metatarsal stress fracture. *Clinical Biomechanics,* 21**,** 412-419.

DONAHUE, S. W., SHARKEY, N. A., MODANLOU, K. A., SEQUEIRA, L. N. & MARTIN, R. B. 2000. Bone strain and microcracks at stress fracture sites in human metatarsals. *Bone,* 27**,** 827-833.

DORSEY, S. W., IRENE, S. M. & KURT, T. M. 2000. Lower Extremity Mechanics in Runners with a Converted Forefoot Strike Pattern. *Journal of Applied Biomechanics,* 16**,** 210-218.

DRAKE, R. L., WAYNE VOGL, A. & MITCHELL, A. W. M. 2015. *Gray's Anatomy for Students,* Philadelphia, Churchill Livingstone Elsevier.

DREZ, D., YOUNG, J. C., JOHNSTON, R. D. & PARKER, W. D. 1980. Metatarsal stress fractures. *The American Journal of Sports Medicine,* 8**,** 123-125.

DUNCAN, R. L. & TURNER, C. H. 1995. Mechanotransduction and the functional response of bone to mechanical strain. *Calcif Tissue Int,* 57**,** 344-358.

EDWARDS, W. B., TAYLOR, D., RUDOLPHI, T. J., GILLETTE, J. C. & DERRICK, T. R. 2009. Effects of Stride Length and Running Mileage on a Probabilistic Stress Fracture Model. *Medicine & Science in Sports & Exercise,* 41**,** 2177-2184.

ERDEMIR, A., SAUCERMAN, J. J., LEMMON, D., LOPPNOW, B., TURSO, B., ULBRECHT, J. S. & CAVANAGH, P. R. 2005. Local plantar pressure relief in therapeutic footwear: design guidelines from finite element models. *J Biomech,* 38**,** 1798-1806.

FAUL, F., ERDFELDER, E., LANG, A.-G. & BUCHNER, A. 2007. G*Power 3: A flexible statistical power analysis program for the social, behavioral, and biomedical sciences. *Behavior Research Methods,* 39**,** 175-191.

FERBER, R., MCCLAY DAVIS, I., WILLIAMS III, D. S. & LAUGHTON, C. 2002. A comparison of within- and between-day reliability of discrete 3D lower extremity variables in runners. *Journal of Orthopaedic Research,* 20**,** 1139-1145.

FIELDS, K. B., SYKES, J. C., WALKER, K. M. & JACKSON, J. C. 2010. Prevention of Running Injuries. *Current Sports Medicine Reports,* 9**,** 176-182.

FIRMINGER, C. R. & EDWARDS, W. B. 2016. The influence of minimalist footwear and stride length reduction on lower-extremity running mechanics and cumulative loading. *Journal of Science and Medicine in Sport,* 19**,** 975-979.

FIRMINGER, C. R., FUNG, A., LOUNDAGIN, L. L. & EDWARDS, W. B. 2017. Effects of footwear and stride length on metatarsal strains and failure in running. *Clinical Biomechanics,* 49**,** 8-15.

FLAVIN, R., HALPIN, T., O'SULLIVAN, R., FITZPATRICK, D., IVANKOVIC, A. & STEPHENS, M. 2008. A finite-element analysis study of the metatarsophalangeal joint of the hallux rigidus. *Bone & Joint Journal,* 90**,** 1334-1340.

FROST, H. M. 1987. Bone "mass" and the "mechanostat": a proposal. *Anat Rec,* 219**,** 1-9.

FUNG, A., LOUNDAGIN, L. L. & EDWARDS, W. B. 2017. Experimental validation of finite element predicted bone strain in the human metatarsal. *J Biomech,* 60**,** 22-29.

FUTRELL, E. E., GROSS, K. D., REISMAN, D., MULLINEAUX, D. R. & DAVIS, I. S. 2020. Transition to forefoot strike reduces load rates more effectively than altered cadence. *Journal of Sport and Health Science,* 9**,** 248-257.

GARCIA-AZNAR, J. M., BAYOD, J., ROSAS, A., LARRAINZAR, R., GARCIA-BOGALO, R., DOBLARE, M. & LLANOS, L. F. 2009. Load transfer mechanism for different metatarsal geometries: a finite element study. *J Biomech Eng,* 131**,** 021011.

GARCIA-GONZALEZ, A., BAYOD, J., PRADOS-FRUTOS, J. C., LOSA-IGLESIAS, M., JULES, K. T., BECERRO DE BENGOA-VALLEJO, R. & DOBLARE, M. 2009. Finite-element simulation of flexor digitorum longus or flexor digitorum brevis tendon transfer for the treatment of claw toe deformity. *J Biomech,* 42**,** 1697-1704.

GEFEN, A. 2002. Stress analysis of the standing foot following surgical plantar fascia release. *J Biomech,* 35**,** 629-637.

GEFEN, A. 2003a. The in vivo elastic properties of the plantar fascia during the contact phase of walking. *Foot Ankle Int,* 24**,** 238-244.

GEFEN, A. 2003b. Plantar soft tissue loading under the medial metatarsals in the standing diabetic foot. *Med Eng Phys,* 25**,** 491-499.

GEFEN, A., MEGIDO-RAVID, M., ITZCHAK, Y. & ARCAN, M. 2000. Biomechanical analysis of the three-dimensional foot structure during gait: a basic tool for clinical applications. *J Biomech Eng,* 122**,** 630-639.

GÍSLASON, M. K. & NASH, D. H. Finite Element Modelling of a Multi-Bone Joint : The Human Wrist. 2012. InTechOpen.

GROSS, T. S. & BUNCH, R. P. 1989. A mechanical model of metatarsal stress fracture during distance running. *Am J Sports Med,* 17**,** 669-674.

GU, Y. & LI, Z. 2012. Mechanical Information of Plantar Fascia during Normal Gait. *Physics Procedia,* 33**,** 63-66.

GU, Y. D., REN, X. J., LI, J. S., LAKE, M. J., ZHANG, Q. Y. & ZENG, Y. J. 2010. Computer simulation of stress distribution in the metatarsals at different inversion landing angles using the finite element method. *Int Orthop,* 34**,** 669-676.

GU, Y. D., REN, X. J., RUAN, G. Q., ZENG, Y. J. & LI, J. S. 2011. Foot contact surface effect to the metatarsals loading character during inversion landing. *International Journal for Numerical Methods in Biomedical Engineering,* 27**,** 476-484.

GUIOTTO, A., SAWACHA, Z., GUARNERI, G., AVOGARO, A. & COBELLI, C. 2014. 3D finite element model of the diabetic neuropathic foot: a gait analysis driven approach. *J Biomech,* 47**,** 3064-3071.

HALLORAN, J. P., ERDEMIR, A. & VAN DEN BOGERT, A. J. 2009. Adaptive surrogate modeling for efficient coupling of musculoskeletal control and tissue deformation models. *J Biomech Eng,* 131**,** 011014.

HALLORAN, J. P., SIBOLE, S., VAN DONKELAAR, C. C., VAN TURNHOUT, M. C., OOMENS, C. W., WEISS, J. A., GUILAK, F. & ERDEMIR, A. 2012. Multiscale mechanics of articular cartilage: potentials and challenges of coupling musculoskeletal, joint, and microscale computational models. *Ann Biomed Eng,* 40**,** 2456-2474.

HAMILL, J. & GRUBER, A. H. 2017. Is changing footstrike pattern beneficial to runners? *Journal of Sport and Health Science,* 6**,** 146-153.

HANNAH, I., HARLAND, A., PRICE, D. & LUCAS, T. 2012. Centre of pressure output in a kinematically driven finite element footstrike model. *Procedia Engineering,* 34**,** 278-283.

HART, N. H., NIMPHIUS, S., RANTALAINEN, T., IRELAND, A., SIAFARIKAS, A. & NEWTON, R. U. 2017. Mechanical basis of bone strength: influence of bone material, bone structure and muscle action. *Journal of musculoskeletal & neuronal interactions,* 17**,** 114-139.

HAYAFUNE, N., HAYAFUNE, Y. & JACOB, H. A. C. 1999. Pressure and force distribution characteristics under the normal foot during the push-off phase in gait. *The Foot,* 9**,** 88-92.

HILEY, M. J. & YEADON, M. R. 2005. Maximal dismounts from high bar. *J Biomech,* 38**,** 2221-2227.

HSU, Y.-C., GUNG, Y.-W., SHIH, S.-L., FENG, C.-K., WEI, S.-H., YU, C.-H. & CHEN, C.-S. 2008. Using an Optimization Approach to Design an Insole for Lowering Plantar Fascia Stress—A Finite Element Study. *Annals of Biomedical Engineering,* 36**,** 1345.

ISVILANONDA, V., DENGLER, E., IAQUINTO, J. M., SANGEORZAN, B. J. & LEDOUX, W. R. 2012. Finite element analysis of the foot: model validation and comparison between two common treatments of the clawed hallux deformity. *Clin Biomech (Bristol, Avon),* 27**,** 837-844.

IWAMOTO, J. & TAKEDA, T. 2003. Stress fractures in athletes: review of 196 cases. *J Orthop Sci,* 8**,** 273-278.

JACOB, H. A. 2001. Forces acting in the forefoot during normal gait--an estimate. *Clin Biomech (Bristol, Avon),* 16**,** 783-792.

JACOB, S., PATIL, K. M., BRAAK, L. H. & HUSON, A. 1996. Stresses in a 3D two arch model of a normal human foot. *Mechanics Research Communications,* 23**,** 387-393.

KELLY, L. A., CRESSWELL, A. G. & FARRIS, D. J. 2018a. The energetic behaviour of the human foot across a range of running speeds. *Scientific Reports,* 8**,** 10576.

KELLY, L. A., FARRIS, D. J., CRESSWELL, A. G. & LICHTWARK, G. A. 2018b. Intrinsic foot muscles contribute to elastic energy storage and return in the human foot. *Journal of Applied Physiology,* 126**,** 231-238.

KENNY, M., ELLISON, M. & RICE, H. 2019. Matlab code to digitise MR bone images and calculate properties of shape: cross-sectional area, area moment of inertia, product moment of area. 1.0 ed. Open Research Exeter: University of Exeter.

KER, R. F., BENNETT, M. B., BIBBY, S. R., KESTER, R. C. & ALEXANDER, R. M. 1987. The spring in the arch of the human foot. *Nature,* 325**,** 147-149.

KRALL, E. A. & DAWSON-HUGHES, B. 1993. Heritable and life-style determinants of bone mineral density. *Journal of Bone and Mineral Research,* 8**,** 1-9.

LAPPE, J. M., STEGMAN, M. R. & RECKER, R. R. 2001. The Impact of Lifestyle Factors on Stress Fractures in Female Army Recruits. *Osteoporosis International,* 12**,** 35-42.

LASSUS, J., TULIKOURA, I., KONTTINEN, Y. T., SALO, J. & SANTAVIRTA, S. 2002. Bone stress injuries of the lower extremity: a review. *Acta Orthop Scand,* 73**,** 359-368.

LAUGHTON, C. A., DAVIS, I. M. & HAMILL, J. 2003. Effect of Strike Pattern and Orthotic Intervention on Tibial Shock during Running. *Journal of Applied Biomechanics,* 19**,** 153-168.

LEE, D.-C., PATE, R. R., LAVIE, C. J., SUI, X., CHURCH, T. S. & BLAIR, S. N. 2014. Leisure-Time Running Reduces All-Cause and Cardiovascular Mortality Risk. *Journal of the American College of Cardiology,* 64**,** 472-481.

LEE, I. M., PAFFENBARGER, R. S. & HENNEKENS, C. H. 1997. Physical activity, physical fitness and longevity. *Aging Clinical and Experimental Research,* 9**,** 2-11.

LEE, I. M., SHIROMA, E. J., LOBELO, F., PUSKA, P., BLAIR, S. N. & KATZMARZYK, P. T. 2012. Impact of Physical Inactivity on the World's Major Non-Communicable Diseases. *Lancet,* 380**,** 219-229.

LEMMON, D. & CAVANAGH, P. 1997. Finite element modelling of plantar pressure beneath the second ray with flexor muscle loading. *Clin Biomech (Bristol, Avon),* 12**,** S13-S14.

LEMMON, D., SHIANG, T., HASHMI, A., ULBRECHT, J. S. & CAVANAGH, P. R. 1997a. The effect of insoles in therapeutic footwear—a finite element approach. *Journal of biomechanics,* 30**,** 615-620.

LEMMON, D., SHIANG, T. Y., HASHMI, A., ULBRECHT, J. S. & CAVANAGH, P. R. 1997b. The effect of insoles in therapeutic footwear--a finite element approach. *J Biomech,* 30**,** 615-620.

LI, S., ZHANG, Y., GU, Y. & REN, J. 2017. Stress distribution of metatarsals during forefoot strike versus rearfoot strike: A finite element study. *Computers in Biology and Medicine,* 91**,** 38-46.

LIEBERMAN, D. E. 2012. What We Can Learn About Running from Barefoot Running: An Evolutionary Medical Perspective. *Exercise and Sport Sciences Reviews,* 40**,** 63-72.

LIEBERMAN, D. E., VENKADESAN, M., WERBEL, W. A., DAOUD, A. I., D'ANDREA, S., DAVIS, I. S., MANG'ENI, R. O. & PITSILADIS, Y. 2010. Foot strike patterns and collision forces in habitually barefoot versus shod runners. *Nature,* 463**,** 531.

LOW, D. C. & DIXON, S. J. 2010. Footscan pressure insoles: Accuracy and reliability of force and pressure measurements in running. *Gait & Posture,* 32**,** 664-666.

MANTER, J. T. 1946. Distribution of compression forces in the joints of the human foot. *Anat Rec,* 96**,** 313-321.

MARTIN, B. 1992. A theory of fatigue damage accumulation and repair in cortical bone. *J Orthop Res,* 10**,** 818-825.

MARTIN, R. B., BURR, D. B., SHARKEY, N. A. & FYHRIE, D. P. 2015. *Skeletal tissue mechanics*, Springer New York.

MATHESON, G. O., CLEMENT, D. B., MCKENZIE, D. C., TAUNTON, J. E., LLOYD-SMITH, D. R. & MACINTYRE, J. G. 1987. Stress fractures in athletes. *The American Journal of Sports Medicine,* 15**,** 46-58.

MATIJEVICH, E. S., BRANSCOMBE, L. M., SCOTT, L. R. & ZELIK, K. E. 2019. Ground reaction force metrics are not strongly correlated with tibial bone load when running across speeds and slopes: Implications for science, sport and wearable tech. *PloS one,* 14**,** e0210000.

MEARDON, S. A. & DERRICK, T. R. 2014. Effect of step width manipulation on tibial stress during running. *J Biomech,* 47**,** 2738-2744.

MILGROM, C., FINESTONE, A., SHARKEY, N., HAMEL, A., MANDES, V., BURR, D., ARNDT, A. & EKENMAN, I. 2002. Metatarsal strains are sufficient to cause fatigue fracture during cyclic overloading. *Foot Ankle Int,* 23**,** 230-235.

MILGROM, C., GILADI, M., STEIN, M., KASHTAN, H., MARGULIES, J., CHISIN, R., STEINBERG, R. & AHARONSON, Z. 1985. Stress fractures in military recruits. A prospective study showing an unusually high incidence. *Journal of Bone & Joint Surgery, British Volume,* 67-B**,** 732-735.

MILGROM, C., SIMKIN, A., ELDAD, A., NYSKA, M. & FINESTONE, A. 2000. Using Bone's Adaptation Ability to Lower the Incidence of Stress Fractures. *The American Journal of Sports Medicine,* 28**,** 245-251.

MILLS, C., PAIN, M. T. & YEADON, M. R. 2008. The influence of simulation model complexity on the estimation of internal loading in gymnastics landings. *J Biomech,* 41**,** 620-628.

MORALES-ORCAJO, E., BAYOD, J., BECERRO-DE-BENGOA-VALLEJO, R., LOSA-IGLESIAS, M. & DOBLARE, M. 2015a. Influence of first proximal phalanx geometry on hallux valgus deformity: a finite element analysis. *Med Biol Eng Comput,* 53**,** 645-653.

MORALES-ORCAJO, E., BAYOD, J. & DE LAS CASAS, E. B. 2015b. Computational Foot Modeling: Scope and Applications. *Archives of Computational Methods in Engineering,* 23**,** 1-28.

MORALES-ORCAJO, E., BECERRO DE BENGOA VALLEJO, R., LOSA IGLESIAS, M., BAYOD, J. & BARBOSA DE LAS CASAS, E. 2018. Foot internal stress distribution during impact in barefoot running as function of the strike pattern. *Computer Methods in Biomechanics and Biomedical Engineering,* 21**,** 1-8.

MOSLEY, J. R. & LANYON, L. E. 1998. Strain rate as a controlling influence on adaptive modeling in response to dynamic loading of the ulna in growing male rats. *Bone,* 23**,** 313-318.

MURPHY, D. F., CONNOLLY, D. A. J. & BEYNNON, B. D. 2003. Risk factors for lower extremity injury: a review of the literature. *British Journal of Sports Medicine,* 37**,** 13.

NAGEL, A., FERNHOLZ, F., KIBELE, C. & ROSENBAUM, D. 2008. Long distance running increases plantar pressures beneath the metatarsal heads. A barefoot walking investigation of 200 marathon runners. *Gait and Posture,* 27**,** 152-155.

NAJAFI, A. R., ARSHI, A. R., ESLAMI, M. R., FARIBORZ, S. & MOEINZADEH, M. H. 2007. Micromechanics fracture in osteonal cortical bone: a study of the interactions between microcrack propagation, microstructure and the material properties. *J Biomech,* 40**,** 2788-2795.

NAKAMURA, S., CROWNINSHIELD, R. D. & COOPER, R. R. 1981. An analysis of soft tissue loading in the foot--a preliminary report. *Bull Prosthet Res,* 10-35**,** 27-34.

NATALI, A. N., FORESTIERO, A., CARNIEL, E. L., PAVAN, P. G. & DAL ZOVO, C. 2010. Investigation of foot plantar pressure: experimental and numerical analysis. *Med Biol Eng Comput,* 48**,** 1167-1174.

NUNNS, M., HOUSE, C., FALLOWFIELD, J., ALLSOPP, A. & DIXON, S. 2013. Biomechanical characteristics of barefoot footstrike modalities. *J Biomech,* 46**,** 2603-2610.

NUNNS, M., STILES, V., FULFORD, J. & DIXON, S. 2017. Estimated third metatarsal bending stresses are highly susceptible to variations in bone geometry. *Footwear Science***,** 1-11.

ORAVA, S. 1980. Stress fractures. *British Journal of Sports Medicine,* 14**,** 40-44.

PAIN, M. T. & CHALLIS, J. H. 2006. The influence of soft tissue movement on ground reaction forces, joint torques and joint reaction forces in drop landings. *J Biomech,* 39**,** 119-124.

PATAKY, T. C., ROBINSON, M. A. & VANRENTERGHEM, J. 2016. Region-of-interest analyses of one-dimensional biomechanical trajectories: bridging 0D and 1D theory, augmenting statistical power. *PeerJ,* 4**,** e2652.

POPOVICH, R. M., GARDNER, J. W., POTTER, R., KNAPIK, J. J. & JONES, B. H. 2000. Effect of rest from running on overuse injuries in army basic training. *Am J Prev Med,* 18**,** 147-155.

QIAN, Z.-H., REN, L., REN, L.-Q. & BOONPRATATONG, A. 2010a. A Three-Dimensional Finite Element Musculoskeletal Model of the Human Foot Complex. *In:* LIM, C. T. & GOH, J. C. H. (eds.) *6th World Congress of Biomechanics (WCB 2010). August 1-6, 2010 Singapore: In Conjunction with 14th International Conference on Biomedical Engineering (ICBME) and 5th Asia Pacific Conference on Biomechanics (APBiomech).* Berlin, Heidelberg: Springer Berlin Heidelberg.

QIAN, Z., REN, L., DING, Y., HUTCHINSON, J. R. & REN, L. 2013. A dynamic finite element analysis of human foot complex in the sagittal plane during level walking. *PLoS One,* 8**,** e79424.

QIAN, Z., REN, L. & REN, L. 2010b. A Coupling Analysis of the Biomechanical Functions of Human Foot Complex during Locomotion. *Journal of Bionic Engineering,* 7**,** S150-S157.

QIN, Y. X., RUBIN, C. T. & MCLEOD, K. J. 1998. Nonlinear dependence of loading intensity and cycle number in the maintenance of bone mass and morphology. *J Orthop Res,* 16**,** 482-489.

RAUH, M. J., MACERA, C. A., TRONE, D. W., SHAFFER, R. A. & BRODINE, S. K. 2006. Epidemiology of Stress Fracture and Lower-Extremity Overuse Injury in Female Recruits. *Medicine & Science in Sports & Exercise,* 38**,** 1571-1577.

RICE, H. & PATEL, M. 2017. Manipulation of Foot Strike and Footwear Increases Achilles Tendon Loading During Running. *The American Journal of Sports Medicine,* 45**,** 2411-2417.

RICE, H. M. 2015. *Potential mechanisms for the occurrence of tibial stress fractures, metatarsal stress fractures and ankle inversion injuries in Royal Marine recruits.* Ph.D., University of Exeter.

RICE, H. M., JAMISON, S. T. & DAVIS, I. S. 2016. Footwear Matters: Influence of Footwear and Foot Strike on Load Rates during Running. *Med Sci Sports Exerc,* 48**,** 2462-2468.

SALZLER, M. J., BLUMAN, E. M., NOONAN, S., CHIODO, C. P. & DE ASLA, R. J. 2012. Injuries Observed in Minimalist Runners. *Foot & Ankle International,* 33**,** 262-266.

SAMITZ, G., EGGER, M. & ZWAHLEN, M. 2011. Domains of physical activity and all-cause mortality: systematic review and dose–response meta-analysis of cohort studies. *International Journal of Epidemiology,* 40**,** 1382-1400.

SCHAFFLER, M. B. & JEPSEN, K. J. 2000. Fatigue and repair in bone. *International Journal of Fatigue,* 22**,** 839-846.

SCHAFFLER, M. B., RADIN, E. L. & BURR, D. B. 1989. Mechanical and morphological effects of strain rate on fatigue of compact bone. *Bone,* 10**,** 207-214.

SCHNOHR, P., MAROTT, J. L., LANGE, P. & JENSEN, G. B. 2013. Longevity in Male and Female Joggers: The Copenhagen City Heart Study. *American Journal of Epidemiology,* 177**,** 683-689.

SCOTT, S. H. & WINTER, D. A. 1990. Internal forces of chronic running injury sites. *Med Sci Sports Exerc,* 22**,** 357-369.

SHARKEY, N. A. & HAMEL, A. J. 1998. A dynamic cadaver model of the stance phase of gait: performance characteristics and kinetic validation. *Clinical Biomechanics,* 13**,** 420-433.

SIMKIN, A., LEICHTER, I., GILADI, M., STEIN, M. & MILGROM, C. 1989. Combined Effect of Foot Arch Structure and an Orthotic Device on Stress Fractures. *Foot & Ankle,* 10**,** 25-29.

SPIRKA, T. A., ERDEMIR, A., EWERS SPAULDING, S., YAMANE, A., TELFER, S. & CAVANAGH, P. R. 2014. Simple finite element models for use in the design of therapeutic footwear. *J Biomech,* 47**,** 2948-2955.

SPORT ENGLAND 2018. Active Lives Adult Survey.

SPYROU, L. A. & ARAVAS, N. 2012. Muscle-driven finite element simulation of human foot movements. *Comput Methods Biomech Biomed Engin,* 15**,** 925-934.

STOKES, I. A., HUTTON, W. C. & STOTT, J. R. 1979. Forces acting on the metatarsals during normal walking. *J Anat,* 129**,** 579-590.

SUN, P. C., SHIH, S. L., CHEN, Y. L., HSU, Y. C., YANG, R. C. & CHEN, C. S. 2012. Biomechanical analysis of foot with different foot arch heights: a finite element analysis. *Comput Methods Biomech Biomed Engin,* 15**,** 563-569.

TELFER, S., ERDEMIR, A., WOODBURN, J. & CAVANAGH, P. R. 2016. Simplified versus geometrically accurate models of forefoot anatomy to predict plantar pressures: A finite element study. *J Biomech,* 49**,** 289-294.

THOMAS, V. J., PATIL, K. M. & RADHAKRISHNAN, S. 2004. Three-dimensional stress analysis for the mechanics of plantar ulcers in diabetic neuropathy. *Med Biol Eng Comput,* 42**,** 230-235.

VÄLIMÄKI, V.-V., ALFTHAN, H., LEHMUSKALLIO, E., LÖYTTYNIEMI, E., SAHI, T., SUOMINEN, H. & VÄLIMÄKI, M. J. 2005. Risk factors for clinical stress fractures in male military recruits: A prospective cohort study. *Bone,* 37**,** 267-273.

VAN DER WORP, M. P., TEN HAAF, D. S. M., VAN CINGEL, R., DE WIJER, A., NIJHUIS-VAN DER SANDEN, M. W. G. & STAAL, J. B. 2015. Injuries in Runners; A Systematic Review on Risk Factors and Sex Differences. *PLOS ONE,* 10**,** e0114937.

VAN GENT, R. N., SIEM, D., VAN MIDDELKOOP, M., VAN OS, A. G., BIERMA-ZEINSTRA, S. M. A. & KOES, B. W. 2007. Incidence and determinants of lower extremity running injuries in long distance runners: a systematic review. *British Journal of Sports Medicine,* 41**,** 469-480.

VIGOTSKY, A. D., ZELIK, K. E., LAKE, J. & HINRICHS, R. N. 2019. Mechanical misconceptions: Have we lost the "mechanics" in "sports biomechanics"? *Journal of Biomechanics,* 93**,** 1-5.

WANG, N., ZHANG, X., XIANG, Y.-B., LI, H., YANG, G., GAO, J., ZHENG, W. & SHU, X.-O. 2013. Associations of Tai Chi, Walking, and Jogging With Mortality in Chinese Men. *American Journal of Epidemiology,* 178**,** 791-796.

WARNE, J. P., KILDUFF, S. M., GREGAN, B. C., NEVILL, A. M., MORAN, K. A. & WARRINGTON, G. D. 2014. A 4-week instructed minimalist running transition and gait-retraining changes plantar pressure and force. *Scandinavian Journal of Medicine & Science in Sports,* 24**,** 964-973.

WILLIAMS III, D. S., MCCLAY, I. S. & HAMILL, J. 2001. Arch structure and injury patterns in runners. *Clinical Biomechanics,* 16**,** 341-347.

WOLFRAM, U. & SCHWIEDRZIK, J. 2016. Post-yield and failure properties of cortical bone. *BoneKEy reports* [Online], 5. [Accessed 2016].

WOOD, A. M., HALES, R., KEENAN, A., MOSS, A., CHAPMAN, M., DAVEY, T. & NELSTROP, A. 2014. Incidence and Time to Return to Training for Stress Fractures during Military Basic Training. *Journal of Sports Medicine***,** 5.

WRIGHT, C. J., ARNOLD, B. L., COFFEY, T. G. & PIDCOE, P. E. 2011. Repeatability of the modified Oxford foot model during gait in healthy adults. *Gait & Posture,* 33**,** 108-112.

WU, L. 2007. Nonlinear finite element analysis for musculoskeletal biomechanics of medial and lateral plantar longitudinal arch of Virtual Chinese Human after plantar ligamentous structure failures. *Clin Biomech (Bristol, Avon),* 22**,** 221-229.

YARNITZKY, G., YIZHAR, Z. & GEFEN, A. 2006. Real-time subject-specific monitoring of internal deformations and stresses in the soft tissues of the foot: a new approach in gait analysis. *J Biomech,* 39**,** 2673-2689.

YEADON, M. R., ATHA, J. & HALES, F. D. 1990. The simulation of aerial movement--IV. A computer simulation model. *J Biomech,* 23**,** 85-89.

YEADON, M. R. & KING, M. A. 2002. Evaluation of a Torque-Driven Simulation Model of Tumbling. *Journal of Applied Biomechanics,* 18**,** 195-206.

YETTRAM, A. L. & CAMILLERI, N. N. 1993. The forces acting on the human calcaneus. *J Biomed Eng,* 15**,** 46-50.

YU, J., CHEUNG, J. T.-M., FAN, Y., ZHANG, Y., LEUNG, A. K.-L. & ZHANG, M. 2008. Development of a finite element model of female foot for high-heeled shoe design. *Clinical Biomechanics,* 23**,** S31-S38.

Appendix 1 - Manual Zone Adjustment within RSscan Software

To identify the cells on the pressure plate corresponding to the second metatarsal head and second toe the mask function in the RS Scan software was used. The manual procedure followed has documented excellent intra- and inter-observer reliability (ICC ≥ 0.995 and 0.985 respectively with $P < 0.001$) (Rice, 2015). In brief the steps are as follows.

1. Adjust the size and position of the last, to accommodate the outline of the foot.
2. Adjust the two horizontal lines separating the metatarsal heads from the toes and midfoot.
3. Adjust the vertical lines separating the rays of the foot. Individual toes were used to estimate these positions.
4. Make any corrections using the individual cell painter. The cells were checked against the pressure distribution to ensure closeness of fit.
5. A mask that is not a region of interest (i.e. metatarsal 5) was used to divide the second toe from the remaining toes.

Appendix 2 – Inter-Segmental Foot Kinematics during Running with Different Habitual Foot Strike Patterns

It has been observed that foot strike influences the kinematics between the foot and the shank, with greater dorsiflexion range of motion observed in those who run with a forefoot than a rearfoot strike (Laughton et al., 2003, Nunns et al., 2013, Dorsey et al., 2000) and greater rearfoot eversion range of motion in those who run with a forefoot than a rearfoot strike (Dorsey et al., 2000, Nunns et al., 2013). However, these findings have been observed when the foot has been simplified into a single rigid segment. The foot is in fact a highly complex multi-segment structure. The aim of this section is to characterise the inter-segment foot kinematics of rearfoot and non-rearfoot strike runners. It was hypothesised that there would be greater range of motion between segments in runners who run with a non-rearfoot strike compared with those who run with a rearfoot strike.

Data for this appendix is taken from the data set collected in Chapter 3 using the marker sets shown in Figures 60 - 62. Briefly, inter-segment foot kinematic data were collected from 18 participants and a static trial obtained whilst standing in a relaxed position. The value of each inter-segment angle during standing was subtracted from each corresponding angle during dynamic trials. The dynamic trials were first reviewed to ensure sufficient marker tracking in at least 5 trials per participant. Five participants were removed from the analysis for this reason. The static trials were then reviewed and where there was insufficient marker data to define a particular segment, that angle was excluded for that participant whilst their other angles were included. The exclusions due to static trials only occurred in the rearfoot strike group, such that time histories were averaged from three or four participants in this group, compared with 6 in the non-rearfoot strike group.

Five trials from each of the 11 included participants were analysed. Participants were categorised according to their corresponding pressure data as either rearfoot (n = 5) or non-rearfoot (n = 6) strikers. Euler angles in three planes were extracted to determine the angle between the following segments: hindfoot in relation to the tibia; forefoot in relation to the hindfoot; forefoot in relation to the tibia. Additionally, a two-dimensional vector angle between the hallux and first metatarsal was obtained in both the sagittal and frontal plane. Angles were time-normalized to 101 points and averaged for each participant. Group mean time histories were presented for each foot strike classification (Figures 63 to 65).

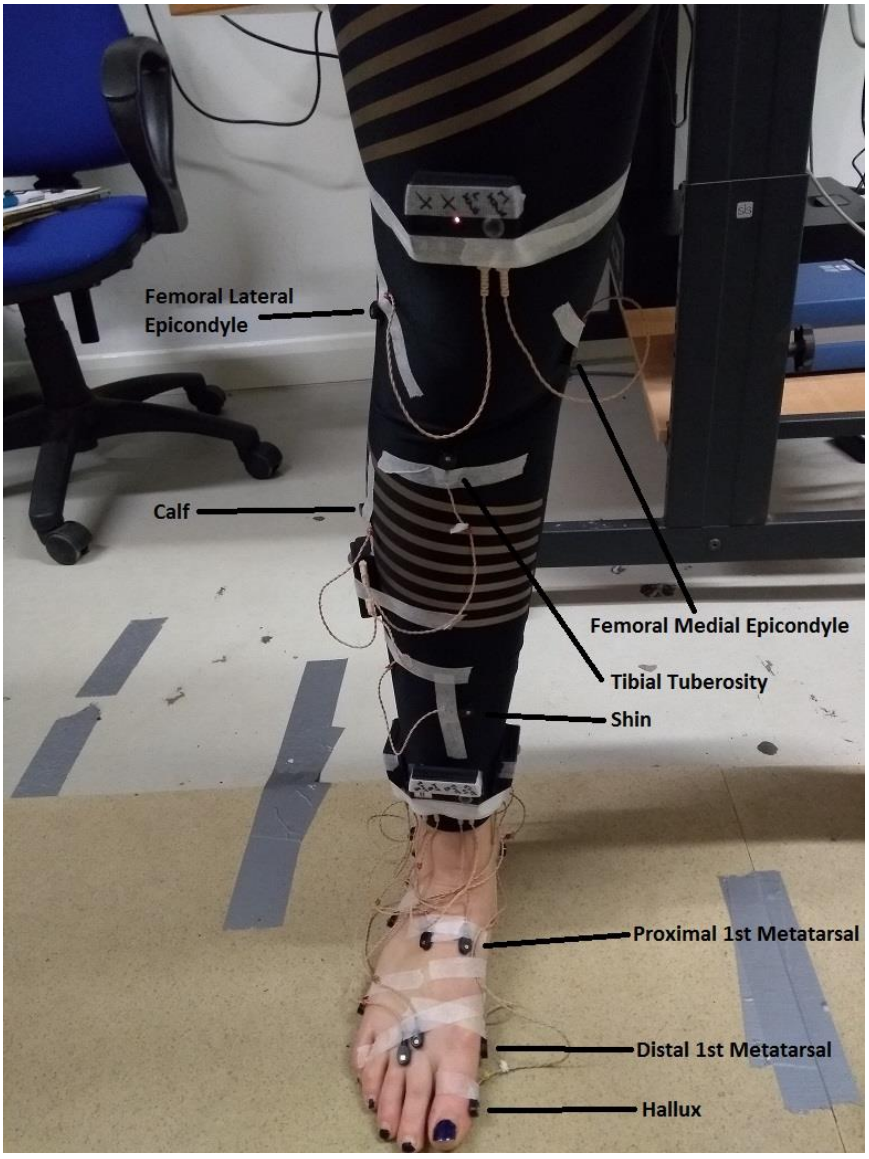

Figure 60: Markers of the leg and medial aspect of the foot

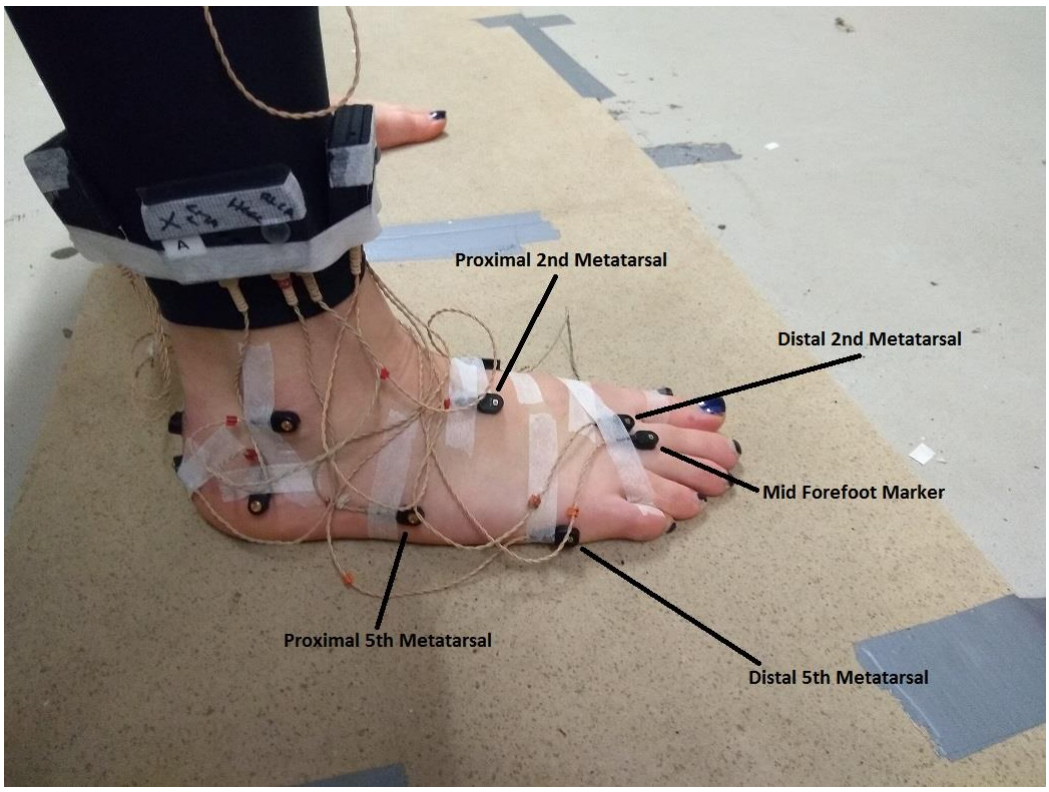

Figure 61: Markers of the lateral aspect of the foot

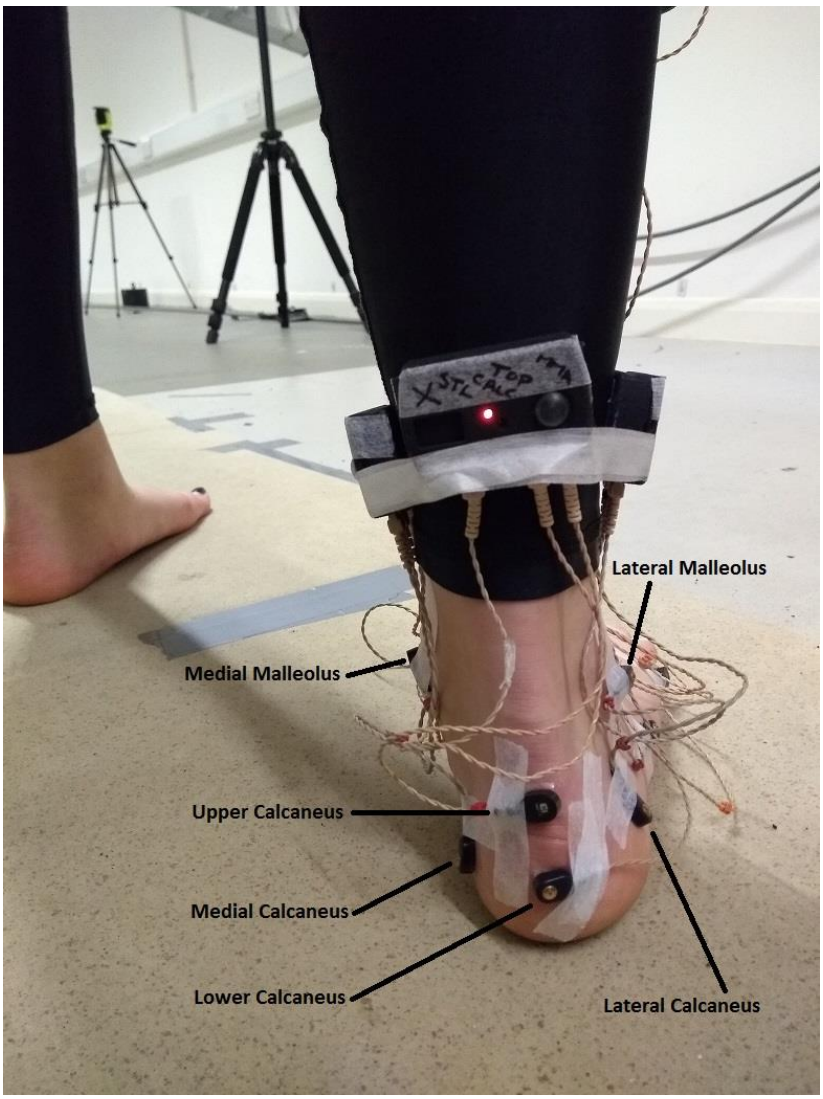

Figure 62: Markers of the rear aspect of the foot

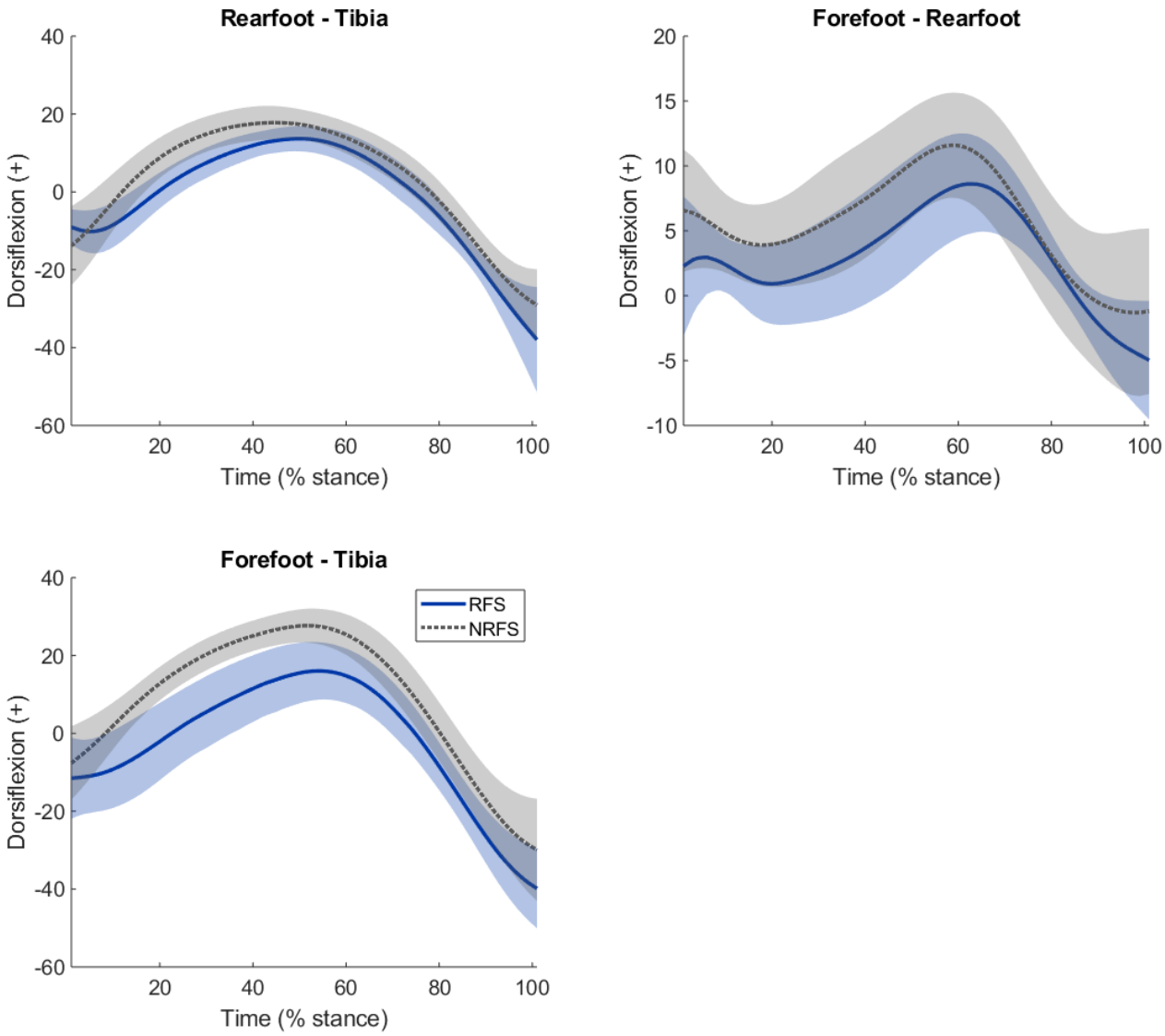

Figure 63: Sagittal plane angles between rigid foot segments during running stance in rearfoot strike and non-rearfoot strike runners.

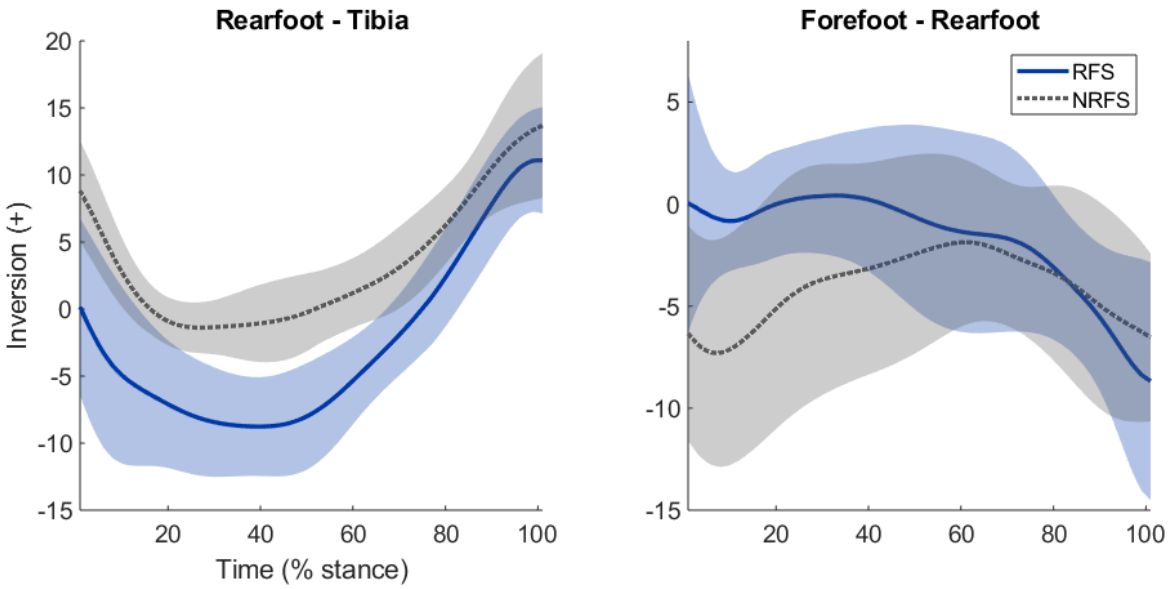

Figure 64: Frontal plane angles between rigid foot segments during running stance in rearfoot strike and non-rearfoot strike runners

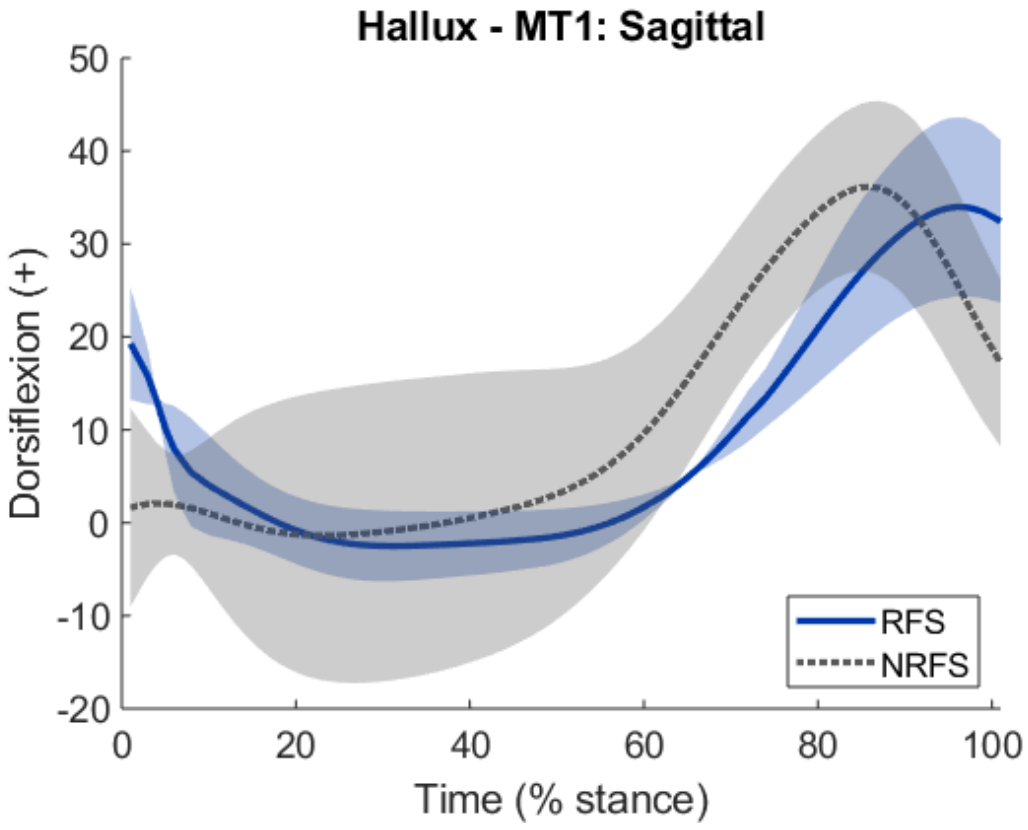

Figure 65: Sagittal plane vector angle between the hallux and first metatarsal during running in rearfoot strike and non-rearfoot strike runners. Note the RFS group includes only two participants.

Range of motion is not influenced by the static angle, therefore was obtained from all 11 participants. Range of motion in the sagittal plane and frontal plane was reported for the angle for which it was most relevant. These values are presented

in Table 17. Note that in the frontal plane, due to the shape of the curves, the range of motion between forefoot and rearfoot was not obtained, whereas it was obtained between the forefoot and tibia. However the figure displaying the average frontal plane angle between forefoot and tibia is not presented, as there were too many exclusions due to unusable static trials. Independent t-tests were conducted to identify differences between groups, but there was insufficient power for this to be meaningful.

Table 17: Range of motion in degrees between foot segments during running stance in the sagittal and frontal planes

ROM (°)	Mean (SD)	
	RFS (n = 5)	NRFS (n = 6)
Sagittal plane		
RF_Tib	23.5 (2.8)	32.0 (8.6)
FF_RF (TD to Peak)	2.8 (3.0)	4.4 (3.7)
FF_RF (Min to Max)	9.1 (2.0)	10.4 (3.3)
FF_Tib	28.1 (2.7)	35.7 (7.3)
Frontal plane		
RF_Tib	8.8 (2.7)	11.0 (5.1)
FF_Tib	11.2 (4.7)	9.4 (4.1)

Note: TD to Peak is the angle between touchdown and the peak value, whereas Min to Max is the difference between the local minima and local maxima.

These values would tend to support previous literature suggestions of a greater range of motion in the sagittal plane between the rearfoot and tibia, and forefoot and tibia in non-rearfoot compared with rearfoot strikers. This does not appear to be the case in the frontal plane.

Appendix 3 – Graphical Representations of all Metatarsal Bones at the Time of Greatest Braking and Propulsive Forces

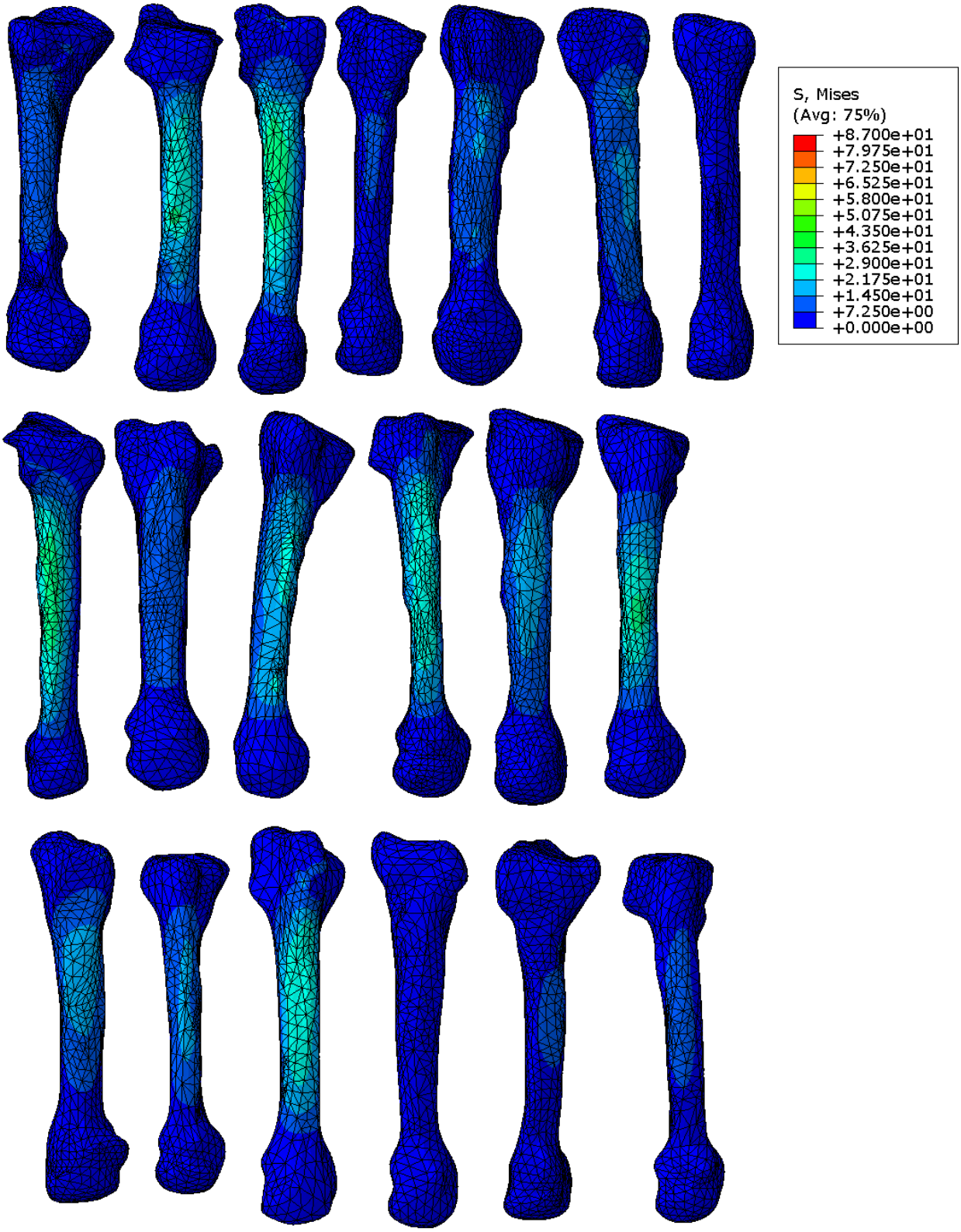

Figure 66: Finite element representations of the stress distribution on all participant's metatarsals at the point of greatest braking forces, dorsal aspect. Figures are scaled for presentation purposes.

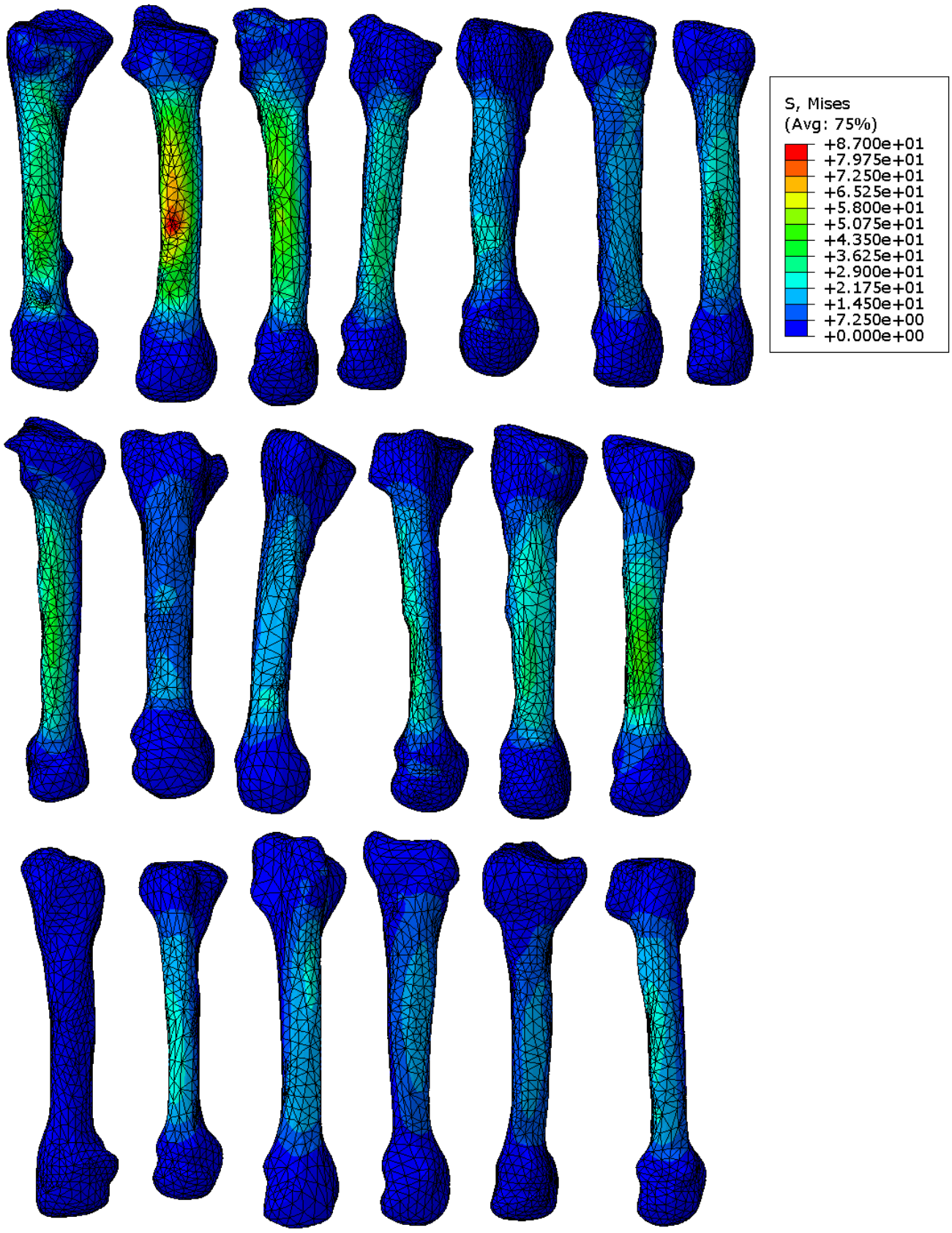

Figure 67: Finite element representations of the stress distribution on all participant's metatarsals at the point of greatest propulsive forces, dorsal aspect. Figures are scaled for presentation purposes.